Lawrence Berkeley National Laboratory
Recent Work

Title
MASS AND HEAT TRANSFER PROCESSES IN LAMINAR, TWO-PHASE FLOW

Permalink
https://escholarship.org/uc/item/4j73z4zt

Authors
Clark, Michael W.
King, C. Judson.

Publication Date
1967-06-01

eScholarship.org Powered by the California Digital Library
University of California

UCRL-17527

Cy. 2

University of California

Ernest O. Lawrence Radiation Laboratory

MASS AND HEAT TRANSFER PROCESSES IN LAMINAR, TWO-PHASE FLOW

Michael W. Clark and C. Judson King

June 1967

TWO-WEEK LOAN COPY

This is a Library Circulating Copy which may be borrowed for two weeks. For a personal retention copy, call Tech. Info. Division, Ext. 5545

Berkeley, California

UCRL-17527 Cy. 2

DISCLAIMER

This document was prepared as an account of work sponsored by the United States Government. While this document is believed to contain correct information, neither the United States Government nor any agency thereof, nor the Regents of the University of California, nor any of their employees, makes any warranty, express or implied, or assumes any legal responsibility for the accuracy, completeness, or usefulness of any information, apparatus, product, or process disclosed, or represents that its use would not infringe privately owned rights. Reference herein to any specific commercial product, process, or service by its trade name, trademark, manufacturer, or otherwise, does not necessarily constitute or imply its endorsement, recommendation, or favoring by the United States Government or any agency thereof, or the Regents of the University of California. The views and opinions of authors expressed herein do not necessarily state or reflect those of the United States Government or any agency thereof or the Regents of the University of California.

Research and Development

UCRL-17527

UNIVERSITY OF CALIFORNIA

Lawrence Radiation Laboratory
Berkeley, California

AEC Contract No. W-7405-eng-48

MASS AND HEAT TRANSFER PROCESSES IN LAMINAR, TWO-PHASE FLOW

Michael W. Clark and C. Judson King

June 1967

MASS AND HEAT TRANSFER PROCESSES IN LAMINAR, TWO-PHASE FLOW

Contents

MASS AND HEAT TRANSFER PROCESSES IN LAMINAR, TWO-PHASE FLOW

Michael W. Clark and C. Judson King
Lawrence Radiation Laboratory and Chemical Engineering Department
University of California
Berkeley, California

June 1967

ABSTRACT

High flux and high concentration level heat and mass transfer experiments have been carried out for several gas-liquid systems which exhibited resistance to transfer in both the liquid and gaseous phases. These experiments were carried out in a horizontal, rectangular duct of high aspect ratio, in which the gaseous and liquid phases were contacted while moving in stratified, laminar cocurrent flow. A calculational method, which utilizes the principle of addition of the individual phase resistances in a trial and error manner, was developed and utilized to predict the interphase high flux, high concentration level mass transfer behavior of the system. In order to ascertain the gas phase resistance for this model accurately, the equation of convective diffusion was solved numerically for the case of a finite interfacial mass flux (high flux) combined with a linear velocity profile away from the mass transfer interface (the Leveque model). The flux level correction factor obtained from this solution, which differed only slightly from the penetration model correction factor, was confirmed experimentally by evaporating isopentane and n-pentane into a flowing nitrogen stream.

During the course of the interphase mass transfer experiments a large reduction in the liquid phase resistance to mass transfer was observed at higher concentration levels of the volatile components. This reduction was ultimately traced to a form of cellular convection in the liquid phase which appeared to be driven by surface tension variations brought about by the concentration gradients existing in the system. The effect of this type of cellular convection upon the experimentally observed, liquid-phase mass transfer coefficients for several systems was well represented by a single correlation involving the Thompson number.

I. INTRODUCTION

One of the most frequent problems facing the chemical engineer is that of transferring material from one phase to another. For example, this is almost invariably the route chosen for separation of two different chemical species. Industrial examples include such processes as distillation, absorption, desorption, partial condensation, and partial flash operations. All of the above processes have some factors in common; first, they usually involve only two phases, a gas and a liquid. A second important, but more subtle, point is that they all involve a certain amount of heat transfer, as well as mass transfer.

At present there exists a large body of both experimental correlations and analytical methods for the prediction of mass transfer rates for processes such as the above. A closer examination of this work, however, will reveal a number of assumptions which are usually, but not always, made. A few of these which are of interest with respect to this study are the following:

1) Mass transfer rates are generally calculated on a low flux, low solute concentration level basis; or else the simple P_{BM} correction factor is used.

2) The heat transfer that is almost invariably associated with the mass transfer is frequently ignored.

3) Quite often the problem is over-simplified by assuming that the resistance to transfer lies entirely within one phase, or that it can be calculated simply by invoking the "addition of resistances" principle with respect to the two phases involved.

4) The pertinent physical properties associated with each phase are commonly assumed to be constant, often at the conditions prevailing in that phase prior to the transfer operation.

5) A number of physicochemical phenomena which have been observed at high flux and concentration levels are not taken into account. Examples of the above might include Marangoni and Benard cells (surface tension and density driven convection cells).

6) Frequently unexpected hydrodynamic effects are encountered; such as retardation of interfacial velocities due to the accumulation of surfactant films.

7) Local supersaturation and nucleation (mist or bubble formation can occur; particularly when concentration gradients are very steep.

In recognition of the above deficiencies, a long term study was initiated with the goal of experimentally and analytically investigating as many of the above listed subject areas as possible. For convenience the work would be carried out utilizing a single experimental geometry. Also, the decision was made to limit the study to laminar, gas-liquid stratified flow. The first investigator in this overall study was Charles H. Byers, whose contributions will be discussed in the following section.

A. Previous Work

Since a number of texts have been written within the general area of mass transfer, it would be impossible to do justice to the subject in a few pages. Consequently, the approach taken here will be to list a few of the more important works which are directly applicable to the material covered in this study. For a review of the general areas of heat and mass transfer, the texts by Sherwood and Pigford;[68] Bird, Stewart and Lightfoot;[11] and Schlichting[67] are recommended.

Within recent years, by far the most profitable approach to the solution of mass transfer problems has been through the use of the partial differential equations of convective transport as a starting point. Although the number of successful analytic solutions to these equations is quite limited, they have been found to cover a broad spectrum of mass transfer problems. If we limit ourselves to the laminar flow region for example, we find that the "penetration model" due to Higbie[29] is applicable to a wide range of problems involving mass transfer from, or into, a freely flowing liquid surface. Similarly the solutions due to Graetz[27] and Leveque[43] have been found applicable to many problems involving transfer from a solid boundary into a flowing fluid stream. Within the

last thirty years a large number of contributions[28] have been made through the use of the "laminar boundary layer" assumptions

In his work, Byers[13,14,15] set out to obtain experimental results for a situation where the mass transfer resistance was divided between two phases in a predictable manner. In order to do this he first tried to design a simple contacting apparatus wherein the fluid dynamics of both phases could be simply described. The equipment which was finally decided upon was a rectangular horizontal duct, with a large width to height, (aspect) ratio. The gaseous phase was to flow above the liquid in either cocurrent or countercurrent flow, with both phases having equal depth. The velocity profiles could then be established in both phases by separating them with a very thin boundary prior to their entering the contacting section.

Such a contractor has several advantages; some of which are listed below.

1) A large aspect ratio means we need only deal with a two dimensional problem for the fluid flow and convective transport equations.

2) The horizontal position of the equipment makes the problem of surface waves and ripples much less severe. In fact if the flow Reynolds numbers are kept below a value of approximately 2000 in the liquid phase the surface does not show any evidence of wave formation provided the gaseous phase is maintained within the laminar flow regime.

3) The exact fluid dynamics of the system are easily obtained for both phases (see Appendix A in Byers' Thesis).[13]

4) It is possible to view the transfer area by constructing the duct of a transparent material.

Having decided upon the geometry of the apparatus, Byers then obtained an exact solution to the convective diffusion equations in both phases using appropriate interfacial equilibrium boundary conditions.[14] However, as is usually the case in exact solutions of most mass transport problems, his solution involved the assumptions of low mass flux rate, low concentration level of the solute, and no coupling of the associated heat transfer to the mass transfer problem.

Byers also constructed the proposed experimental equipment,[15] and carried out a number of runs involving systems where mass transfer resistance was divided between the gaseous and liquid phases. The bulk of his work involved the evaporation of either a pure liquid (ethanol); or the evaporation of a solute (ethyl ether) from a liquid binary mixture (ethyl ether-ethanol), into a flowing gas stream (N_2, He, or CO_2). His experimental results agreed very well with the theoretical approach; thus confirming its applicability under the laminar co-current flow conditions. He also carried out a few counter-current runs; and developed an approach which predicted these results quite well.

B. Objectives of the Present Study

After it had been shown that the horizontal duct performed as expected under the low flux and low concentration level conditions, the next logical step in the overall study was to extend the conditions of the experiment to involve some of the interesting complications that were previously listed. With a little thought, one can see that two changes in the run conditions of the channel could conceivably introduce nearly all of these complications. That is, if we increase the concentration level of the transferring species and simultaneously increase the flux level (for example by using a more volatile liquid), then we will certainly violate our low flux, low concentration assumption. Also, the associated heat transfer problem will become more acute; since a higher rate of transfer will involve an increase in the amount of energy associated with the change of phase through which the solute must go. In addition, the variability of properties, particularly in the liquid phase, will become a factor, since viscosity, diffusivity, and density are generally strong functions of concentration and the concentration gradients will be large.

Thus the objectives of the present work were formulated along the following lines:

1) The thermal characteristics of the system should be evaluated, primarily the heat losses to the outside and between phases prior to entering the test section.

2) A suitable system whereby the conditions of high flux and high concentration level could be achieved, should be found and evaluated experimentally.

3) Theoretical studies should be carried out which would be capable of predicting as many as possible of the effects which might be encountered in the course of the experimental work. These should include variable physical properties, simultaneous heat and mass transfer and their linking conditions, and a high flux solution of the physical problem at hand.

4) A close watch should be kept on the system in anticipation of any anomalous behavior which might occur (see 5), 6), and 7), pages 1 and 2).

II. EXISTING EXPERIMENTAL APPARATUS

The horizontal rectangular duct design which Byers utilized in his work will be described briefly below. For a more detailed account the reader is referred to Refs. 13, 14, and 15.

The major piece of equipment is the horizontal contacting device, which is rectangular in cross section with inside dimensions of 0.500 by 3.00 in. for each phase. The channel was constructed of Lexan polycarbonate, which is a clear, transparent plastic capable of being used over a wide temperature range (up to 100°C). The overall length is 6.5 ft, with this being divided into three sections. The first, an inlet or calming section, is 2.5 ft in length. This is followed by an 18.0 in. test section, and the last 2.5 ft are an exit calming section. The gas and liquid phases are separated from each other by a thin metal divider plate in the inlet and exit sections; thus the total exposure length is only 18.0 in.

Several pieces of analytical equipment were used by Byers to obtain his basic experimental data; these included an Aerograph gas chromatograph, a Brown electronic recorder for thermocouple readout, and an Atkins thermistor temperature detector. Also, a liquid re-circulation loop with flow meters and a gas feed system were in existence; however, after several preliminary calculations it became apparent that a large portion of this equipment would have to be re-designed. This was primarily due to a number of thermal considerations which were important to the present study and not to the work carried out by Byers.

III. EQUIPMENT ALTERATIONS

After the general experimental plan had been decided upon, it was necessary to evaluate the feasibility of carrying out these experiments on the existing equipment. The work which Byers had carried out had been nearly isothermal; therefore he did not have to construct a very elaborate temperature measuring system. Since a large portion of the experimental plans involved heat transfer measurements, it was decided that the existing temperature measuring facilities were inadequate, and work was started on the design and construction of a more accurate system.

A. Test Section

The first change which was necessary was the insertion of several temperature sensors in the test section, to yield temperature profiles at several points along the exposure length. Figure 1 is an isometric drawing of the test section, showing the position of five 1/2 in. diameter holes drilled through the top of the test section. T_1, T_2, and T_3 indicate the position of three separate temperature probes located at 1/2, 10 and 17-1/2 in. from the inlet end of the channel. C_1, and C_2 indicate the position of two concentration probes at 10 in. and 17-1/2 in. respectively. The basic design of the concentration probes remained essentially the same as that employed by Byers; however, the thermistor temperature probes that he had used were both too bulky (too large a heat capacitance, and insufficient resolution) and not accurate enough for the present work. Consequently, a new thermoprobe design was necessary. The basic requirements of such a probe were as follows:

1) The unit must be capable of measuring temperature as a function of position. The could be accomplished by continuing to use a micrometer body as the basis for design, thus allowing a position accurate to 0.0005 in.

2) The sensing element should be small compared to the total distance over which the profile is to be measured; i.e., 1/2 in. This is what was meant by the term "resolution". If we restrict the physical dimensions of the probe tip to 1.0% of the distance covered, then the tip diameter should be less than 0.005 in.

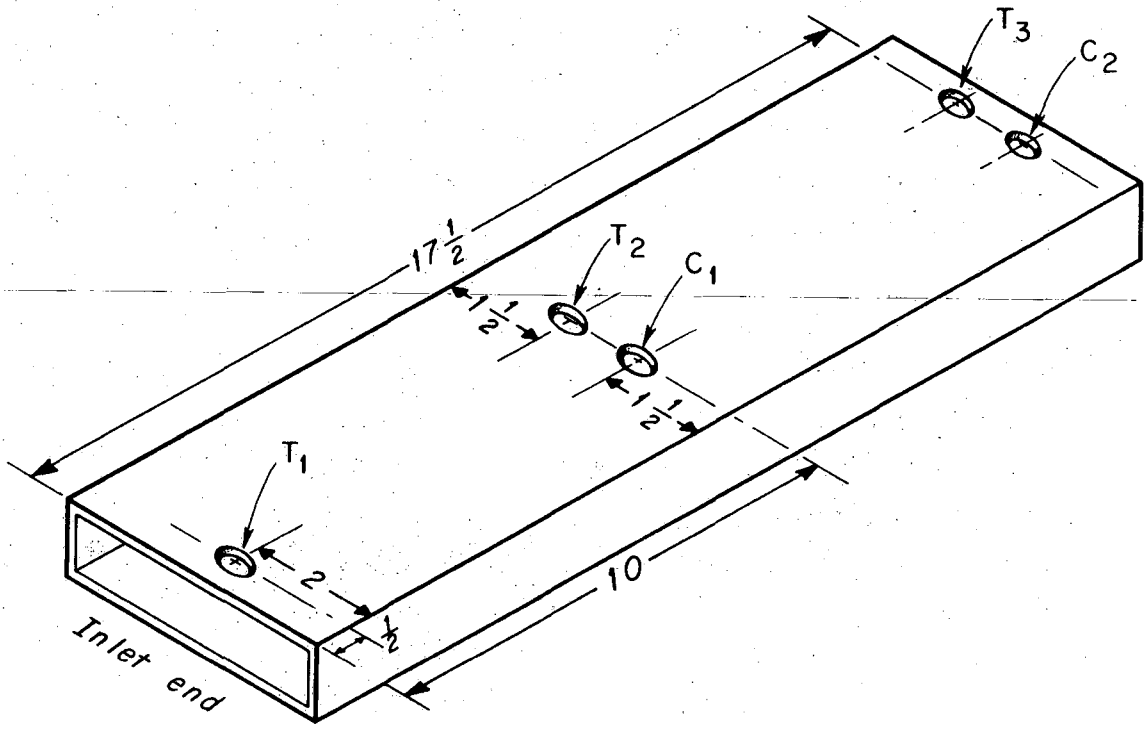

Fig. 1. Test Section, with overall dimensions and placement of the temperature and concentration probes indicated.

3) The sensing portion of the probe should ideally be sensitive to small time and spatial variations in temperature. Thus in addition to a low thermal capacitance, as was stated previously, the thermal conductivity of the probe material should be as low as possible.

The upper portion of the probe (the micrometer barrel) is large enough that it will be at ambient temperature. This adds an added incentive towards obtaining a low thermal conductivity material, because the axial heat conduction could force the probe tip to be at a temperature different from the adjacent gas stream. As the design of the probe advanced this problem became very acute, primarily because a gas in laminar flow has a very small heat removal capability.

One method of partially solving the problem of axial conduction is to bend the probe tip, so that a portion of the tip is horizontal prior to the extreme end where the thermocouple junction would be made. This method was used in the final probe design (see Fig. 3). The advantage of such a design is that the length of wire immediately adjacent to the thermocouple junction is now within a lamina of constant gas velocity and temperature. Thus the physical problem which must be solved is that of a cylinder of length L, exposed to a flowing gas stream with a temperature T_G, and a velocity V_G. The diameter of the cylinder is d_a, and one end of the cylinder is fixed at a temperature T_s. We would now like to solve for the temperature of the cylinder at the position z = L, if the length parameter is measured from the fixed end of the cylinder. This situation is depicted in Fig. 2. If a differential heat balance is written for a small length of the cylinder, dz, equating the heat flowing in from the gas to Q_z, the axial heat flux, we obtain:

$$\frac{-d_a}{4}(dQ_z) = h_G(T-T_G)dz \qquad (3\text{-}1)$$

where T = probe temperature and h_G = exterior heat transfer coefficient. Using the Fourier expression for the axial heat flux,

$$Q_z = -k_t \frac{dT}{dz} \qquad (3\text{-}2)$$

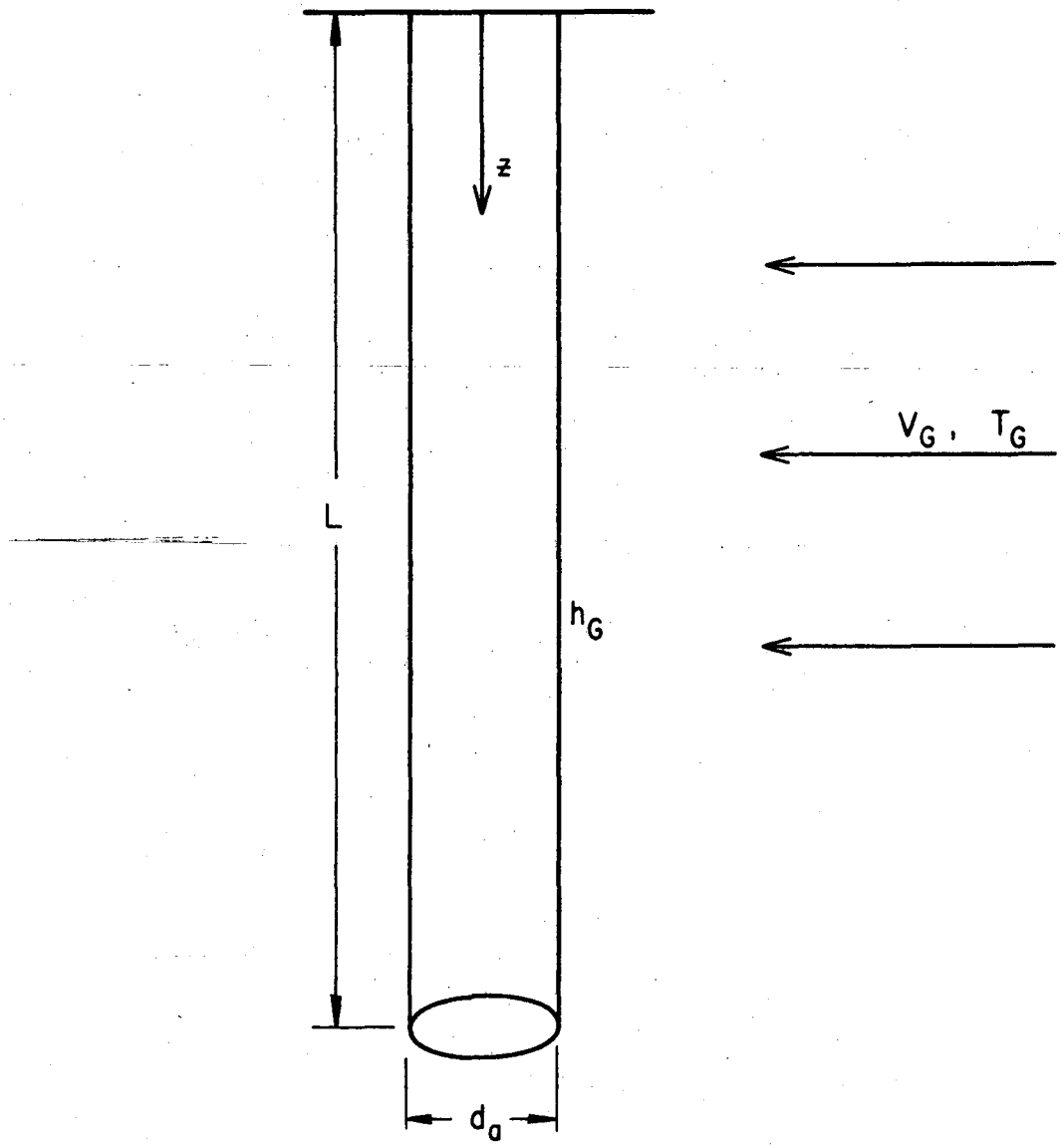

Fig. 2. Physical model used for solution of the problem of heat transfer to a thermocouple tip exposed to a flowing gas stream.

where k_t = thermal conductivity of the probe, and substituting (3-2) into (3-1) we obtain:

$$\frac{d^2T}{dz^2} = (4h_G/k_t d_a)(T-T_G) \quad . \tag{3-3}$$

The solution to the above differential equation is quite straightforward. First substitute the following variables:

$$\zeta = z/L \ , \quad \Phi = \frac{T-T_G}{T_s-T_G} \quad , \text{ and } \quad N = \sqrt{4h_G L^2/k_t d_a} \tag{3-4}$$

to yield the final equation in dimensionless form:

$$\frac{d^2\Phi}{d\zeta^2} = N^2\Phi \quad . \tag{3-5}$$

The boundary conditions for the problem are that the probe temperature is equal to T_s at z = 0, and the probe temperature is equal to T_G at z = infinity. Writing these in dimensionless form we would have:

$$\Phi = 1 \text{ at } \zeta = 0.0 \quad \text{and} \quad \Phi = 0.0 \quad \text{as} \quad \zeta \to \infty \tag{3-6}$$

The solution to Eq. (3-5) subject to the conditions expressed in (3-6), can be obtained by two successive integrations;

$$\Phi = \cosh(N\zeta) - \tanh(N)\sinh(N\zeta) \tag{3-7}$$

A quick glance at the behavior of the above function, holding in mind that our objective is to have θ approach zero at z/L = 1.0, shows that we want to increase the value of N as high as possible. This was used as the design criterion for the resulting thermocouple probe.

Since the value of h_G is dependent on the exterior gas velocity it is not one of the independent parameters; however, the other terms entering into the expression for N could all be varied to some extent. The value of k_t could be varied through the choice of different metals for construction of the probe. Listed below are the thermal conductivities of several metals and alloys:[31]

Copper	....	0.918	cal/cm sec °C
Constantan	....	0.054	"
Iron	....	0.161	"
Chromel	....	0.043	"
Platinum	....	0.161	"

In view of these values two systems were picked for investigation – Iron-Constantan and Chromel-Constantan, with the latter having superior values of thermal conductivity, but poorer mechanical qualities. The above metals could be obtained in several diameters, with the optimum appearing to be a 5 mil diameter wire coated with a 1/2 mil Teflon coating. Smaller diameters tended to be too flexible to support their own weight, and also did not come with a factory insulation. Calculations based on the preceding equations indicated that the Iron system would require a value of L = 1.7 times the value for the Chromel-Constantan system, thus the latter system was used. This entailed a minor inconvenience, since there were no existing calibration curves, but the much lower thermal conductivity of the system overshadowed the effort required to calibrate the system.

Substitution into Eq. (3-7), using as a criterion $\Phi = 0.02$ and the value of $k_t = 0.054$, yields a value of L = 0.6 for the Chromel-Constantan probe. In the final design the value of L varied from 0.5 to 0.6 in. This means that the probe temperature should be from 2 to 4% of the value of $(T_G - T_s)$ lower than the actual gas stream temperature. This was confirmed experimentally, and the Chromel-Constantan probes were found to be quite insensitive to axial-conduction induced errors.

Figure 3 shows the complete probe design. Point G indicates the tip of the 5 mil diameter probe wires. B illustrates a piece of 23 mil diameter stainless steel tubing, through which the thermocouple wires were threaded. This acted as a support in the flowing gas stream, except for the last 0.6 in. discussed above. The wires were kept approximately 1/16 in. apart from the S.S. tube to their tip. Point H illustrates the o-ring seals, which allowed the shell of the probe to rotate, while the inside remained pointing in a fixed direction.

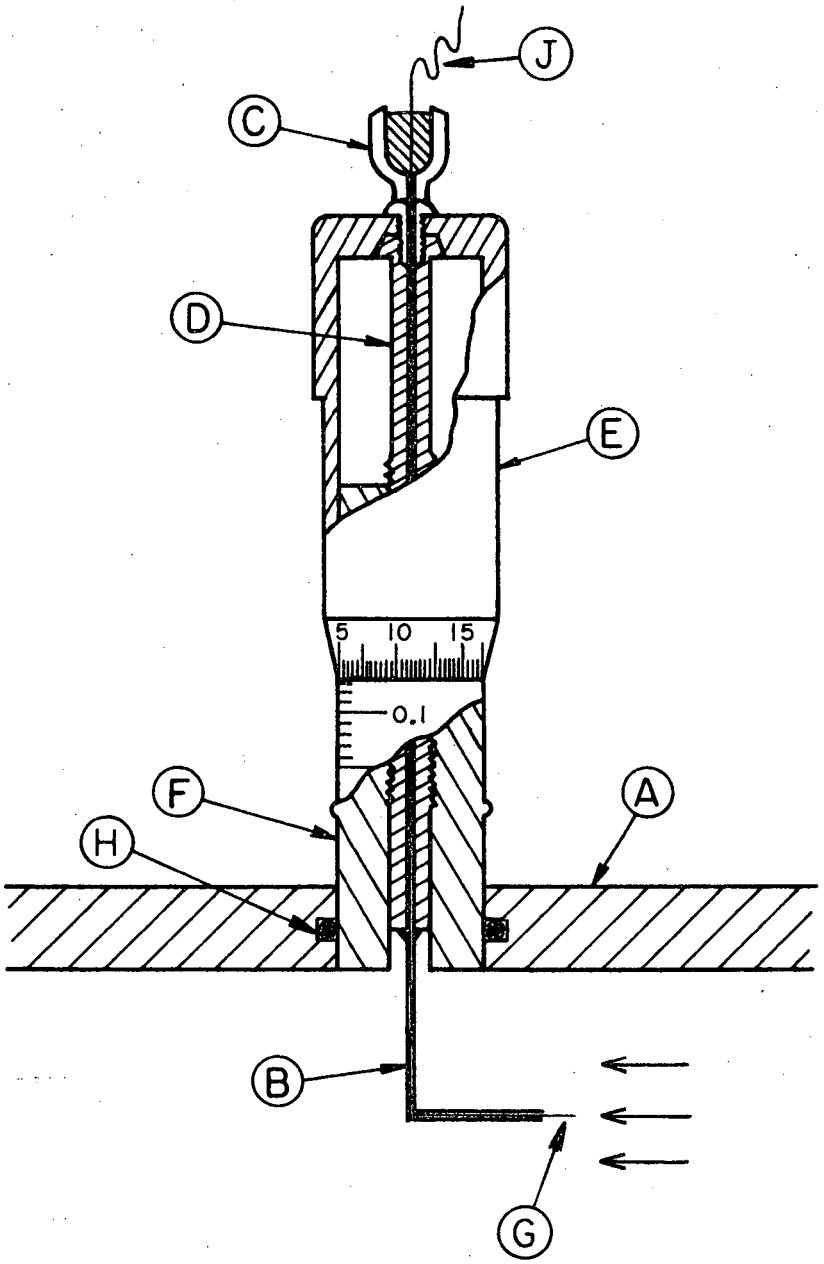

XBL 676-4142

Fig. 3. Cross sectional view of thermocouple probe.

This was a necessary design change, as the thermocouple metals were very brittle and would not take the constant twisting that would have resulted from fixing the barrel of the micrometer and turning the inside in the usual manner. The thin thermocouple wires were further supported from point J to the ice bath by threading them through 20 mil diameter Teflon tubing.

A Sargent Model SR recorder was used to record the thermocouple output as a function of time and vertical position. The scale used was 0.0 to 0.5 mV. This meant that temperature could be read to an accuracy of 0.1°C.

B. Inlet and Exit Sections

The existing inlet and exit calming sections utilized a thin metalic divider plate to separate the gaseous and liquid phases. Actually this divider plate was made up in a sandwich arrangement, composed of a layer of metal, a layer of cork, and another layer of metal, with the total thickness being only 1/16 in. A preliminary heat transfer calculation was carried out for this inlet design, and it was found that the heat transferred in the inlet section before the streams entered the test section would be approximately twice the transfer which would take place in the test section. Provisions had been made for evacuation of the cork filled center section; however, even assuming a good vacuum (2 to 3 mm Hg), the heat conduction through the cork matrix promised to contribute a large fraction (compared to the test section) of the total heat transferred from the liquid to the gas. Also the extremely thin metal plates (0.0156 in.) did not have sufficient strength, and would collapse under an atomosphere of pressure, should the cork have been removed.

In order to confirm the above calculations, several experimental runs were carried out using the existing equipment for heat transfer between a gas and liquid phase. Figure 4 shows the profile results for one of these runs under favorable gas flow conditions. The "zero heat transfer" curve represents a theoretical calculation for the inlet probe position at 1/2 in. from inlet assuming no prior heat transfer in the inlet section. The gas temperature prior to entering the inlet section was 22.0°; the liquid temperature, 16.8°.

The results shown in Fig. 4, indicated that an improved inlet section would be desirable prior to any attempts to carry out a simultaneous heat and mass transfer experiment. After several designs were carried out, it was realized that although vacuum insulation could substantially reduce the heat leaks, this was very impractical from a structural point of view. In order to obtain sufficient strength to keep a four in. wide plate from flexing, it had to be made almost 1/8 in. thick. This would mean a total divider plate thickness of over 1/4 in., which was undesirable from a hydrodynamic standpoint. Also, the vacuum

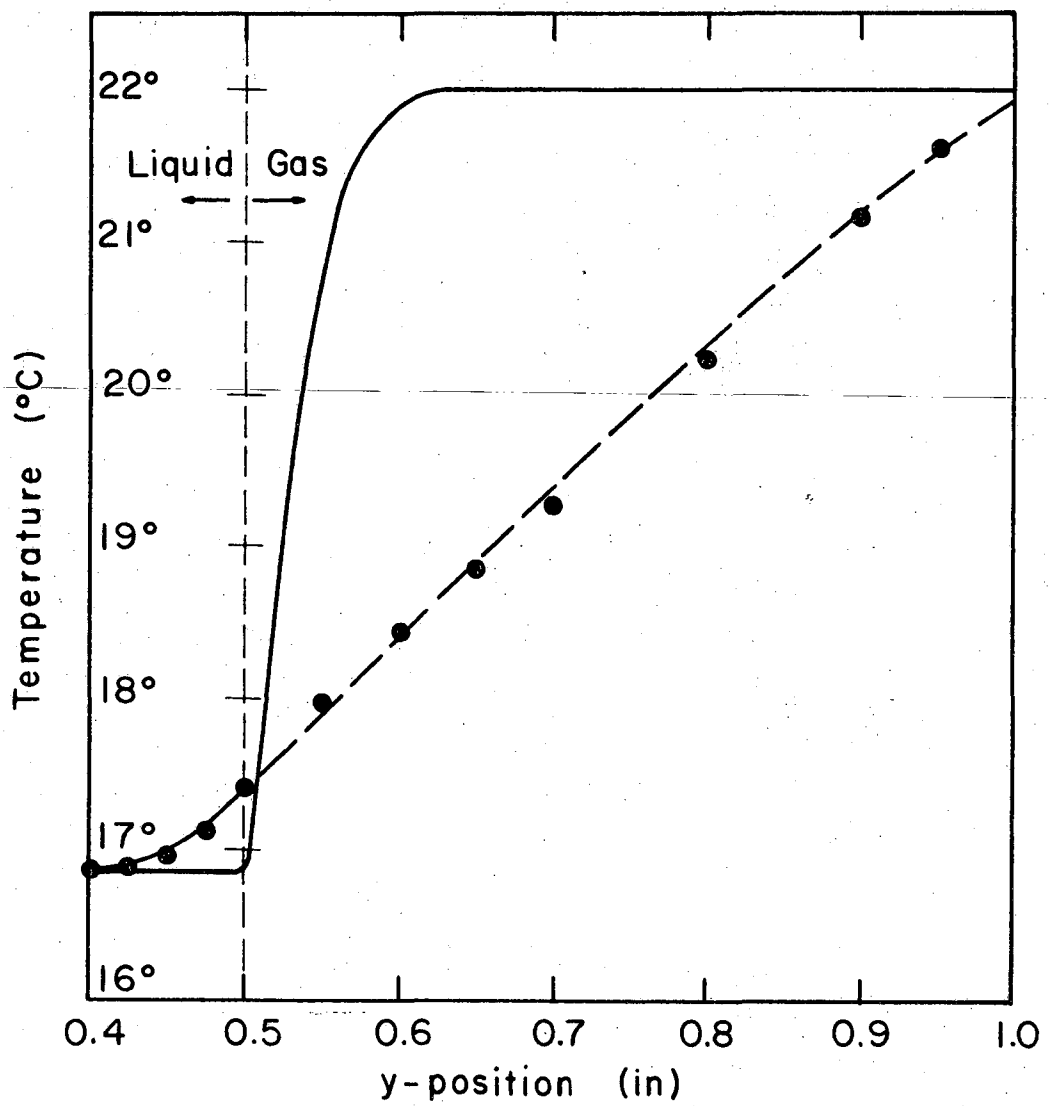

XBL675-3210

Fig. 4. Comparison of experimental temperature profile for existing inlet section with theoretical profile assuming zero heat transfer in the inlet section. Data taken at 1/2 in. from test section inlet; QG = 750 cm^3/sec; QL = 0.580 gpm.
System: air/tridecane

design would have been expensive, and difficult to construct and operate. An alternate approach, which was finally adopted, was to spatially separate the two phases until just prior to entering the test section. In this way, ordinary insulation could be used. The entry section was slightly curved, in a parabolic shape. This allowed a final entry angle of 6°, with a minimum of heat transfer between phases prior to entering the test section. A cross-sectional view of the parabolic entry way is shown in Fig. 5. The construction was carried out using 1/16 in. polycarbonate plate. A preliminary estimate indicated that the gas phase hydrodynamics should not be appreciably altered as long as the Reynolds number was maintained below a given critical value. This value (N_{Re} = 1200) was determined experimentally by locating the point at which the heat transfer coefficient first began to deviate from its predicted value. Figure 6 shows a comparison of inlet temperature profiles (on a dimensionless basis of $\Phi = (T-T_G)/(T_L-T_G)$), with the metal-cork divider, the parabolic entry and the "zero heat transfer" curves all being shown for the gas phase. As can be seen, the parabolic entry section shows a very definite advantage over the old design. A number of runs at widely varying flow conditions indicated that the small amount of heat transfer which was occuring in the entry section could be accurately predicted by adding 1.5 in. to the total test section length for all heat transfer calculations. Thus an exposure length of 2.0 in. would accurately predict the temperature profile observed by the probe at 0.5 in. from the start of the test section.

Another problem which had to be overcome was that of insulating the gas from ambient conditions. This was usually not too important, since the majority of the runs were made with the gas phase at ambient conditions, and the liquid phase temperature being controlled to yield the desired temperature difference. However, a few runs were made with the gas phase being heated, and for these the equipment was insulated on the exterior using a combination of styrofoam and asbestos wool to a total thickness of several inches. This was still not totally satisfactory, and a final adjustment of the temperature profile at the upper exterior boundary of the test section was achieved by wrapping fine Nichrome

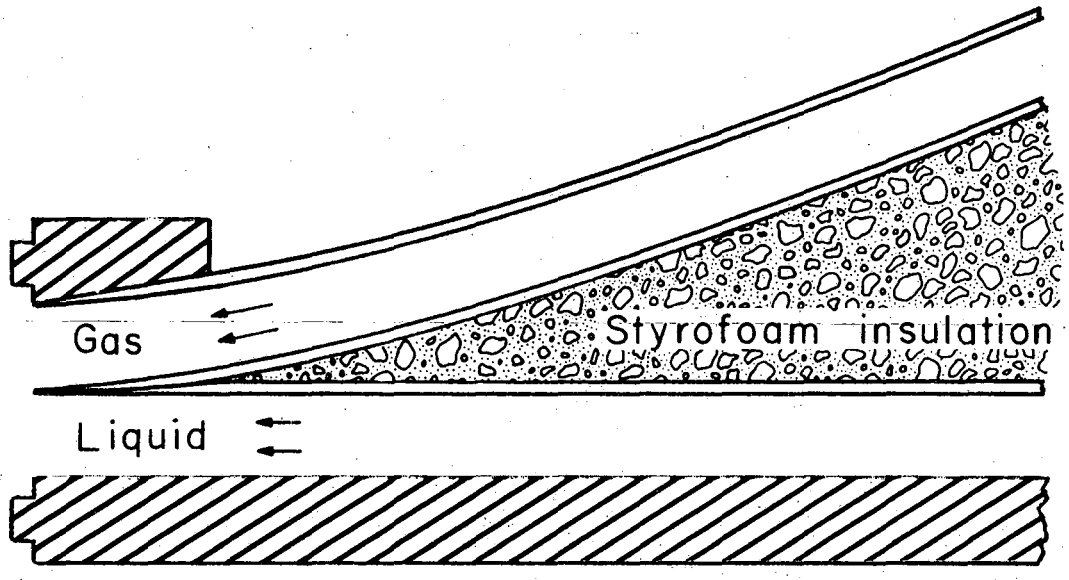

XBL675-3211

Fig. 5. Cross sectional view of parabolic entryway. The channel walls were constructed with polycarbonate plastic.

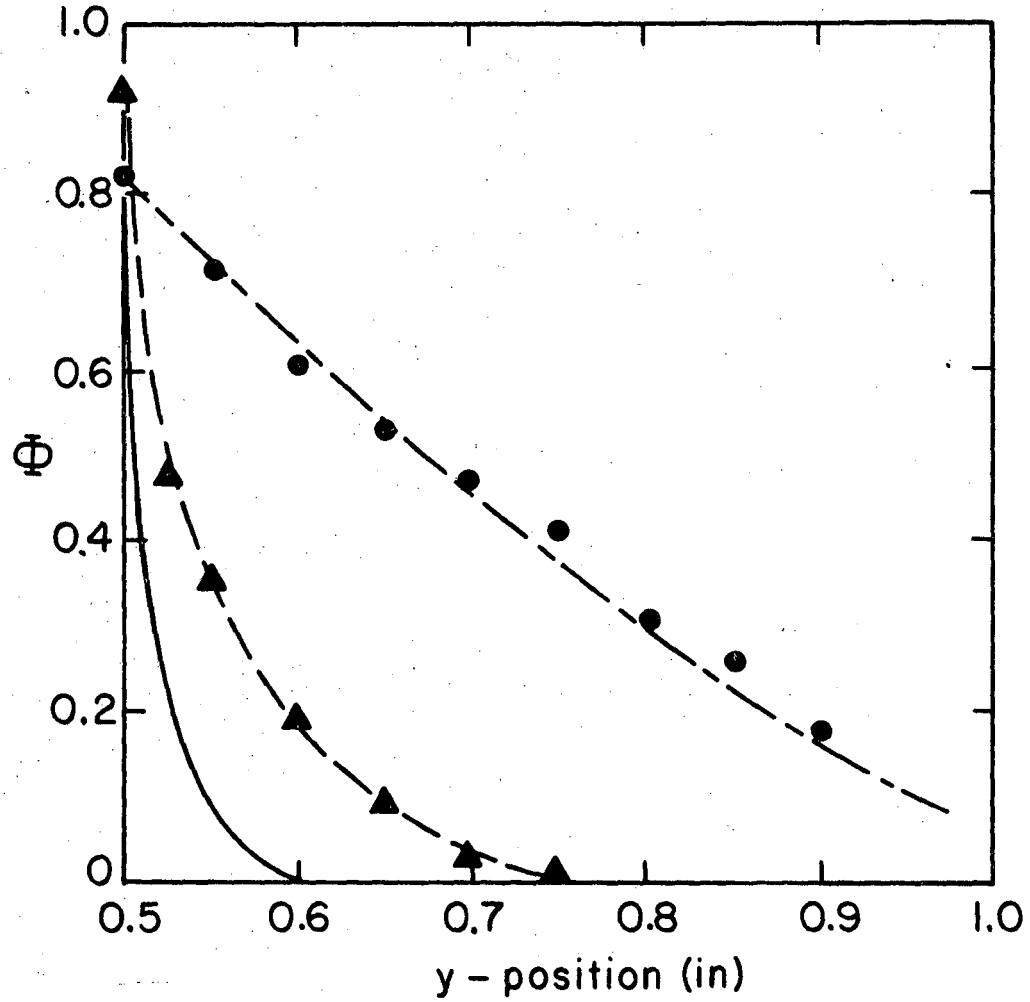

XBL675-3212

Fig. 6. Dimensionless temperature profiles taken at 1/2 in. from test section inlet. ● ... results using previous inlet section design, △ ... results using parabolic inlet section, the solid line indicates the theoretical prediction for zero inlet heat transfer. QG = 750 cm^3/sec, QL = 0.580 gpm.
System: air/tridecane

heating wire around the outside, and passing a carefully controlled current through the wire. Using this technique, an upper boundary which very closely approached the desired isothermal wall condition could be achieved.

Since all thermal data were taken using probe techniques, the exit section remained the same as designed by Byers except for the replacement of several gaskets, which had begun to crack and leak.

C. Integrated Experimental System

Figure 7 is a view of the overall experimental arrangement, showing both the gas and liquid flow systems. The major changes from the previous system were:

1) A liquid make-up system was installed to allow an accurate, continuous addition of the volatile component under conditions of high liquid evaporation rates.

2) A bypass was constructed around the channel, so that the liquid bulk temperature could be established prior to admitting flow into the test section.

3) The gas inlet supply system was altered in several places; including the removal of a gas saturator, insertion of an accurately controlled gas phase heater, and installation of better gas flow control.

4) The liquid level control was slightly improved by placing needle valves on the lines to the "vacuum" and "air pressure" from the lower surge tank.

5) The gas sampling system was improved, primarily by using a vacuum system after the gas chromatograph so that the sample flow rate could be accurately controlled, without depending on the channel pressure level to force the samples through the chromatograph.

6) Several changes which have already been discussed, were carried out on the inlet and test sections.

7) A major alteration was the construction of a temperature measuring system which utilized thermistors and thermocouple probes to obtain temperatures at a number of points around the system. Figure 8

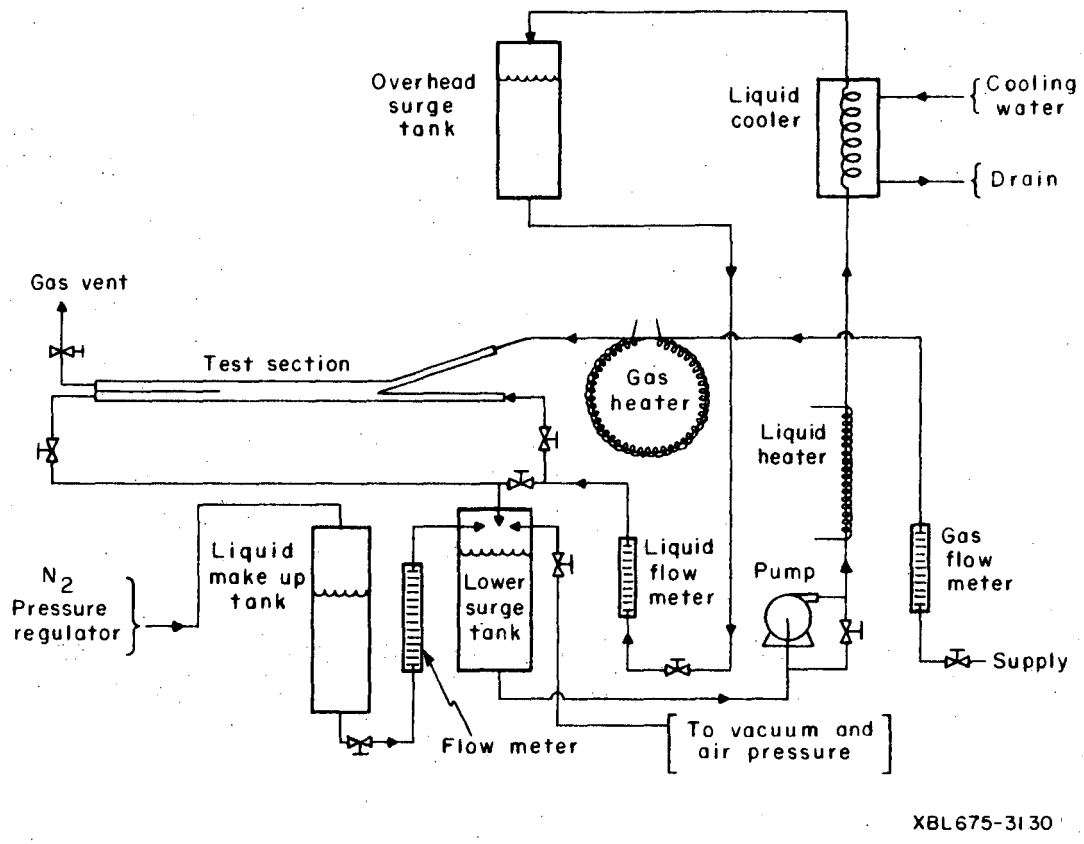

Fig. 7. Schematic view of experimental apparatus, showing liquid and gas flow geometries.

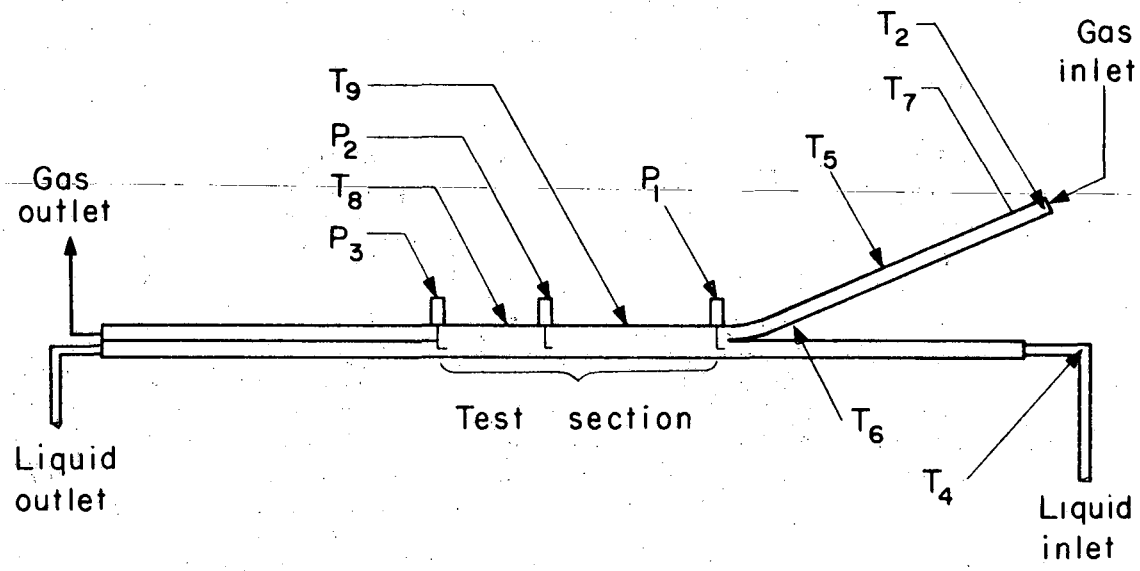

Fig. 8. Cross sectional view of channel, with the position of all the points for temperature determination indicated.

shows a schematic cross-section of the channel, with the location of each of these sensing points indicated. T_1 thru T_9 indicate fixed thermistor probes, whereas P_1, P_2, and P_3 are the micrometer mounted thermocouple probes, capable of recording temperature as a function of vertical position. The thermistors labeled T_5, T_7, T_8, and T_9, were glued to the exterior surface of the polycarbonate channel, then covered with two or more inches of insulation. The temperature measured at these points, when compared with the gas stream temperature and the ambient temperature gave a good indication of the gas phase heat losses thru the upper exterior wall.

The probes T_2 and T_4, were used to measure the inlet cup mixing temperature of the gas and liquid streams respectively. Each of these probes were inserted into the fluid stream, well away from the influence of the ambient temperature.

The probe T_6, was used for a variety of purposes. It is shown inserted in the styrofoam insulation in Fig. 8; where it was frequently placed to help determine the heat transfer between the phases prior to entering the test section.

All of the thermistors were connected to an Atkins, Model 3L01J Resistance Thermometer, which provided a direct temperature read-out in degrees Centigrade.

IV. HEAT TRANSFER EXPERIMENTS

The first objective of the present study, was to evaluate the thermal characteristics of the system. In order to accomplish this, a number of experiments were planned involving pure heat transfer between a non-condensable gas and a non-volatile liquid. In view of the subsequent simultaneous heat and mass transfer runs which were planned, careful consideration was given to the choice of materials to be used in the study.

The readily available gases included nitrogen, air, helium, carbon dioxide, and oxygen. Air and helium were chosen for use in this portion of the work because of their large difference in thermal diffusivity.

The choice of a liquid had to be made under more stringent requirements. The factors which were important were a low vapor pressure, low viscosity (less than 2 cp), and low cost. Another consideration, which turned out to be the most difficult to meet, was that the liquid had to be compatible with polycarbonate plastics, the material used throughout the channel construction. After an exhaustive literature survey, the most promising series of compounds appeared to be the linear, long-chain aliphatic hydrocarbons. A detailed listing of the properties of these compounds can be found in Appendix D. A carbon chain length of thirteen (n-Tridecane) offers all of the above requirements except that of ready availability. After several inquiries, the desired material was obtained in a relatively impure form as a "still cut" from the Atlantic Refining Co., made by the Iso-sieve process. The composition of the material is listed in Appendix D, however, the important facet is that only C_{12} to C_{15} linear alkanes were included in the mixture. Because of the regular behavior of the properties of normal alkanes of this length with carbon number, the physical properties could all be predicted quite accurately. Another advantage of the n-alkanes was that the envisioned mass transfer experiments could be carried out by evaporating lighter n-alkanes from the Tridecane. Having both of the liquids from a single homologous series should result in more predictable behavior of the variation of physical properties with respect to liquid concentration.

A. Theoretical Background

As was pointed out earlier, the most profitable starting point for the solution of either heat or mass transfer problems in laminar flow is the equation of convective diffusion of either heat or mass. Since these problems (i.e. heat or mass transfer) have the same basic form, the remarks which follow, although written in heat transfer terminology, apply equally well to the low flux, low concentration level mass transfer situation. In vector notation the equation for heat transfer to a moving fluid is given by

$$\rho C_p \frac{DT}{Dt} = k\nabla^2 T \quad . \tag{4-1}$$

This form of the equation implies the assumption of constant properties (ρ, C_p, k), an incompressible fluid, and negligible viscous dissipation of fluid bulk motion to thermal energy. It should be noted that Eq. (4-1) can be written for both the liquid and gaseous phases when the resistance to transfer does not reside entirely in one phase. When this is the case the two equations must be solved simultaneously, resulting in a more complicated problem than the solution for a single phase.

A number of important solutions of Eq. (4-1) have been carried out, corresponding to several different physical problems. These solutions will be outlined below in order of increasing physical and mathematical complexity.

1. The Leveque Solution

The problem solved by Leveque[43] was for the case of heat transfer from a solid boundary into an adjacent fluid stream. He postulated that in a region near the wall, the velocity profile could be approximated by the linear form

$$u = ay \quad . \tag{4-2}$$

If the fluid is assumed to be semi-infinite in extent, and the following transformations are carried out,

$$\Phi = \frac{T-T_o}{T_{in}-T_o} \quad , \quad \eta = y/L \quad , \quad \text{and} \quad \lambda = \alpha x/aL^3 \quad , \tag{4-3}$$

then Eq. (4-1) reduces to a form which can be solved as an ordinary differential equation by first introducing the variable

$$\xi = \eta/(9\lambda)^{1/3} \quad , \tag{4-4}$$

and then integrating subject to the boundary conditions:

$$\Phi = 1.0 \quad \text{at} \quad \xi = \infty \quad \text{and} \quad \Phi = 0 \quad \text{at} \quad \xi = 0 \quad . \tag{4-5}$$

The final solution can then be expressed as

$$\Phi = \frac{3}{\Gamma(1/3)} \int_{\xi}^{\infty} x e^{-x^3} dx \quad . \tag{4-6}$$

The local heat transfer coefficient is given by

$$h = \frac{-k}{T_{in}-T_o} \left(\frac{\partial T}{\partial y}\right)_{y=o} = \frac{k}{0.893} \left[\frac{a}{9\alpha x}\right]^{1/3} \tag{4-7}$$

2. The Graetz Solution

The next problem of interest is that of the heat transfer from a solid boundary to a fluid in laminar flow between two semi-inifinte flat plates. This is a special form of the problem first solved by Graetz,[27] in 1885 for a cylindrical geometry. The solution for flow between two flat plates was carried out by Butler and Plewes.[12] In this problem the velocity profile is now assumed to be parabolic, and is given by the expression

$$u = 6U_m(y/b - (y/b)^2) \tag{4-8}$$

The solution to the convective transport equation can be carried out using the separation of variables technique. The final solution requires the evaluation of eigenvalues and eigenfunctions, and can be expressed in series form as

$$\Phi = -2.1766\, e^{-14.58\, X}(\mathcal{f}_1(Y)) - 1.431\, e^{-141\, X}(\mathcal{f}_2(Y)) + \ldots, \quad (4\text{-}9)$$

where the variables X (a modified form of the Graetz number) and Y are defined by the expressions

$$X = \alpha x/6U_m b^2 \qquad \text{and} \qquad Y = y/b \quad . \qquad (4\text{-}10$$

The values of the eigenfunctions, $\mathcal{f}_1$, $\mathcal{f}_2$, etc., as well as the exponential constants, are tabulated by Butler and Plewes.[12]

3. The Modified Graetz Solution

If we now consider the physical problem depicted in Fig. 9, the solution which results is very similar to that of the Graetz problem, with the additional parameter of interfacial velocity to be considered. The same method of solution that was applied to the Graetz problem could be used to solve the problem at hand; unfortunately, one would have to generate a whole series of eigenfunctions and eigenvalues for each different value of interfacial velocity. An alternate approach is to solve the equation numerically, thus generating Nusselt numbers and heat transfer profiles in a graphical manner.

Byers and King[14] have carried out the above outlined numerical solution; and Fig. 10 represents their results in graphical form. Here the fraction saturation of the gas phase is plotted versus the Graetz number. The third parameter which identifies each member of the family of curves is the ratio of the mean gas velocity to the interfacial velocity, U_m/U_i. The results can be applied to heat transfer calculations by substituting $\Phi_{\text{cup mixing}}$, for the fraction saturation, and replacing D, the molecular diffusivity, with α, the thermal diffusivity. The same computer technique can be used to predict temperature profiles. Examples of these profiles can be found in the paper by Byers and King.[14]

4. The Beek and Bakker Solution

In the same way that the semi-infinite Leveque solution can be used to approximate the solution to the Graetz problem, one can also postulate a semi-infinite model having a finite interfacial velocity and

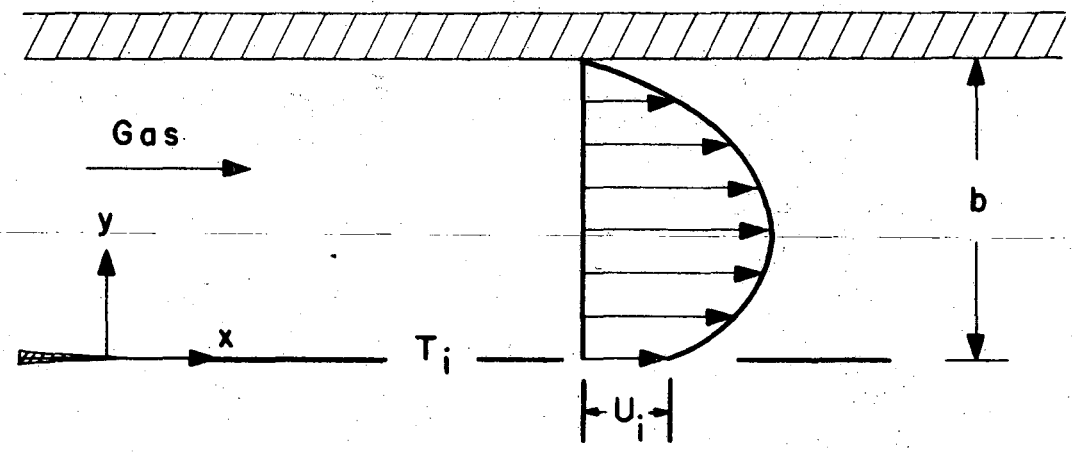

XBL675-3204

Fig. 9. Velocity profile in the gaseous phase used in the Modified Graetz Solution. Liquid interface is located at y = 0.

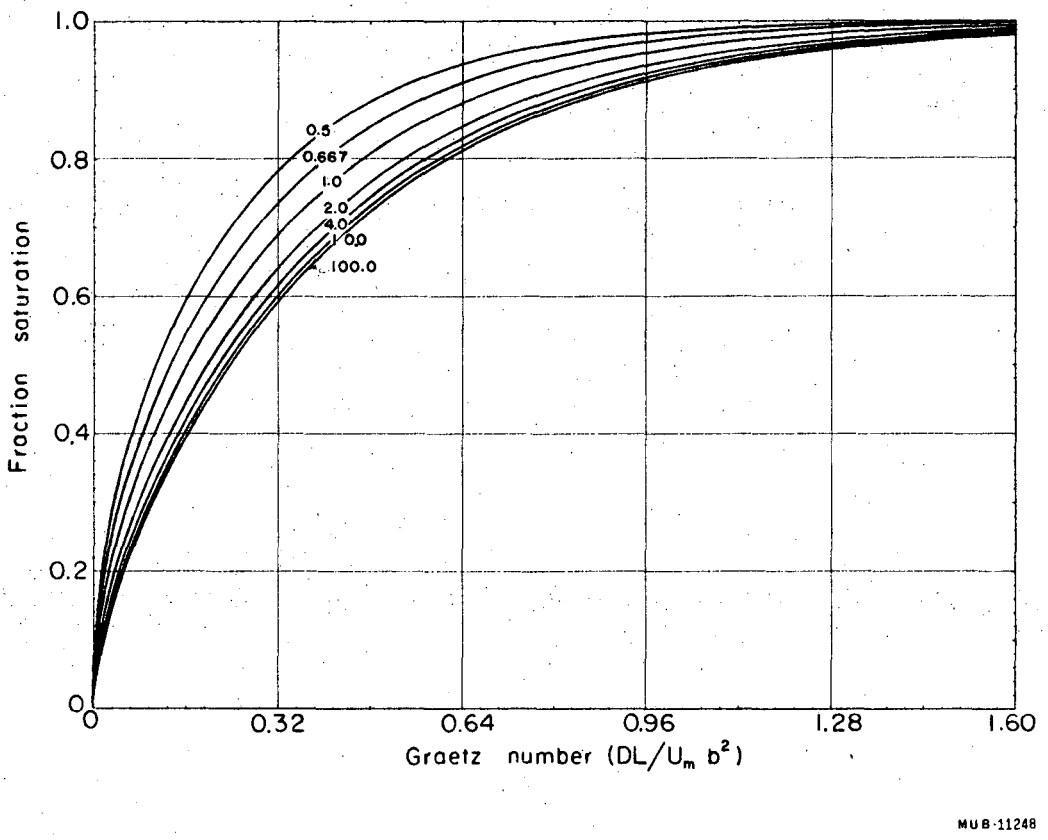

Fig. 10. Mean Fraction Saturation as a Function of the Graetz Number, for various values of the parameter U_m/U_i.

linear velocity slope as an approximation to the modified Graetz problem. Such a solution has been carried out by Beek and Bakker.[6] Unfortunately, their solution is only asymptotically correct for large or small values of the Graetz number. Furthermore, it is awkward to use and somewhat limited since it predicts only transfer coefficients and not temperature profiles. Byers[13,14] has shown that for a mean exit percent saturation of less than 50%, the results of Beek and Bakker agree quite well with his computer approach, provided care is taken in the interpolation of their solution between the two asymptotic curves.

The experimental heat transfer results taken during this work were predicted using a numerical technique (GRAGRA) developed by Byers, which solved the Graetz problem for resistance in both fluid phases. This approach had a very distinct advantage: Since the experimental heat transfer data were taken in profile form, these could be compared directly with the profiles obtained from the computer solution. After several runs, it became apparent that for the flow rates used in this study the major portion of the heat transfer resistance resided in the gaseous phase. The phase resistance was commonly 98.5 to 99.5 percent of the total heat transfer resistance. Thus, when the desired heat transfer results were in the form of fraction saturation, interpolation from Fig. 10 could be utilized without any appreciable loss in accuracy.

B. Experimental Results

A total of 16 experimental heat transfer runs were carried out, using tridecane as the liquid phase and both helium and air as the gaseous phases. In all cases the runs were made by transferring heat from a warm gas to a cooler liquid stream. This was done to prevent initiation of natural convection in the gas phase, which would occur if the gas phase were being heated rather than cooled from below. Both inlet and exit profiles were taken for each experimental run condition. The inlet profiles were used to establish the inlet temperature driving force $(T_L - T_G)$ from the bulk liquid and gas temperatures entering the test section. Since the liquid did not undergo any appreciable temperature change, the

interfacial temperature was nearly equal to the bulk liquid temperature for all of these runs. The inlet temperatures were first established; then the exit profiles were taken and calculated on a dimensionless basis of

$$\Phi = \frac{T-T_G}{T_L-T_G} \quad , \qquad Y = y/2b \qquad (4\text{-}11)$$

where y = distance from bottom of the channel.

Figures 11 and 12 show the experimentally obtained points for the two extreme values of exposure time (Graetz No. = 0.075 and Graetz No. = 0.590). Figure 11 shows the results using air at a very high flow rate (N_{Re} = 1200); whereas the results shown in Fig. 12, are for the helium system at a relatively low flow rate, (N_{Re} = 155). The results of several other profile runs at intermediate Graetz numbers can be found in Appendix B. Also shown on each of the figures is the theoretically predicted profile for the given run conditions. The overall agreement of these profiles was excellent; however, the results did tend to scatter somewhat in the neighborhood of the exterior boundary (Y = 1). This was primarily due to the difficulty in establishing a truly adiabatic boundary. As long as the gas temperature immediately adjacent to the channel wall was not a strong function of distance downstream, the Nichrome heating wire was effective. When the run conditions resulted in a large degree of gas phase equilibration the exterior boundary temperature was not constant, and the desired adiabatic boundary condition could not be achieved closely.

A second source of experimental error resulted from the tendency of the liquid to "bridge" to the thermocouple-probe when the tip was close to the liquid interface. This frequently occured at the Y = 0.525 point, and generally was quite obvious in the resultant profile when it occurred. Examples of this can be seen in the results from Runs 20 and 25, shown in the Appendix.

After the experimental profile had been obtained, a curve was drawn through the points. Values of ϕ were then taken for every 0.025 in. (a total of 21 points) and used as input data for the program TOHETR (see Appendix D). The experimental profile was integrated by a numerical

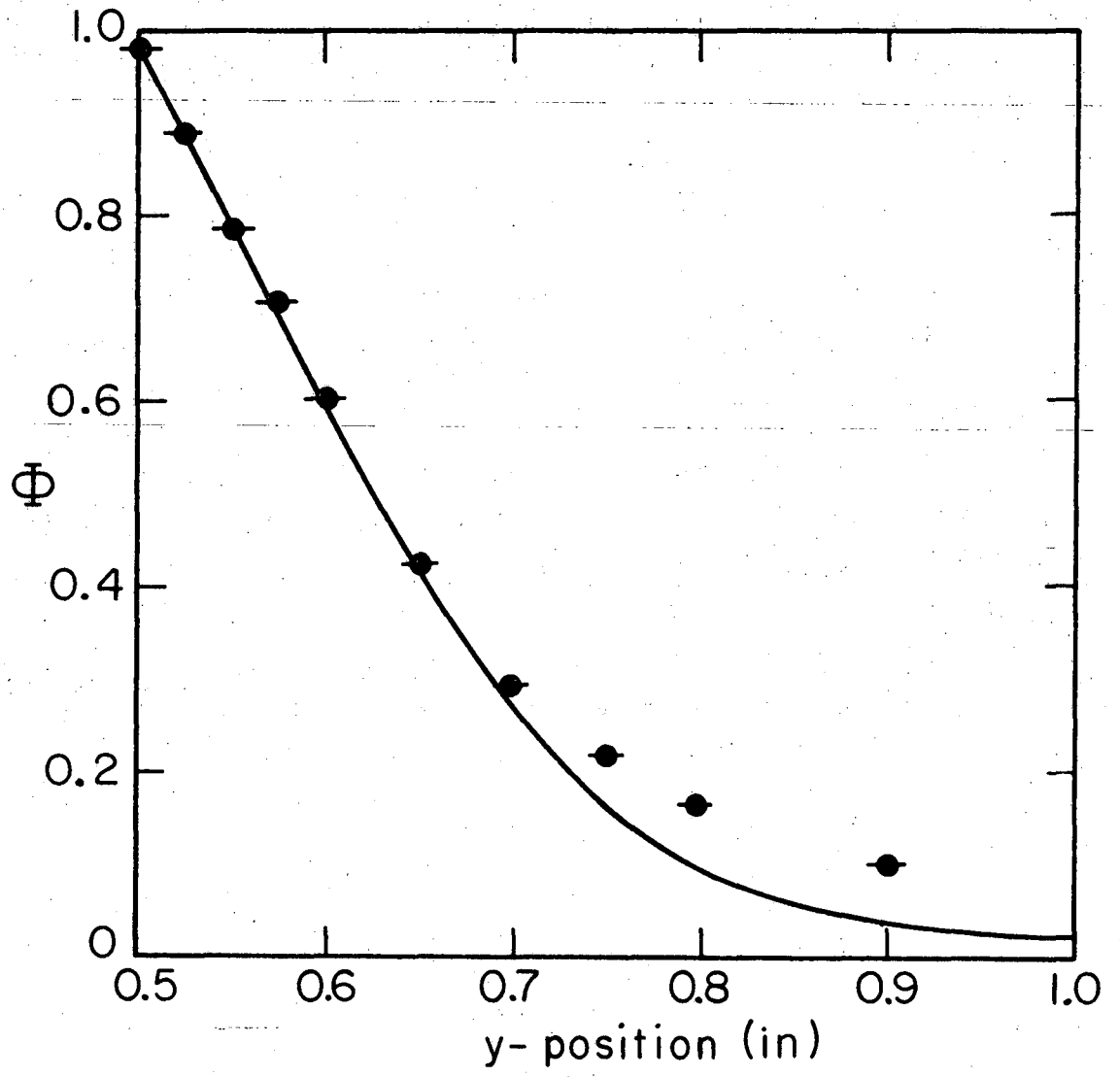

XBL675-3208

Fig. 11. Dimensionless experimental temperature profile taken at 17.5 in. from the test section inlet; QG = 690 cm^3/sec, QL = 0.810 gpm.
Run # 15, System: air/tridecane
● = experimental data
— = theoretically predicted curve

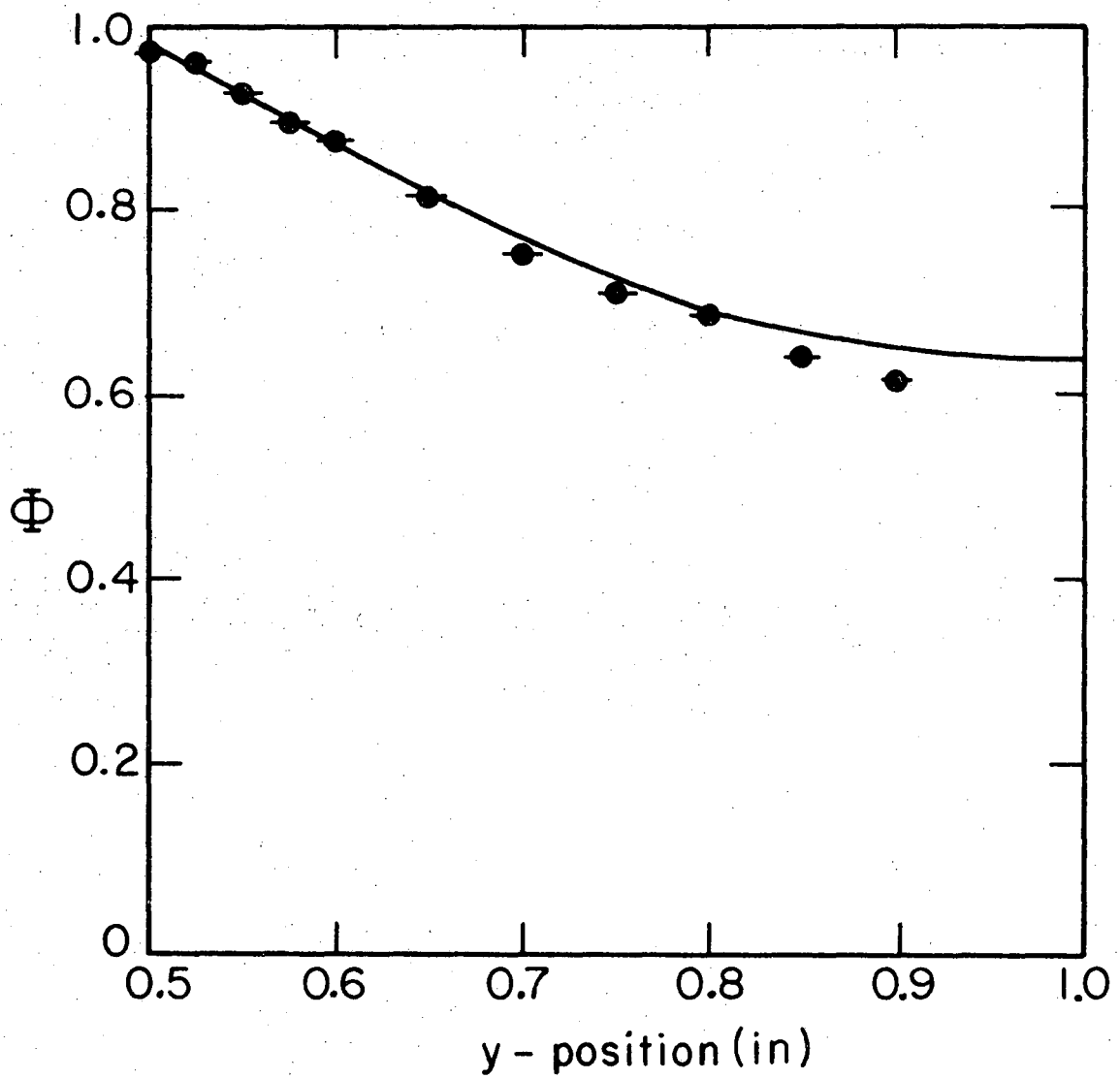

XBL675-3209

Fig. 12. Dimensionless experimental temperature profile taken at 17.5 in. from the test section inlet; QG = 780 cm^3/sec, QL = 0.360 gpm.
Run # 23, System: helium/tridecane
● = experimental data
— = theoretically predicted curve

technique to yield a cup mixing temperature, or, on a dimensionless basis, a fraction saturation. Table I gives a comparison of these experimentally obtained values with the theoretically predicted values obtained from the GRINT program.[13] Again the agreement was quite good; with the average error less than 3% and the maximum error less than 12%.

Table I. Gas-liquid heat transfer results

Run No.	U_m/U_i	Graetz No.	Fs (Theory)	Fs (Experimental)	% deviation
14	15.7	0.075	0.247	0.231	- 6.5
15	7.83	0.075	0.253	0.287	+11.8
16	12.8	0.105	0.306	0.345	+11.3
17	5.56	0.105	0.316	0.351	+11.1
18	7.63	0.105	0.311	0.346	+11.3
19	5.05	0.173	0.429	0.446	+ 3.8
20	3.42	0.175	0.442	0.442	0.0
21	1.89	0.310	0.629	0.564	-10.3
22	8.55	0.282	0.556	0.524	- 5.8
23	19.8	0.590	0.766	0.733	- 4.3
24	37.6	0.306	0.570	0.636	+11.6
25	39.0	0.326	0.587	0.585	- 0.3
				Average % error	+ 2.8

V. THE EVAPORATION OF PURE LIQUIDS

The rate of evaporation of a pure liquid into an adjacent flowing gas stream can usually be predicted by the solution of a simplified form of Eq. (4-1), the equation of convective diffusion. If the vapor pressure of the fluid in question is sufficiently high, the assumptions of low concentration level and low mass flux, which were outlined briefly in Sec. I, are no longer valid, and one must take these effects into account in the calculation of the mass transfer coefficient. In order to demonstrate how the concentration level and mass flux level influence the calculation of mass transfer rates, we shall briefly consider each of the above factors.

Effect of Concentration Level upon Mass Transfer

In order to show the effect of concentration level upon the interfacial mass transfer coefficient conveniently, let us first examine two forms of Fick's first law:

$$J_A^* = -cD_{AB}\nabla x_A \tag{5-1}$$

$$J_A^o = -(D_{AB}/\tilde{V}_A)\nabla \phi_A \tag{5-2}$$

The value of D_{AB} in the above two equations is the same, even if there are gradients in temperature and pressure, as long as $\tilde{V}_A$ remains constant and the substance to which Eq. (5-2) is applied is incompressible and has a zero coefficient of expansion.[34]

Since the solution to most mass transfer problems requires the integration of a Fick's law expression similar to those given above, it is convenient to use (5-1) for situations where the group cD_{AB} does not vary throughout the fluid. This is found to be true for most gases at moderate pressures as long as long as the temperature does not vary greatly; therefore Eq. (5-1) is the simplest form of Fick's law to use under these conditions. In a similar manner, the group $D_{AB}/\tilde{V}_A$ is generally found to be more nearly constant for most liquid solutions; therefore the application of (5-2) is found to be advantageous, again due to the greater ease of integration of the differential equation.

Both J_A° and J_A^{*} are molar diffusion fluxes that are taken with respect to the fluid itself; in order to obtain a flux relative to stationary coordinates, if we limit ourselves to binary systems, we may use the following equations:

$$N_A - x_A(N_A + N_B) = -c\, D_{AB} \nabla x_A \qquad (5\text{-}3)$$

$$N_A - \phi_A(N_A + N_B \tilde{V}_B/\tilde{V}_A) = -(D_{AB}/\tilde{V}_A) \nabla \phi_A \qquad (5\text{-}4)$$

Let us now consider Eq. (5-3), which is applicable to most binary gas mixtures at low pressure. If the value of $(N_A + N_B)$ is not equal to zero, then it is obvious from this equation that the value of the molar flux of component A relative to a stationary coordinate (i.e. N_A) is dependent upon the concentration level of that component (x_A) as well as Δx_A. If Eq. (5-3) is written at the gas-liquid interface, then the interfacial flux of A is concentration dependent; this is what is meant by the "concentration level effect". Since the value of x_A is always less than 1.0, we see that an increase in concentration level of the transferred species will usually result in an increase in total flux, provided $(N_A + N_B)$ is of the same sign as N_A.

Effect of Flux Level upon Mass Transfer

Whereas the effect of concentration level can be demonstrated by considering the magnitude of certain terms in the Fick's law expression, the effect of high flux upon the mass transfer rate enters in a more subtle manner. Usually the solution of the convective diffusion equation is carried out by first achieving a solution for the velocity profiles within the system, then substituting these into the appropriate places in the equation of convective diffusion; i.e., the flow equations and the mass transfer equations are solved independently. However, if the mass flux becomes sufficiently high, these equations can no longer be "de-coupled", since a flux of mass also represents a physical flow of material and hence a velocity.

Thus a "high flux mass transfer solution" represents the solution to a physical problem where the mass flux of material has been considered as an additional velocity term, comparable in magnitude to the velocities present in the absence of mass transfer. This type of solution yields a different concentration profile shape from the low flux solution; whereas the shape of the concentration profile is not altered by the concentration level effect, discussed earlier.

In order to differentiate between the low and high flux solutions, it is convenient to make the following definitions. First, let us define the local mass transfer coefficient, $k'_{x,loc}$, as done by Bird et al.,[11]

$$k'_{x,loc} = \frac{N_{Ao} - x_{Ao}(N_{Ao} + N_{Bo})}{x_{Ao} - x_{A\infty}} \tag{5-5}$$

With the preceding general definition in hand, we can now define the mass transfer coefficient for the limit of low mass flux as:

$$\left[\lim_{(N_{Ao} + N_{Bo}) \to 0} k'_{x,loc}\right] = k_{x,loc} \tag{5-6}$$

Since most of the existing mass transfer correlations are based on the assumption of low flux conditions, it is much more convenient to predict the high flux performance by applying a numerical correction factor to the low flux results. In order to accomplish the above, the following dimensionless variables are useful,

$$R_{AB} = \frac{N_{Ao}+N_{Bo}}{k'_{x,loc}} = \frac{x_{Ao} - x_{A\infty}}{\frac{N_{Ao}}{N_{Ao}+N_{Bo}} - x_{Ao}} \tag{5-7}$$

$$\phi_{AB} = \frac{N_{Ao}+N_{Bo}}{k_{x,loc}} \tag{5-8}$$

$$\theta_{AB} = k'_{x,loc}/k_{x,loc} \tag{5-9}$$

Both R_{AB} and ϕ_{AB} are convenient dimensionless expressions for the absolute value of the interfacial mass flux rate. θ_{AB} is the correction factor, which, when applied to the existing low flux expression for the mass transfer coefficient, yields the "high flux rate" transfer coefficient. Thus if one is able to obtain a solution to the high flux problem for a given flow situation, the results can be presented graphically in terms of any two of the above variables. This has been done for several flow geometries, and will be discussed later. The graphical results can be found in Figs. 21.7-2 and 21.7-3 in the text by Bird, Stewart and Lightfoot.[11]

Another complication that frequently arises at high flux levels is the variation of the important physical properties, since these are frequently strong functions of concentration. However, this is not a necessary consequence of increased flux level, and therefore can be considered separately.

A final result of the high flux effect in an evaporation experiment is the variation of temperature due to the large heat flux created by the enthalpy of vaporization. This effect will be ignored for the present and the system will be assumed to be isothermal. A detailed treatment of the temperature gradient effect is given in Sec. 5-D.

A. Prior Theoretical Work

1. Concentration Level Effect

It has already been shown that the effect of concentration level upon the mass transfer rate can be predicted by selecting the appropriate form of Fick's law to be applied at the interface (see Eqs. 5-3 and 5-4). King[34] has shown that the inclusion of a single concentration-dependent term of the form $(1 - z_{Ao}(1+S))$ in the Sherwood group yields a satisfactory correlation for the mass transfer coefficient of component A in a binary mixture. He also points out that the form of Fick's law which is used should be based upon the best physical representation for the system (i.e. for gases use a mole fraction dependent form; for liquids a volume fraction dependent form is more appropriate). Olander[58]

had previously presented the above concentration level effect for mass fraction driving forces, and had shown that the effect can be important at high concentration levels. Vivian and Behrmann[82] used the equivalent of Eq. (5-3) to explain the concentration dependence of the molar solute flux in a binary gaseous system. Several other works, such as those by Shulman and Delaney,[67] and Westkaemper and White[84] have discussed the combined effect of solute concentration level and high flux level by applying the "P_{BM}" correction factor, which is obtained by carrying out a solution to the high-flux, film-theory problem with $N_{B_o} = 0$.

It should be noted that when the mass transfer coefficients are defined as in Eqs. (5-5) and (5-6), the concentration level effect is included; i.e., the value of $k'_{x,loc}$ is not a function of concentration level and varies only with changes in the value of $(\partial x_A/\partial y)/\Delta x_A$. An equation similar to (5-5) can be written for other forms of Fick's law (such as Eq. (5-2).) This will be covered in Chapter VI, which deals with interphase transfer problems.

2. High Flux Level Effect

The calculation of the effect of high flux level upon the mass transfer coefficient for a given system cannot be generalized in the manner used for the concentration level, since the high flux solution is dependent on the assumed fluid flow situation. In order to illustrate the form taken by the high flux level solutions, let us consider the three important flow geometries for which such a solution exists.

a. Film theory. This approach postulates that there is a film of stagnant fluid with a finite thickness, δ, immediately adjacent to the steady state mass-transfer interface. The solution to this problem has been obtained by several independent investigators (Lewis and Chang,[44] 1928; Ackermann,[1] 1937; and Colburn and Drew,[20] 1937), and a detailed development can be found on pages 658-668, Bird et al.[11] The results of the high flux approach can be given in the form,

$$1 + \frac{(x_{Ao}-x_A)(N_{Ao}+N_{Bo})}{N_{Ao}-x_{Ao}(N_{Ao}+N_{Bo})} = \exp(N_{Ao}+N_{Bo})\,\frac{\delta}{cD_{AB}} \quad . \qquad (5\text{-}10)$$

If one makes the simplifing assumption of $(N_{Ao} + N_{Bo})$ approaching zero (low rate), then the more familiar form of the film solution results, i.e.

$$\frac{1}{k_{x,loc}} = \frac{\delta}{cD_{AB}} \quad . \tag{5-11}$$

If the interfacial flux of the inert component, B, is set equal to zero, Eq. (5-5) can be simplified to the form,

$$k'_{x,loc} = \frac{N_{Ao}(1-x_{Ao})}{x_{Ao}-x_{A\infty}} \tag{5-12}$$

If we now set $N_{Bo} = 0$ in Eqs. (5-7) and (5-10) and then combine these equations with (5-11), we see that, since $x_A = 1 - x_B$,

$$\frac{k'_{x,loc}}{k_{x,loc}} = \theta_{AB} = \frac{\ln(x_{B\infty}/x_{Bo})}{x_{B\infty}-x_{Bo}} \cdot (1-x_{Ao}) \tag{5-13}$$

In a large number of investigations the low flux mass transfer coefficient is defined as simply $k_G = N_{Ao}/(P_{Ao}-P_{A\infty})$, rather than as defined in this work (where the concentration level effect is taken into account). If this very simple definition of the mass transfer coefficient is used then at one atmosphere total pressure, we see that the total correction factor (for both flux level and concentration level) is given by $1/x_{Bm}$, where x_{Bm} is the log mean mole fraction of the inert component between the interface and the bulk fluid stream. This is the P_{BM} correction factor which was referred to earlier. This method of simultaneously correcting for both the high flux rate and high concentration level has been applied to turbulent mass transfer situations by several investigators with reasonable success[20,82] (see Sec. 5-B).

b. Penetration theory. This approach is characterized by the assumption of a velocity profile, u_x = constant (i.e. bulk flow), and steady state transfer; alternatively, the same equation can be reached by considering unsteady state transfer into a stagnant phase. Once again a generalized solution of the convective transport equation can be reached, although the mathematics become somewhat more complicated than for the

Film Model. The final solution for the mass-transfer rate, first obtained by J. H. Arnold[4] (see pages 594-598, and 668-672, Bird et al. for details), is given in implicit form by:

$$\frac{X_{Ao}-X_{A\infty}}{\frac{N_{Ao}}{N_{Ao}+N_{Bo}}-X_{Ao}} = \sqrt{\pi}\,(1+\operatorname{erf}\psi)\exp\psi^2 \qquad (5\text{-}14)$$

where ψ, is a dimensionless mass transfer rate given by the equation:

$$\psi = \frac{N_{Ao}+N_{Bo}}{c}\sqrt{\frac{t}{D_{AB}}} \qquad (5\text{-}15)$$

Had the limiting assumption of low mass transfer rates been made, the solution would take the much simpler, and more familiar form:

$$k_{x,loc} = c\sqrt{\frac{D_{AB}}{\pi t}} \qquad (5\text{-}16)$$

c. Laminar boundary layer theory. A number of investigators have published solutions for the high flux laminar boundary layer equations. The books by Hartnett and Eckert[28] and Schlichting[67] both give extensive details in the method of solution of these equations. In addition publications by Acrivos,[2] Sparrow,[71] Olander,[58] and Dickson[64] have given solutions to the high flux laminar boundary layer equations for a wide variety of initial and boundary conditions. A detailed account of the basic theoretical approach to the problem of mass transfer into laminar boundary layer flow is given by Bird et al.[11] (pages 608-619); therefore only an outline of the solution will be presented here.

If we assume that, in a binary mixture of components A and B which have equal molecular weights, the following physical properties are constant: k, c, D_{AB}, C_p, μ, and ρ; then the boundary layer equations for this system become

$$\text{(continuity)} \qquad \frac{\partial u_x}{\partial x} + \frac{\partial v_y}{\partial y} = 0 \qquad (5\text{-}17)$$

(motion) $$u_x \frac{\partial u_x}{\partial x} + v_y \frac{\partial u_x}{\partial y} = \nu \frac{\partial^2 u_x}{\partial y^2} \qquad (5\text{-}18)$$

(convective transport) $$u_x \frac{\partial x_A}{\partial x} + v_y \frac{\partial x_A}{\partial y} = D_{AB} \frac{\partial^2 x_A}{\partial y^2} \qquad (5\text{-}19)$$

If the gas (B) is not soluble in the liquid phase, then the boundary conditions can be given as below:

at $y = \infty$: $u_x = u_\infty$, $x_A = x_{A\infty}$

at $y = o$: $u_x = o$, $x_A = x_{Ao}$, $N_B = o$

Following the development given by Bird et al.,[11] the equation of continuity may be integrated to yield:

$$v_y = v_{yo} - \int_o^y \frac{\partial u_x}{\partial x}\, dy \qquad (5\text{-}20)$$

By utilizing Eq. (5-3), an alternate form for the above equation may be obtained,

$$v_y = - \frac{M_A}{\rho} \left[\frac{c\, D_{AB}}{(1-x_{Ao})}\right] \frac{\partial x_A}{\partial y}\Big|_{y=o} - \int_o^y \frac{\partial u_x}{\partial x}\, dy \qquad (5\text{-}21)$$

In the above expression for v_y, we see that the value of the fluid velocity in the y-direction is a function of the interfacial mass flux, as well as the position variables x and y. This is the way in which the aforementioned linkage of the fluid dynamics and convective transport equations takes place; i.e. the fluid velocity is dependent upon the mass transfer solution at the interface. Also, the solution of the convective transport Eq. (5-19) requires an expression for v_y, which is obtained by using Eq. (5-21). After making the substitution for v_y in (5-19) it is found that, if the interfacial mass flux (which was substituted for v_{yo}) varies as $x^{-1/2}$, then a similarity transformation may be used to convert Eq. (5-19) into an ordinary differential equation. Since the low flux solution yields an $x^{-1/2}$ dependence for the interfacial flux, we see that the high flux correction will change the absolute value of the mass

transfer rate, but will not alter its x-direction dependence. Also, we see that in this solution $u_x = fn(N_{Ao} + N_{Bo})$, because of the connection of u_x and v_y through the equation of continuity.

The ordinary differential equation which results from the similarity transformation of the equation of convective diffusion is non-linear, and requires a rather complex numerical technique for its solution. The results, which have been tabulated on page 614 in Bird et al.,[11] can best be seen in graphical form by making use of the dimensionless variables θ_{AB} and R_{AB} defined in Eqs. (5-7) and (5-9). In this way the correction factor for high flux, θ_{AB}, is given as a function of the dimensionless mass flux, R_{AB}. The results are shown in Fig. 13 for two values of the Schmidt number. In addition the results for the two previously discussed models, film and penetration, are also presented. As can be seen in Fig. 13, although the three models do yield slightly different results, the differences are small except at extremely high values of the interfacial flux. Thus for moderate values of interfacial flux any of the models might be expected to yield a fairly accurate answer for the correction factor, θ_{AB}.

Note that for all the models transfer into a given phase results in a reduction in the transfer coefficient (θ_{AB} less than 1.0); whereas transfer out of a phase increases the transfer coefficient. A rough physical explanation for this is that the existance of a convective or "blowing" velocity into the phase tends to shift the concentration profile slightly away from the interface. This shifting of the profile into the phase results in a decrease in the value of $\partial x_A/\partial y\big|_{y=o}$, i.e., a lower value of the diffusive flux at the interface. A similar arguement can be given for the reverse case of transfer out of a given phase (or an interfacial "suction" velocity) which will tend to increase the diffusive flux.

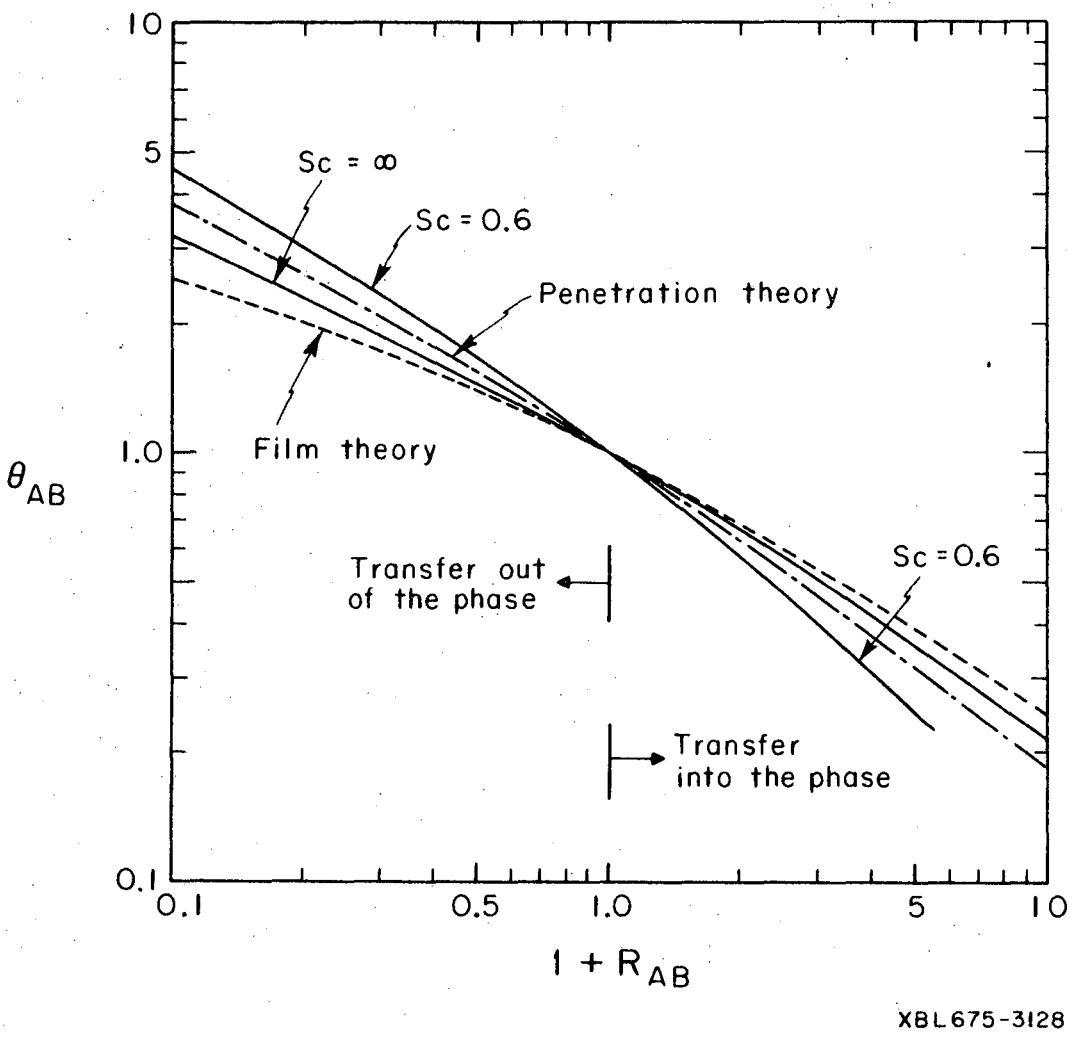

Fig. 13. Flux level correction factor for existing high flux solutions, plotted as a function of dimensionless flux ratio. Solid lines indicate the results for laminar boundary layer theory.

B. Prior Experimental Work

The high flux film theory approach has been experimentally studied by numerous investigators. Colburn and Drew[20] used this theory to develop the P_{BM} concept, then applied their results to an experimental study involving the evaporation of water into a turbulent air stream. Their results agreed fairly well with the theoretical prediction; however, a later study of the same system using a wetted-wall column was carried out by Cairns and Roper,[16] who found k_g to vary as the 0.83 power of P_{BM}. Westkaemper and White[84] attempted to study the combined effects of concentration level and high flux by using the P_{BM} concept to predict the rate of evaporation of carbon tetrachloride into a turbulent air stream; however, their results were inconclusive. Shulman and Delaney[69] also vaporized carbon tetrachloride into air; using a packed column for contacting equipment these authors found a two-thirds power dependence of k_g upon P_{BM}.

A critical review of all of these earlier works has been published by Vivian and Behrman.[82] They concluded that, due to a variety of experimental difficulties, none of the aforementioned data are incompatible with the use of P_{BM} to predict the combined effect of high flux and concentration level. Their experimental program, which consisted of evaporation of pure liquids into a turbulent gas stream within a short wetted-wall column, gave a tentative confirmation of the P_{BM} prediction. Unfortunately their experimental results were difficult to analyze due to a significantly large hydrodynamic entry region.

Several investigators have worked on the experimental confirmation of the laminar boundary layer approach for the region of high interfacial mass transfer rates. Emanuel and Olander[22] confirmed the approach for the physical problem of a rotating soluble disc in a surrounding liquid. Their data gave excellent agreement with theory for the system KBr into water, for values of mass fraction driving force up to 0.404. A study of the sucrose-water system was carried out with a mass fraction driving force of 0.679; however, the agreement for this system was not as good because of large variations of liquid phase viscosity with concentration.

Mendelson and Yerazunis[52] studied the high mass transfer rate effect on the evaporation of a liquid from the stagnation point of a cylinder. They obtained good agreement with the laminar boundary layer equations for the system carbon tetrachloride into air, with mass fraction driving forces up to 0.73. Their study also included the system water into air; however, this system yielded extremely poor results, which the investigators attributed to interfacial resistance to mass transfer.

Ranz and Dickson[64] have presented data for both a stagnation flow and turbulent boundary layer on a flat plate. They evaporated several different organic systems into a hot air stream; however, the data appeared to have a large degree of scatter and agreement with theory was rather poor. The authors state that within the experimental error and within the errors due to variations of properties the experiments confirmed the predicted effect of interfacial flux rate and concentration level.

C. High Flux Leveque Solution

Since none of the existing high flux rate solutions were directly applicable to the flow geometry utilized in this work, a program was initiated with the final goal of obtaining such a solution. Ideally, this would involve a solution of the Graetz problem for confined flow, with the addition of the high flux and high concentration level conditions. Unfortunately the confined flow problem is quite complex, primarily because of the x-direction acceleration of the fluid. This means that an extra term should be retained in the equation of motion; i.e. the $\partial^2 u_x/\partial x^2$ term, and the u_x and v_y terms are now linked through the continuity equation.

Even if this extra term is ignored, the solution cannot be obtained in the relatively simple manner that was used for the boundary layer approach, since the assumption that v_y is proportional to $x^{-1/2}$ is no longer valid for the Graetz problem. The numerical solution to this problem would require an iterative trial and error solution of three linked partial differential equations (the equation of motion, the equation of continuity, and the equation of convective diffusion for one component.)

This appeared to be a formidable task, even using numerical techniques; therefore an approximate solution was carried out.

Since the Leveque solution (Eq. (4-7)) is known to predict the transfer coefficients for the Graetz problem accurately provided the contact times are short, a solution which gives the effect of high flux rates for the Leveque approach should be a reasonable approximation to the problem at hand. Figure 14 illustrates the physical problem to be solved. The assumptions which were necessary in the course of the solution are the following:

1) The high flux rate correction will affect the magnitude of the mass transfer coefficient, but not its x-direction functionality. Thus, v_{yo}, which is proportional to N_{Ao} (since $N_{Bo} = 0$), is given by the expression,

$$v_{yo} = C_2(x)^{-1/3} \tag{5-22}$$

2) The velocity in the x-direction, u_x, is given by $u_x = C_1 y$ and is not altered by the high flux contribution.

3) The inlet concentration of the volatile species, A, is equal to zero. (Note that Bird et al.[11] have shown that the assumptions of $x_{A\infty} = 0$ and $N_{Bo} = 0$, which are made here primarily for convenience, are not necessary and the more general problem which does not involve these assumptions can be solved with suitable definitions of θ_{AB}, R_{AB} and a dimensionless concentration.)

4) The interfacial concentration of component A is given by equilibrium considerations as a constant, C_{Ao}.

Under the above assumptions, the equation for which we shall seek a solution is

$$C_1 y\left(\frac{\partial x_A}{\partial x}\right) + C_2 x^{-1/3}\left(\frac{\partial x_A}{\partial y}\right) = D_{AB}\left(\frac{\partial^2 x_A}{\partial y^2}\right) \tag{5-23}$$

The concentrations are given in mole fraction in (5-23) rather than as absolute concentration for mathematical convenience. If one now defines the following variables,

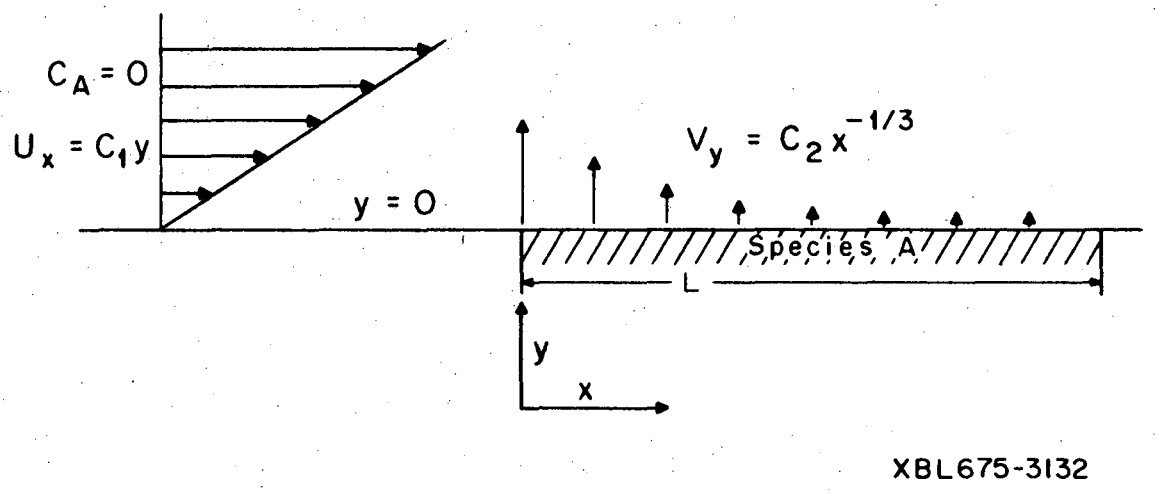

Fig. 14. Hydrodynamics for the high flux Leveque solution.

$$\theta_A = x_A/x_{Ao}\ ,\quad X = x/L\ ,\quad Y = y/L\ ,\quad K_1 = L^{-4/3}C_2/C_1\ ,\quad \text{and}$$
$$K_2 = D_{AB}/C_1L^2\ ; \tag{5-24}$$

then Eq. (5-23) is given in dimensionless form as

$$Y\left(\frac{\partial\theta_A}{\partial X}\right) + K_1X^{-1/3}\left(\frac{\partial\theta_A}{\partial Y}\right) = K_2\left(\frac{\partial^2\theta_A}{\partial Y^2}\right)\ . \tag{5-25}$$

The appropriate boundary conditions for (5-25) in dimensionless form are

$$\begin{aligned} &1.\ \text{at}\quad X = 0,\ \theta_A = 0\ \text{for}\ Y > 0 \\ &2.\ \text{at}\quad Y = 0,\ \theta_A = 1\ \text{for}\ X \geq 0 \\ &3.\ \text{at}\quad Y = \infty,\ \theta_A = 0\ \text{for}\ X \geq 0 \end{aligned} \tag{5-26}$$

It should be noted at this point that the solution to the above problem is dependent on the variable C_2, which is in turn dependent on the absolute value of the mass flux at the interface; i.e.

$$C_2 = \text{fn}\left(x_{Ao},\ \frac{\partial x_A}{\partial Y}\Big|_{Y=0}\right)\ . \tag{5-27}$$

The overall problem was solved by first assuming a fourth degree polynomial dependence of C_2 upon x_{Ao}. Using this assumption, combined with a low flux solution value of $\partial x_A/\partial y$, the solution of (5-25) was carried out to yield the interfacial flux at various value of x_{Ao}. These results were then compared with the assumed polynomial equation. If they differed by more than 1%, a new polynomial was written for C_2 based upon the results of the preceeding calculations and the procedure was carried out again until an accurate agreement was obtained.

Since an analytical solution could not be achieved for Eq. (5-25), a numerical technique was adopted. The equation was first put into an appropriate difference form, and then solved using the Crank-Nicholson six-point implicit formula.[42] This approach yields a tri-diagonal matrix for the coefficients of the concentration vector. This system of equations

can be solved utilizing the method due to Thomas[42]; to give the concentration vector for each step down the channel in the x-direction. The computer program (LEVHIF) which carried out the above calculations is given in Appendix C, along with a brief description of its operation. The results of the Leveque high flux rate solution are presented in Fig. 15. Here θ_{AB}, the high flux correction factor described in Eq. (5-19), is shown plotted versus $1 + R_{AB}$ (given by Eq. (5-17)). Also shown for comparison are the curves for the penetration and laminar boundary layer models (Sc = 1.5, which corresponds to N_2 at the experimental conditions), taken from Fig. 21.7-2, Bird et al.[11] As can be seen in Fig. 15, the calculated results lie between the laminar boundary layer and penetration curves, with the penetration results giving a good first approximation to the high flux Leveque solution.

D. Experimental Results

In order to confirm that the alterations in the experimental apparatus (primarily the revised form of the inlet section) had not changed its performance, a short series of low flux mass transfer runs was carried out. These experiments were conducted by vaporizing normal pentane from a liquid mixture of pentane and tridecane into a flowing nitrogen stream. The pentane concentration was held in the neighborhood of 0.01 mole fraction in the liquid phase to rule out any high flux or concentration level effects. Several of these runs were carried out with simultaneous heat transfer by allowing the gas phase to enter at a slightly higher (approximately 10°C) temperature than the liquid phase. Since the liquid phase temperature does not change appreciably under these conditions, the mass transfer results should have been the same as obtained under isothermal conditions.

Another reason for carrying out the above runs was to ascertain the feasibility of obtaining simultaneous heat and mass transfer data. The mass transfer results are presented in Fig. 16, in the form of percent saturation at the interfacial temperature of the exit gas phase versus Graetz number. The solid line is a theoretical curve from the

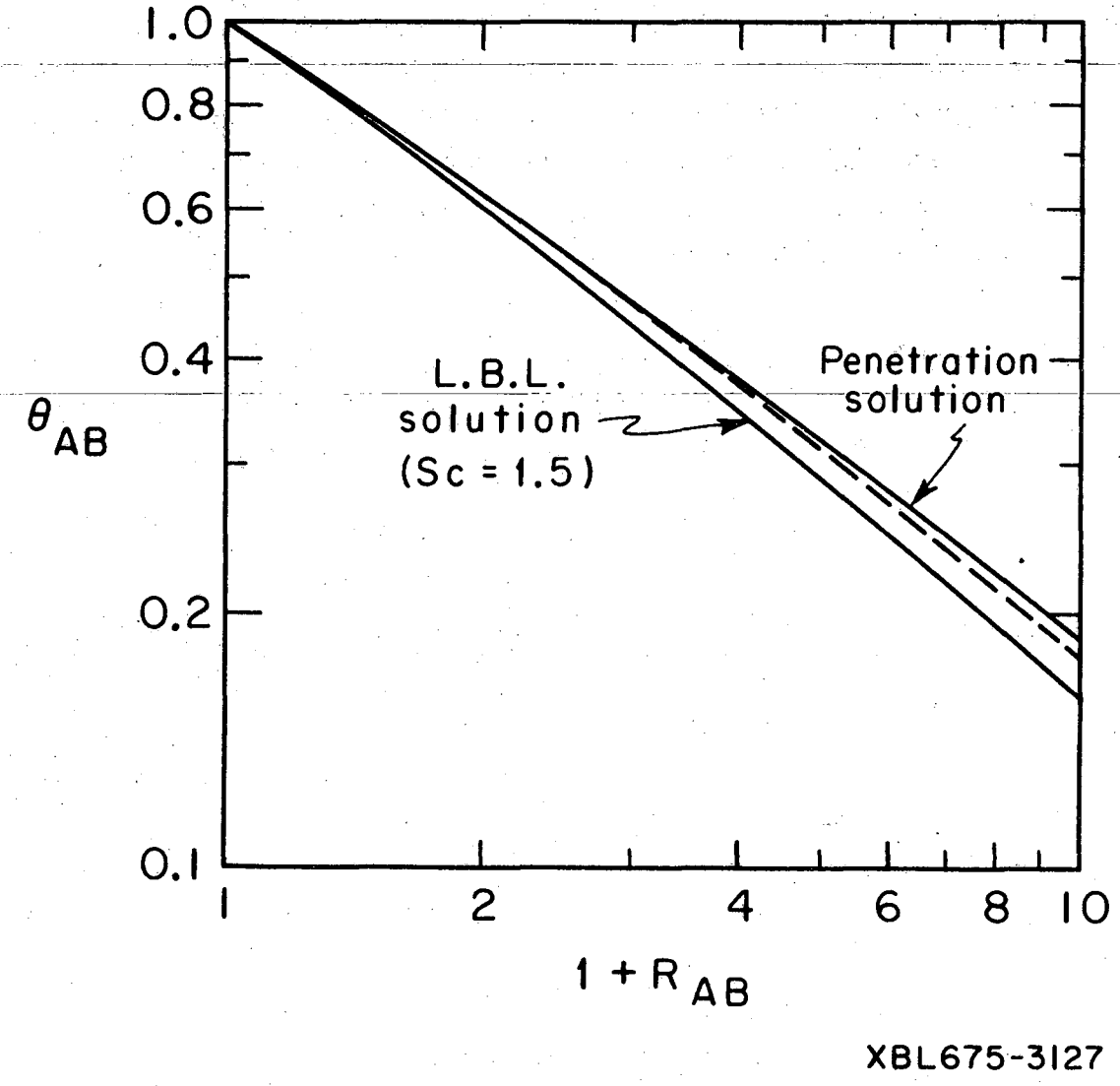

Fig. 15. Results for the high flux Leveque solution (dashed line); also shown are the curves for laminar boundary layer theory (Sc = 1.5) and penetration theory.

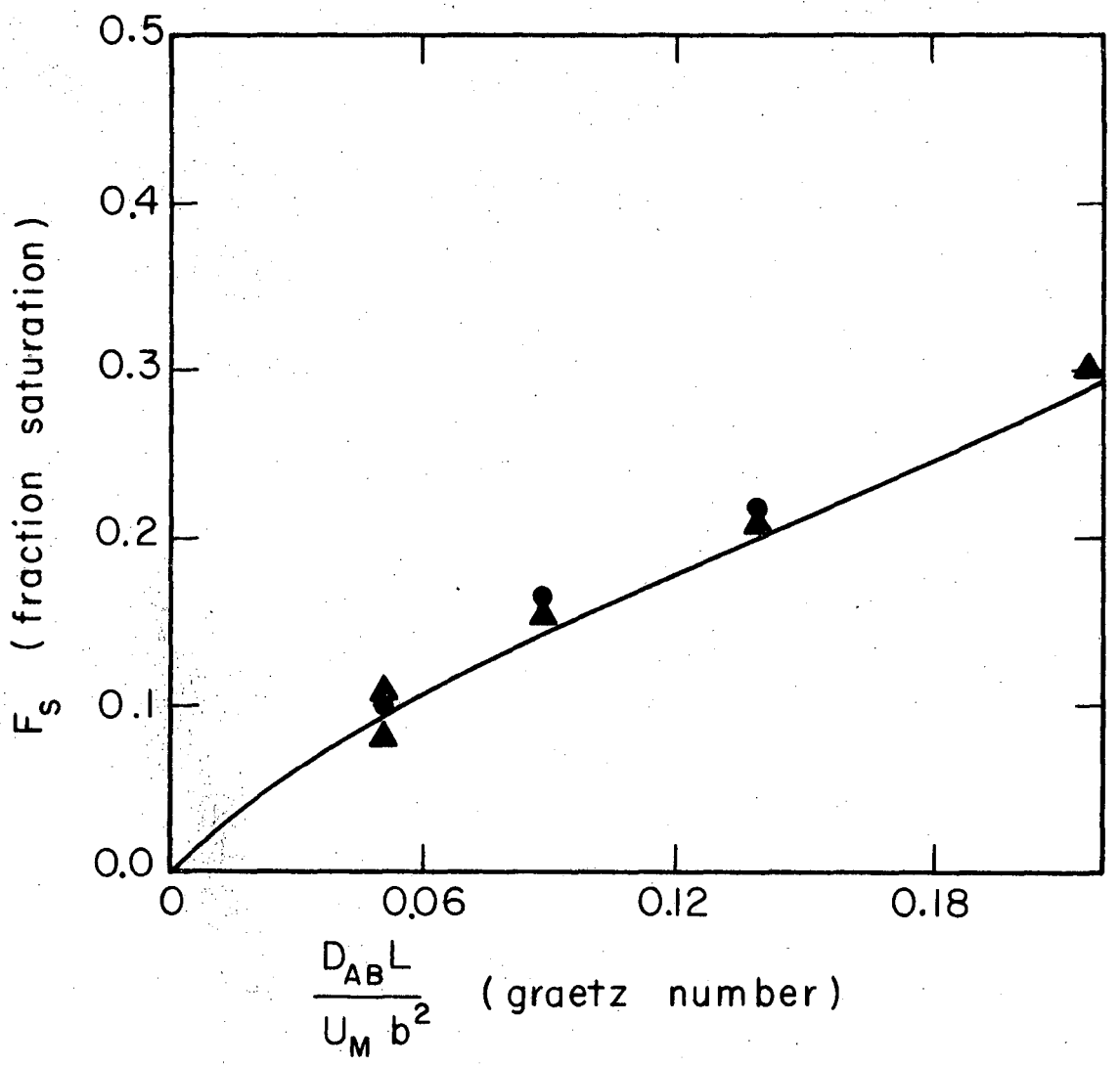

XBL675-3205

Fig. 16. Low Flux Mass Transfer Results. Runs 28-34; System: n-pentane/tridecane in liquid phase, Nitrogen in gas-phase.
● = isothermal system
▲ = gas phase approximately 10°C above liquid phase.

interphase mass transfer solution carried out by Byers. The agreement obtained was very good; indicating that the new inlet section was suitable for gas phase Reynolds numbers up to 1200. (Experimental conditions of all runs can be found in Appendix B).

The Effect of Mass Transfer upon Interfacial Temperature

The high flux mass transfer results were obtained by vaporizing two pure fluids, n-pentane and isopentane into nitrogen. Both of these liquids have boiling points that are only slightly above the run conditions. Consequently the mass flux levels were quite high and the effect of the latent heat of evaporation upon the temperature profiles could no longer be ignored. This effect can be seen in the temperature profiles giving in Fig. 17. The interfacial temperature was decreased by an average value of 1.5° for this run, which consisted of normal pentane being evaporated into nitrogen. This effect can be accurately predicted by assuming that the heat supplied by the gas phase is negligible compared to that supplied by the liquid phase. Thus we only need to consider the liquid phase heat transfer problem, with the interfacial flux given by an arbitrary function of distance. This function is actually dependent upon the overall mass transfer problem, so that the gas phase mass transfer is coupled with the liquid phase heat transfer. A solution for this type of problem has been obtained by Modine, Parrish, and Toor[55] for the case of thin liquid films. In this situation the interfacial heat transfer results in a large decrease in the bulk liquid temperature. Their approach reguires the evaluation of a number of eigenfunctions and eigenvalues, and is therefore rather awkward and difficult to apply. In view of the liquid depths used in this study; the decrease in bulk liquid temperature was not as significant. Consequently a somewhat simpler approach was used, and found to yield an acceptable prediction of the interfacial temperature.

The first step in this procedure is to calculate the mass transfer rate assuming a constant interfacial temperature equal to the inlet liquid temperature. An approximate expression can then be written for the interfacial heat flux as a function of distance downstream by assuming a constant bulk velocity for the liquid phase. The temperature behavior

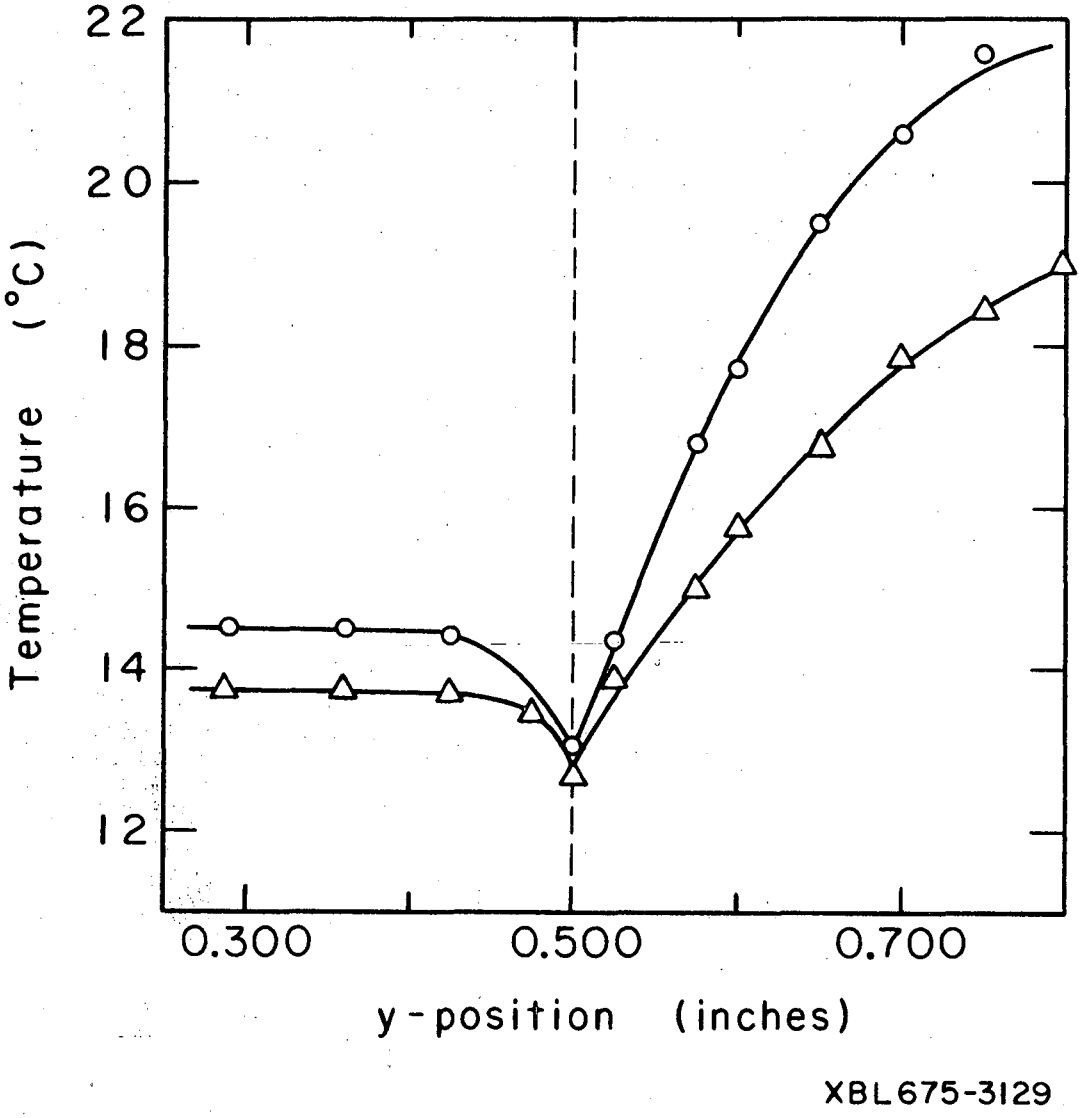

Fig. 17. Temperature profiles showing the depression of the interfacial temperature due to evaporation of n-pentane. Run # 231; o ... indicates data taken at 1/2 in. from inlet, Δ ... indicates data taken at 17.5 in. from the test section inlet.

of the liquid phase was obtained by applying penetration theory, with the interfacial heat flux as a boundary condition. The details of the above calculations can be found in Appendix E.

In general this procedure predicted an interfacial temperature that was somewhat lower than the values obtained experimentally; particularly for the runs at extremely high flux rates. This discrepancy was attributed to the formation of density and surface tension driven convection cells, which would tend to decrease the temperature difference between the bulk liquid and the interface. These cells will be discussed at greater length in Chapter VI. Also, the lower liquid boundary was not truly isothermal, so that heat transfer from the exterior could contribute to the complexity of the problem.

In practice the experimentally determined temperature profiles were used in obtaining the equilibrium concentration of the evaporating fluid at the gas-liquid interface.

The high flux mass transfer data were taken in two ways; i.e. both gas phase concentration profiles and cup mixing concentrations were obtained. In either case the mole fraction of the volatile species was obtained by sampling a continuous flow from either the concentration probe or the exit stream using the gas chromatograph. In general, from three to six chromatograms were carried out for each experimental point and an average value was obtained. The chromatograms for a single data point usually gave between five and ten percent spread.

Figures 18 and 19 represent two of the experimental profiles taken at the exit probe for interfacial mole fractions of 0.403 and 0.584, respectively. In both cases the experimental system was normal pentane evaporating into pure nitrogen, and Fs is based upon the experimentally observed interfacial temperature.

Figure 20 is a comparison of several experimental concentration profiles taken at the same flow conditions, with varying values of interfacial concentration. The increase in overall transfer rate and the decrease of k'_x as the value of x_{Ao} is raised can easily be seen. For comparison the low flux, low concentration profile for the same flow conditions is given by the dashed curve.

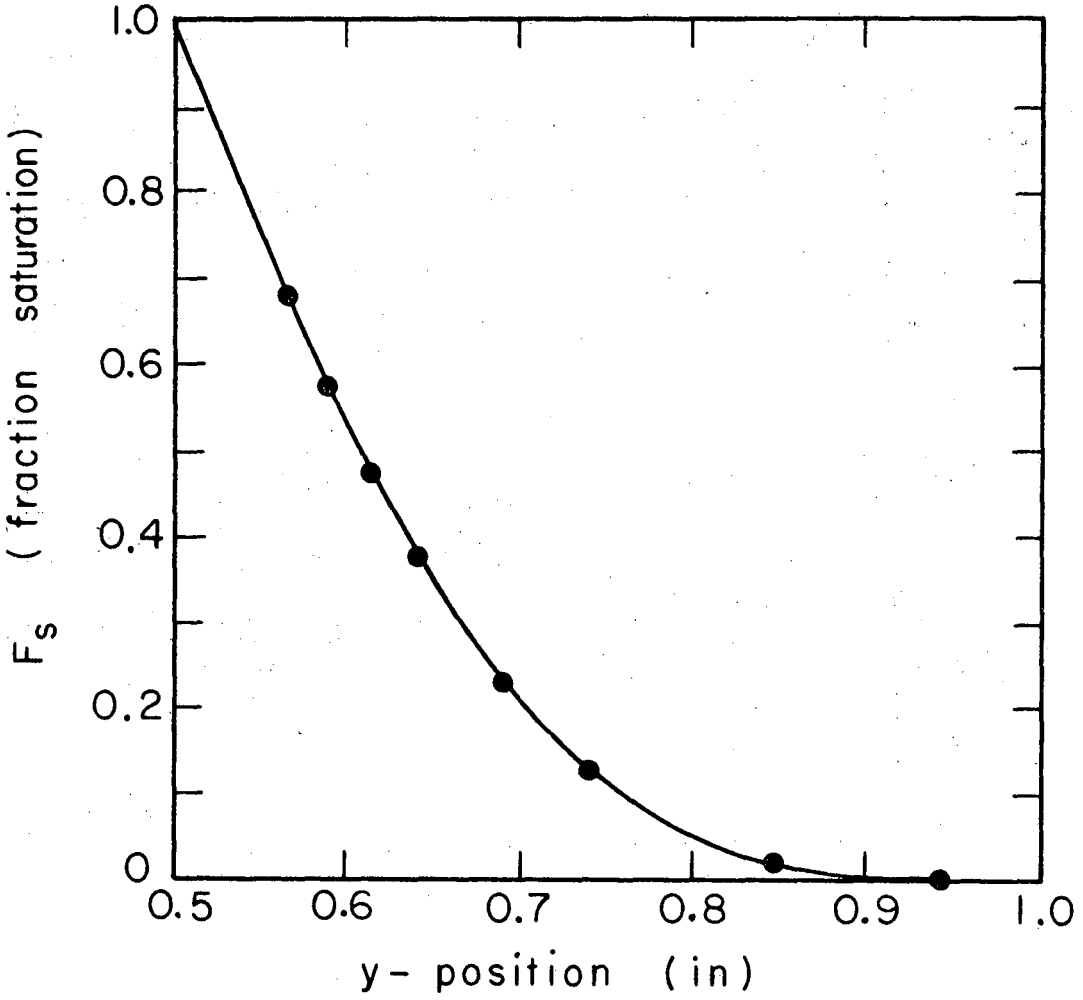

XBL675-3207

Fig. 18. Exit concentration profile for Run # 233.
$x_{Ao} = 0.403$
System: n-Pentane - Nitrogen

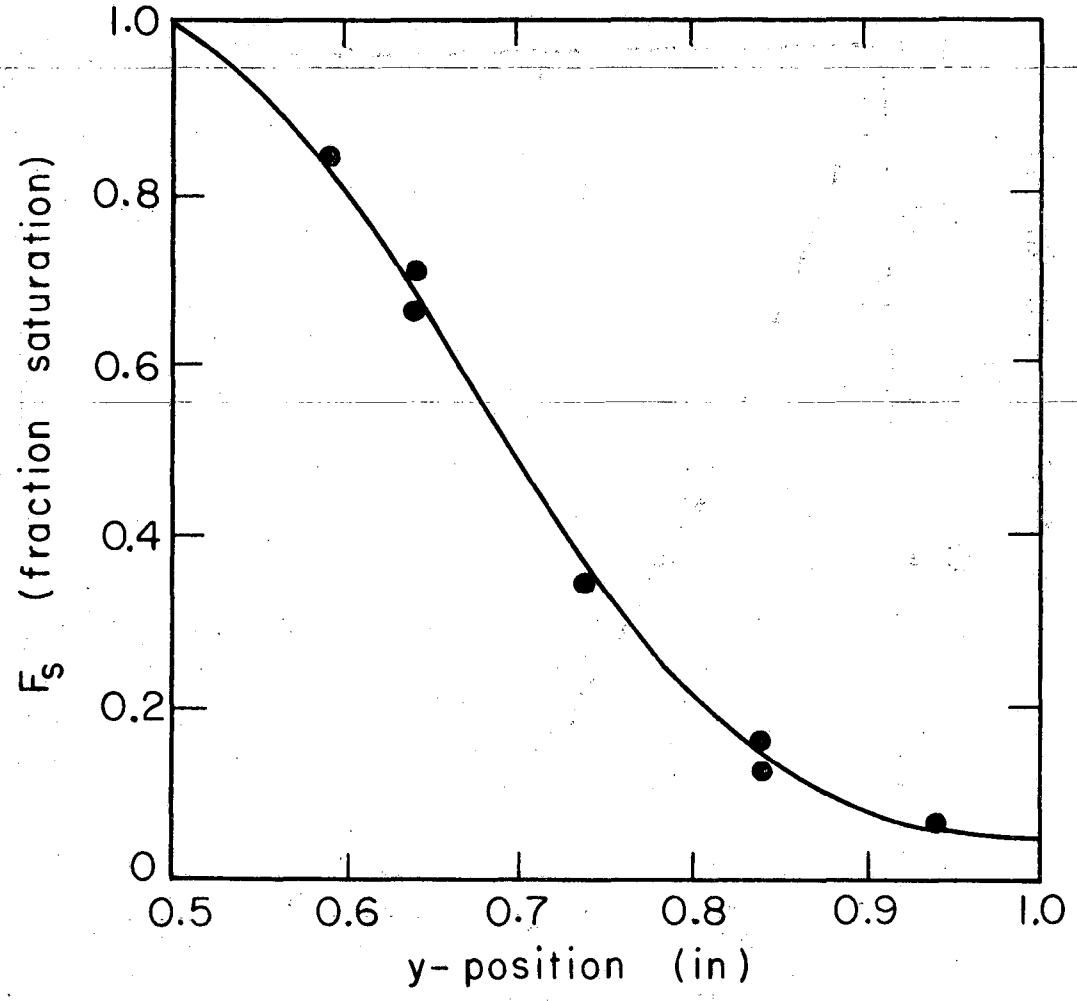

XBL675 - 3206

Fig. 19. Exit concentration profile for Run # 240.
$x_{Ao} = 0.584$
System: n-Pentane - Nitrogen

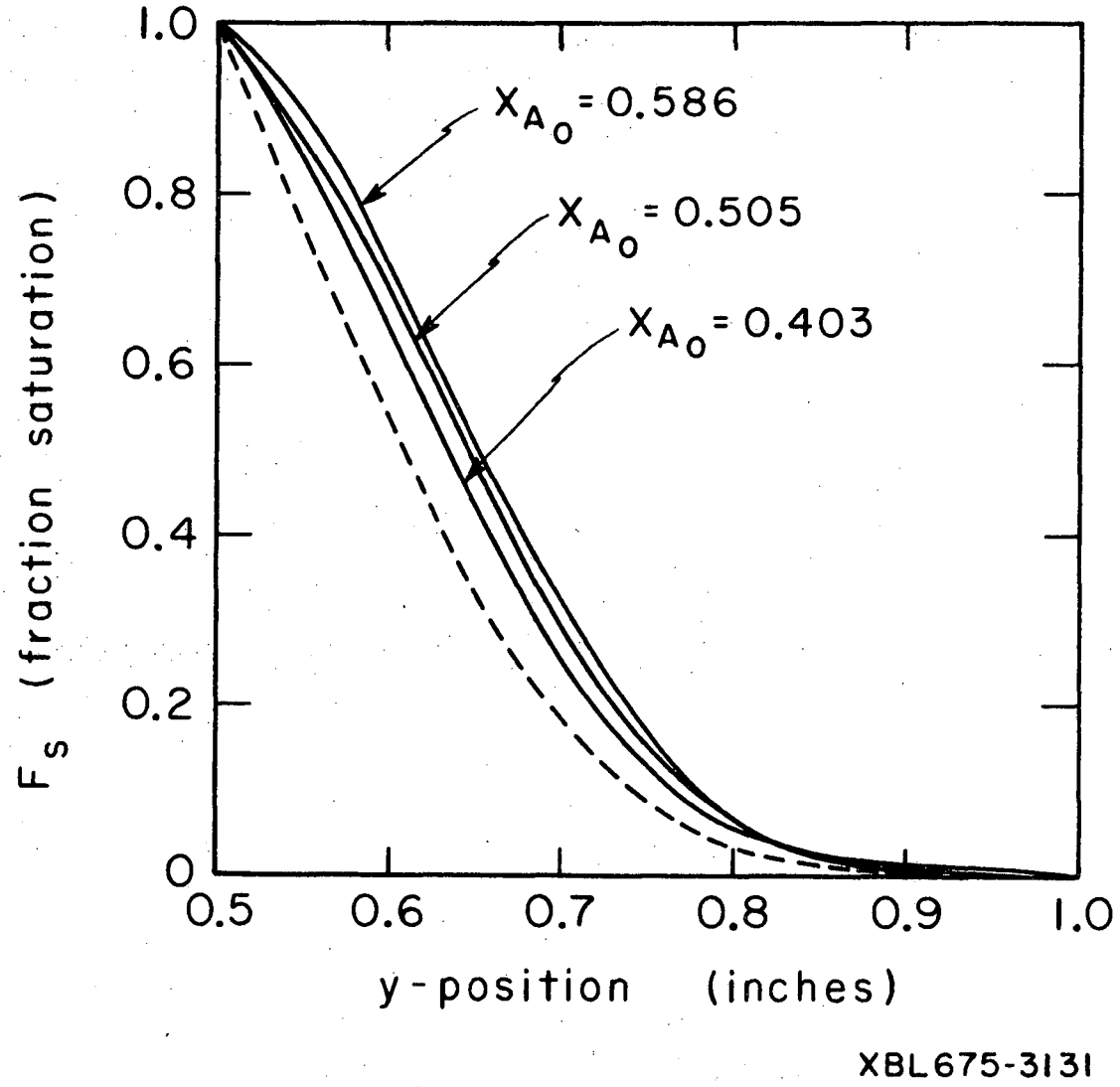

Fig. 20. Dimensionless exit concentration profiles for various values of interfacial gas phase mole fraction. The dashed line represents a theoretical profile for the case of low flux and low concentration level. QG = 308 cm^3/sec, QL = 0.400 gpm.
System: n-pentane/nitrogen

In order to compare the experimentally obtained profiles with a theoretical approach, it was first necessary to integrate these profiles to obtain a cup mixing concentration according to the equation:

$$x_{A,\ \text{cup mix}} = \int_0^b \frac{u_x(y)\ x_A(y)\ dy}{b\ u_{x,avg}} \qquad (5\text{-}28)$$

The experimental cup mixing mole fraction was then converted to a fraction saturation by dividing it by the equilibrium mole fraction at the interfacial conditions. A theoretical value of the fraction saturation was obtained in the following manner.

First a "low flux" value was obtained for the experimental flow conditions (Graetz number and velocity ratio based upon the inlet flow conditions) by interpolation from Fig. 10. Note at this point that if we take into account the fluid acceleration due to mass transfer the fraction saturation should increase. For example, using a bulk velocity representing the value at $N_A = 1/2\ N_A(\text{TOTAL})$ for calculation of the Graetz number, then for an interfacial mole fraction of $x_{Ao} = 0.500$ and the experimental conditions of Run # 231, we obtain a 10% (relative) increase in fraction saturation due to the acceleration effect.

The fraction saturation is directly related to the average mass transfer coefficient for the low flux, low concentration level case, i.e.

$$\begin{aligned} k_{x,avg}\quad \Delta x_A &= N_{A,avg} \\ N_{A,avg}\ (L) &= c(x_{A,avg})\ u_{x,avg}\ (b) \end{aligned} \qquad (5\text{-}29)$$

By manipulation of the above equations along with (5-5) and (5-9) we see that the correction factors which have been derived for the average mass transfer coefficient to account for flux level and interfacial concentration level are also applicable to the cup mixing concentration. Thus, the flux correction can be obtained by multiplying by θ_{AB}, and the concentration factor by dividing by $(1\text{-}x_{Ao})$. The appropriate value of θ_{AB} was obtained by first calculating R_{AB} for the experimental conditions, then using the penetration curve in Fig. 15 to obtain θ_{AB}. Actually, due

to the existance of a finite interfacial velocity, the correct value of θ_{AB} should lie somewhere between the penetration and Leveque solutions. Since the difference between the two can be seen to be quite small, the penetration model was utilized in all calculations.

In addition to the integration of the experimental profiles, a number of cup mixing concentrations were obtained directly by sampling the exit gas stream. The overall experimental results are summarized in Table II, with further information being given in Appendix B. The agreement between the calculational approach and the experimental results is quite good; however, there is a slight tendency for the experimental fraction saturation to be somewhat higher than the predicted values. This is not surprising, since one important difference exists between the two situations; i.e. the experimental arrangement was one of confined flow. This meant that as the liquid phase evaporated, it contributed a significant amount of material and therefore acceleration to the gas phase in the region near the interface. It is difficult to predict the exact influence of this acceleration upon the transfer coefficients; however, the qualitative effect should be to increase the mass transfer into the gas phase. The increase in F_s due to acceleration would be 10% for Run # 231 (see above), provided, however, that the velocity profile remained parabolic.

As can be seen from the results given in Table II, a slight increase in the theoretical value for fraction saturation would result in a better agreement between the theoretical and experimentall obtained results.

During the course of the high flux evaporation studies, a film of liquid could frequently be observed on the vertical side walls of the transparent test section, often rising to a height of one-quarter inch or more above the liquid interface. A tentative explanation of this effect was that the temperature induced variation in the liquid surface tension could account for a stable vertical film in an analogous manner to the well known "tears of wine", which is a concentration induced, surface tension driven; phenomenon. A brief search of the recent literature has yielded several references which tend to confirm this hypothesis; most

Table II. High flux rate experimental results

Run #	Graetz #	x_{Ao}	Experimental F_s	Theoretical F_s	Percent Error
233	0.0454	0.403	0.248	0.235	+ 5.6
236	0.0454	0.418	0.278	0.239	+14.0
237	0.0454	0.505	0.291	0.248	+14.8
231	0.0810	0.418	0.357	0.338	+ 5.3
234	0.0842	0.410	0.377	0.353	+ 6.4
239	0.0842	0.580	0.380	0.382	- 0.5
241	0.0842	0.580	0.427	0.382	+10.5
229	0.1510	0.439	0.535	0.481	+10.1
240	0.1510	0.580	0.591	0.525	+11.2
The above runs were made with the system n-pentane into nitrogen; the remainder of the results listed in this table are for the evaporation of iso-pentane into nitrogen.					
242	0.0956	0.560	0.402	0.400	+ 0.2
246	0.0956	0.655	0.435	0.421	+ 3.2
244	0.1368	0.560	0.490	0.483	+ 1.4
245	0.1368	0.681	0.488	0.516	- 5.7
247	0.1368	0.740	0.509	0.536	- 5.3
				Average percent error =	+ 5.1%

notable are the experimental works by Lightfoot,[46] and Lightfoot and Ludviksson.[47] In the latter reference it is demonstrated that a temperature gradient of only 0.4 °C/cm is sufficient to yield a infinitely high vertical film of water one micron in thickness. Since the temperature gradients due to the evaporative heat flux in the present experiment were an order of magnitude higher than the above figure, the observed effect could easily have been supported by a temperature driven mechanism.

VI. EVAPORATION FROM LIQUID MIXTURES

In the previous chapter, which dealt with the evaporation of a pure liquid into an adjacent gaseous stream, the solution for the mass transfer performance of the system was tremendously simplified by the lack of mass transfer resistance in the liquid phase. This meant that one could predict the interfacial concentration of the evaporating fluid by simply utilizing the temperature-vapor pressure curve for the liquid in question. The calculation of the high flux mass transfer rate could then be carried out in a straight-forward manner from the given flow conditions and the interfacial concentration.

If we now focus our attention upon the problem of the evaporation of a volatile substance, A, from a binary liquid mixture, A + B, we find that the complexity of the problem is greatly increased. From a mathematical view-point we see that, since the mass transfer resistance can now be divided between the liquid and gaseous phases, the problem requires the simultaneous solution of two partial differential equations. The equation of convective diffusion can be written for both the gas and liquid phase, yielding two equations linked by the interfacial boundary conditions between the two fluids. If the complicating factors of high flux and high concentration level are also considered, the problem begins to appear quite formidable indeed. Thus before attempting a direct solution to the above problem, let us first review the relatively small amount of existing work within the area of interphase mass transfer.

A. Background Material

1. Interphase Mass Transfer

The first major contributions toward the solution of the general two-phase resistance, mass transfer problem were made by Lewis[45] and Whitman.[85] The "two-film" approach used by these authors resulted in a simple addition of the individual mass transfer resistances to yield the overall mass transfer resistance. In recent years this "addition of resistances" principle has been invoked for many other models besides the simple film approach for which it was originally developed.

King[34] has shown that the following criteria should be satisfied by the physical situation in order for the additivity of independently measured phase resistances to be valid.

1) The liquid and gas concentrations at the interface should be linearly related by an equation of the form:

$$P_A = H(C_A) + (\text{constant}) \qquad (6\text{-}1)$$

2) The resistances which are added should be the only ones present.

3) The flow conditions used in calculating the individual resistances should be identical to those existing in the interphase situation.

4) The existence of either of the individual resistances should not substantially affect the value of the other.

5) The ratio of the two individual resistances should remain constant for all points on the interface.

In practice, it has been found that the effects of the above conditions frequently tend to cancel out one another in equipment providing a single exposure of fluid phases, particularly when the additivity principle is applied to the average rather than the local mass transfer coefficients. In complex contacting equipment, such as packed and plate towers, the departure from additivity can be more severe.

Byers[13] has shown that for the cocurrent laminar flow contacting device used in this study the additivity of resistances principle is accurate to better than 2%, provided the Graetz number is less than 0.50. It should be noted, however, that this was for the special case of low flux and low concentration level. From the few other exact solutions of the interphase mass transfer problem, it can be generally stated that that the addition of resistances tends to be valid if the individual transfer coefficients have the same functionality with respect to exposure time or length of contact between phases. Since it has been shown that the existence of high flux and high concentration level does not effect the x-direction functionality of the mass transfer coefficients, the application of the addition of resistances principle to the problem at hand should lead to a satisfactory prediction of the overall mass transfer behavior of the high flux, high concentration level system.

In order to carry out the addition of resistances under the high flux and high concentration level conditions, it is first necessary to define several useful quantities. As was stated earlier, a convenient and accurate assumption for most liquid phase mass transfer calculations is that of constant partial molal volume. This assumption leads to a mass transfer coefficient for the liquid phase,

$$k'_{\phi,loc} = \frac{N_{Ao} - \phi_{Ao}(N_{Ao} + (\tilde{V}_B/\tilde{V}_A)\, N_{Bo})}{\phi_{Ao} - \phi_{A\infty}} \tag{6-2}$$

which is analogous to Eq. (5-5) for the gas phase.

For the limiting case of low mass flux we may then write in an analogous manner to Eq. (5-6);

$$k_{\phi,loc} = \lim_{(N_{Ao} + (\tilde{V}_B/\tilde{V}_A)\, N_{Bo}) \to 0} \left[k'_{\phi,loc}\right] \tag{6-3}$$

In a similar manner we can also develop the dimensionless high flux parameters on a volume fraction basis for the liquid phase, i.e.

$$R_{AB} = \frac{N_{Ao} + \left(\frac{\tilde{V}_B}{\tilde{V}_A}\right) N_{Bo}}{k'_{\phi,loc}} = \frac{\phi_{Ao} - \phi_{A\infty}}{\frac{N_{Ao}}{N_{Ao} + (\tilde{V}_B/\tilde{V}_A)\, N_{Bo}} - \phi_{Ao}} \tag{6-4}$$

$$\phi_{AB} = \frac{N_{Ao} + (\tilde{V}_B/\tilde{V}_A)\, N_{Bo}}{k_{\phi,loc}} \tag{6-5}$$

$$\theta_{AB} = k'_{\phi,loc}/k_{\phi,loc} \tag{6-6}$$

In addition to the local mass transfer coefficients defined by Eqs. (5-5), (5-6), (6-2), and (6-3), it is also convenient to define a set of average mass transfer coefficients which are similar to the local coefficients except that they employ average values for the interfacial flux and the various concentration variables, for example:

$$k'_{\phi,avg} = \frac{N_{Ao}(avg) - \phi_{Ao}(avg)(N_{Ao}(avg) + (\tilde{V}_B/\tilde{V}_A)\, N_{Bo}(avg))}{\phi_{Ao}(avg) + \phi_{A\infty}(avg)} \quad (6\text{-}7)$$

where the flux and concentration variables are averaged over the entire mass transfer exposure.

In order to simplify the remaining calculations the following assumptions will now be made:

1) The perfect gas laws are applicable to the gas phase; i.e., the gas phase mole fraction can be found from the equation,

$$cx_A = C_A \quad , \quad (6\text{-}8)$$

where c, the total molar concentration, remains constant.

2) The liquid phase is a binary mixture, with the components having a constant partial molal volume, i.e.

$$C_A = \phi_A/\tilde{V}_A \quad (6\text{-}9)$$

3) Species A is the only substance undergoing mass transfer between the two phases; i.e., the liquid solvent is non-volatile and the second gas phase component is non-condensable. ($N_{Bo} = 0$).

If we now divide Eq. (6-7) into its gas phase equivalent, while realizing that N_{Ao} (gas) must be equal to - N_{Ao} (liquid) we obtain:

$$\frac{k'_{x,avg}}{k'_{\phi,avg}} = -\frac{(\phi_{Ao} - \phi_{A\infty})(1 - x_{Ao})}{(x_{Ao} - x_{A\infty})(1 - \phi_{Ao})} = \frac{k_{x,avg}\, \theta_{AB}(gas)}{k_{\phi,avg}\, \theta_{AB}(liq)} \quad (6\text{-}10)$$

Equations (6-1), (6-8) and (6-9) can be combined to yield a relation between the liquid phase volume fraction and the equilibrium value of the gas phase mole fraction,

$$x_A = (H/\rho_T \tilde{V}_A)\, \phi_A + (\text{constant}) \quad (6\text{-}11)$$

The solution of the above two equations, (6-10) and (6-11), determines the two unknown interfacial concentrations, x_{Ao} and ϕ_{Ao}.

Unfortunately upon closer examination of (6-10) we see that the equation is implicit in the unknown interfacial concentrations, because the high flux correction factors, $\theta_{AB}(gas)$ and $\theta_{AB}(liq)$, are both dependent upon the value of the interfacial concentration of the phase in question.

Thus a trial and error procedure was necessary in order to achieve a final solution of Eqs. (6-10) and (6-11). A sample calculation can be found in Appendix E. A brief sketch of the solution technique is given by the following steps:

1) Assume a value for x_{Ao} (and consequently ϕ_{Ao}); usually the value predited by the low flux interphase solution of Byers was utilized.

2) Calculate the value of $\theta_{AB}(liq)$ from the assumed value of ϕ_{Ao} using the curve for the penetration model given in Fig. 12. This is possible since for any given run the value of $\phi_{A\infty}$ is known.

3) Calculate the value of $\theta_{AB}(gas)$ from the assumed value of x_{Ao} using the curve for the Leveque solution given in Fig. 14. This is easily accomplished, since the value of $x_{A\infty} = 0$ throughout this work.

4) Using these values and Eqs. (6-10) and (6-11) a new value of x_{Ao} (and hence ϕ_{Ao}) can be calculated and compared with the initial assumption. If the agreement is poor, then the new values of x_{Ao} and ϕ_{Ao} are inserted in step 1) and the calculations repeated. Usually the second iteration yields a value of x_{Ao} which differs from the assumed value by less than 1%, at which point the calculations can be terminated.

5) Using the final value of ϕ_{Ao}, the average mass transfer coefficient can then be calculated using Eq. (6-7), or alternatively the vapor phase form of this equation. The resulting average mass flux is then converted into a fraction saturation using (5-29) and the results compared with experimental data using a plot of fraction saturation of the gas phase versus inlet liquid bulk concentration.

2. Cellular Convection

The onset of what has been termed "natural" or cellular convection within a fluid can have a profound influence upon the transfer coefficients for the phase in question. These cells are often said to arise "spontaneously", since they occur without an expenditure of mechanical work upon

the system. The actual driving forces which produce the fluid motion have been shown to be related to the spatial variation of two fluid properties, density and surface tension. This variation can be brought about whenever the fluid is undergoing either heat or mass transfer.

To illustrate this behavior, let us consider a thin layer of stagnant liquid which is being heated from below and cooled at the upper surface. Since the density of most liquids increases with decreasing temperature, the fluid adjacent to the upper surface will be more dense than the underlying liquid. This is potentially an unstable situation and the upper fluid may begin to flow downward due to the force of gravity, thereby creating the spontaneous flow, or convection, described above.

The same situation might also arise if a light component were being transferred out of a mixture with a heavier component. The concentration gradient necessary to drive the mass transfer would yield the same sort of adverse density variation if the transfer were taking place from the upper surface. Two other analogous situations could be postulated with the surface tension as the driving force, since a value of surface tension which is higher than the surface tension in equilibrium with the bulk fluid is a potentially unstable situation.

Although the first documented observance of cellular convection is attributed to Cornelius Varley[81] in 1836, probably the first important historical figure in the field was James Thompson. In 1855, in a note to the Royal Society,[77] Thompson explained the surface motions which he had observed in a wine goblet as being caused by variations in surface tension which resulted from the preferential evaporation of alcohol from the wine. In a second note dated 1882,[78] Thompson described convective patterns which he had obsered "in a tub of water, in the yard of a roadside inn." This motion he attributed to a buoyancy mechanism, which resulted when the liquid was cooled at its upper surface while being heated from beneath.

The first systematic experimental study of cellular convection was carried out in 1900 by Henri Benard.[7] In his work Benard measured the size and shape of convection cells produced by heating a thin layer of molten spermaceti from beneath. He also found that there was a certain critical value of the heat flux, below which the cellular pattern did not occur.

An excellent summary of the major contributions to the area of cellular convection is the work by Berg, Acrivos, and Boudart.[8]

(a) Hydrodynamic Stability Analysis

The first successful theoretical approach to the problem of cellular convection was carried out by Lord Rayleigh in 1916.[65] His mathematical approach, which has since been given the name of "hydrodynamic stability analysis", was to consider the flow perturbations about an initially stable flow regime. In this case the initial regime is one of zero flow.

The mathematical representation of the stability problem begins with the following equations of change:

(continuity equation)

$$\partial\rho/\partial t + \text{div}(\rho u) = 0 \tag{6-12}$$

(equation of motion)

$$\rho Du/Dt = f - \text{grad } p - \frac{2}{3}\text{grad}(\mu \text{ div } u) + \text{div}(\mu \text{ def } u) \tag{6-13}$$

(energy equation)

$$\rho D(C_v T)/Dt = \text{div}(k \text{ grad } T) - p \text{ div } u + \frac{\mu}{2}(\text{def } u)\cdot(\text{def } u) - \frac{2}{3}\mu(\text{div } u)^2 \tag{6-14}$$

(species conservation equation)

$$\rho DC_A/Dt = \text{div}(D_{AB} \text{ grad } C_A) \tag{6-15}$$

(equations of state)

$$\rho = \rho_o(1 - \alpha_1(T - T_o)) \tag{6-16}$$

$$\rho = \rho_o(1 - \alpha_2(C_A - C_{Ao})) \tag{6-17}$$

If the flow is driven by heat transfer alone, then the species conservation equation can be ignored, and the appropriate temperature dependent equation of state is utilized, i.e. (6-16). The next step in the approach is to define a number of perturbation variables,

$$u = u^{o} + u' \quad ; \quad T = T^{o} + T' \quad , \quad \text{etc.} \tag{6-18}$$

where ^{o} denotes the initial steady state value of the variable and $'$ represents its perturbation from the steady state value. These variables are then substituted into the equations of change, and the resulting set of equations linearized by assuming that the perturbations are very small. A detailed derivation of these equations and the appropriate methods of solution has been presented by Chandrasekhar.[18]

Perturbation solutions for the density driven convection problem have been carried out by a number of investigators using a variety of boundary conditions for the problem. The initial solution carried out by Lord Rayleigh[65] assumed that both the upper and lower surfaces were at constant temperatures, and that the liquid could circulate freely at the surface with no slip. Subsequent solutions by Pellew and Southwell,[61] Low,[48] and Sparrow[71] et al., have extended the solution to a number of boundary conditions. A listing of the various solutions and the assumptions inherent to each can be found in the summary by Berg, Acrivos, and Boudart.[8] The primary value of all of these solutions is their ability to predict the conditions required for the onset of cellular convection. Although the exact stability criteria of the system are dependent upon the wave length of the initial infintesimal disturbance, the theory is also able to predict a region that is stable to any disturbance provided that a single dimensionless variable, $R = (g\beta_T \frac{\partial T}{\partial y} h^4)/\alpha\nu$, is less than a given critical value. This dimensionless group, which is called the Rayleigh number, has different critical values depending upon the applicable boundary conditions. The critical values vary from 657.5 to 1710; these values have been confirmed experimentally by several investigators for cases where the density variation was dependent upon variations

in temperature. A number of the experiments which involved a free upper surface, however, exhibited convection at values of R well below the theoretical value of R_{cr}.

These experiments prompted J. R. A. Pearson[60] to propose a different mechanism for thermal convection cells, a model which was driven by surface tension rather than density gradients. The physical boundary conditions which Pearson used are listed below:

1) The heat lost at the surface is proportional to the surface temperature, and is balanced by heat conducted up from below.

2) The lower surface could either be isothermal or subject to a constant heat flux, yielding slightly different solutions.

3) The surface forces generated due to temperature induced variations in surface tension are balanced against the shear of the underlying fluid.

4) Both the upper and lower surfaces are rigid and non-deformable. (Actually two boundary conditions, one for each surface).

5) The lower surface is one of zero slip between the fluid and the wall.

The results of Pearson's analysis could be expressed in a manner similar to those of the density driven problem, where the region of stability is defined by one dimensionless variable, the Thompson number,

$$Th = -\left(\frac{\partial \gamma}{\partial T}\right)\left(\frac{\partial T}{\partial y}\right) h^2/\alpha\mu \qquad (6\text{-}19)$$

The critical values for the Thompson number were found to be 80 for the isothermal case and 48 for the constant flux case.

Since Pearson's theoretical work was published in 1958, several experimenters have attempted to verify his theoretical predictions. The experimental results have thus far exhibited a large amount of scatter; however, convection has not been encountered at a Thompson number which was below the theoretically predicted value. The following table is a representative sample of the experimentally obtained results taken from a Ph.D. Thesis by John Berg.[9] Note that the results are one to two orders of magnitude higher than the theoretical values predicted by Pearson's analysis.

Liquid	Experimental Th_{cr}
Acetone	3400
Benzene	950
Carbon Tetrachloride	1400
n-Heptane	700
Isopropyl alcohol	200
Methyl alcohol	650

Another assumption which is inherent to both the density and surface tension driven flows is that of a linear temperature gradient between the upper and lower surfaces. This is usually a good assumption for a temperature profile, but for the analogous problems that are caused by concentration gradients it becomes quite poor. This is primarily because of the exceedingly low values of liquid phase diffusivity, which lead to small penetration depths and therefore non-linear, undeveloped profiles. Another difference between the temperature dependent and the concentration dependent problems is in the properties entering into the Thompson and Rayleigh numbers; these are given in their concentration dependent form below:

$$Th = \left(\frac{\partial \gamma}{\partial C_A}\right)\left(\frac{\partial C_A}{\partial y}\right) h^2/D_{AB}\mu \qquad (6\text{-}20)$$

$$R = g\left(\frac{\partial \rho}{\partial C_A}\right)\left(\frac{\partial C_A}{\partial y}\right) h^4/D_{AB}\nu \qquad (6\text{-}21)$$

(b) Nonlinear Theory

The key to a successful theoretical prediction of the flow patterns and consequently the transfer coefficients for finite cellular convection lies in the non-linear terms in the equations of motion. Thus far the basis of the nonlinear work attempted has been an incomplete form of the equations of motion, obtained by neglecting the temperature dependence of all physical properties except density, (only the density driven problem has been considered using the nonlinear approach). This method of attack is known as the Boussinesq approximation.

Cellular convection was first treated in this manner by Pillow[63] in 1952, who considered the problem of two-dimensional flow between two flat plates at different temperatures. After making several simplifying assumptions, he was able to predict a 5/4 power dependence of heat transfer rate upon the temperature driving force, a number that has been frequently confirmed experimentally for natural convection from a heated horizontal plate.[32] (This is equivalent to the well known experimental relationship for natural convection, which gives $h = (\text{const.})(Gr^{1/4}).$)[62]

Several other solutions have been obtained by various techniques. Malkus and Veronis[49] used a perturbation technique which retained the first three terms in an expansion of the variables. Kuo[40] obtained the 5/4 power dependence (or equivalently a 1/4 power dependence of the Nusselt number upon the Rayleigh number) by expanding the dependent variables in an orthogonal series fashion.

The nonlinear mathematical approach does appear to hold a great deal of promise, since a complete solution would yield the entire flow pattern for the problem under consideration. Unfortunately the high degree of mathematical complexity required for such a solution makes the task appear quite formidable at best. To date there does not appear to have been any attempt to use the nonlinear approach to obtain even an approximate solution for the surface tension driven problem of cellular convection.

(c) Experimental Results

There has been relatively little experimental work carried out in the general area of surface tension driven, cellular convection and its effect upon mass transfer. Of the papers which have been published, the majority are concerned with the photographic observance of the phenomenon and a subsequent description of the physical shapes and flow patterns of the cellular disturbances which were obtained. The study by Orell and Westwater,[59] using a photographic Schlieren technique gives an excellent description of the various types of cell patterns which were observed in a ternary liquid-liquid system involving the transfer of acetic acid out of ethylene glycol into ethyl acetate. The experimental system utilized consisted of a transparent tank, which was separated into two equal portions by a diaphragm. The two liquids were introduced into

the opposite sides of the cell and the diaphragm removed to give a flat, horizontal interface between the two stationary liquid phases. Photographic data were then taken while the two phases slowly equilibrated; in some instances cellular convection could still be detected after 43 hrs. of contact.

A similar photographic study has been carried out by Berg[9] for a number of different gas-liquid systems. In his work Berg allowed both pure liquids and binary liquid mixtures to evaporate from a shallow horizontal vessel into air at ambient conditions. The shapes and sizes of the cells were quite varied, and were found to be dependent upon the particular system involved and even the length of time over which evaporation had been occurring.

Ellis and Biddulph[21] have also carried out an experimental study of gas-liquid interfacial turbulence at a horizontal interface. Using small trace-particles of polyethylene, they observed interfacial velocities as high as 3.5 in./sec for the system acetone-water.

Quinn and co-workers[83,53,54] have reported the existence of Marangoni instabilities in two different liquid-liquid contacting configurations, a liquid-liquid jet and a radially moving film contactor. They state that the Marangoni effect appeared to be reproducible in nature, and furthermore, that it is manifest at very small contact times-as low as 0.04 sec. The net effect of the cellular convection was to increase the overall mass transfer coefficients, but the authors do not offer any form of correlation or quantitative prediction.

Muenz and Marchello[56] observed an increase in mass transfer coefficient which they attributed to concentration-driven Marangoni cells during the course of an experiment on the effect of surface ripples on gas-liquid mass transfer. Again the authors did not give a quantitative correlation of the effect of the cellular convection upon the mass transfer characteristics of the system.

Bakker, Buytenen and Beek[5] have carried out a photographic study of interfacial turbulence in liquid-liquid systems, in which they also obtained quantitative mass transfer data. Using order-of-magnitude physical arguements these authors concluded that the mean cell size

was roughly equal to the depth of penetration of the concentration profile. By making the assumption that the individual cells on either side of the interface reach equilibrium during their exposure these authors estimate the factor by which the mass transfer rate is increased to be in the neighborhood of 2 to 3.

By utilizing a liquid-liquid wetted wall column, Maroudas and Sawistowski[50] obtained quantitative mass transfer data for systems which were undergoing surface tension driven cellular convection. By making use of the Danckwerts theory of surface renewal and their experimentally obtained increases in mass transfer rate, they were able to calculate values of the fractional rate of surface renewal varying from 0.01 to 10, depending upon the contact time involved. Unfortunately, this method of attack does not lead to a prediction of the effect of Marangoni instabilities upon mass transfer rates, as the value of s, the fractional rate of surface renewal cannot be predicted a priori, but must be obtained instead from experimental data.

In view of the work which has been carried out thus far, there does not appear to be any satisfactory method for accurately estimating the quantitative effect of surface tension-driven cellular convection upon the system mass transfer coefficients.

B. Experimental Results

In order to confirm the calculational method outlined in Sec. 6(A)-1 a number of experiments were planned involving evaporation of a volatile component from the n-tridecane solvent into a flowing nitrogen gas stream. The mass transfer flux level of the experimental system could be easily varied by either increasing the volatility of the transferred species, increasing the system temperature level, or increasing the concentration level of the transferred species in the inlet liquid stream. Since the equipment had already demonstrated predictable behavior with respect to the stream flow variables (see Fig. 16 and Table II), the decision was made to fix the bulk velocities of the liquid and gas streams, thereby reducing the number of variables which had to be considered when analyzing the experimental results.

Also, the streams were introduced at the same temperature, so that the only heat flow was that due to the enthalpy of evaporation of the volatile component. The average interfacial temperature was then taken experimentally, and all subsequent equilibrium calculations were based upon this temperature. In practice the value of interfacial temperature desired was fixed prior to running, and the bulk inlet temperature of the liquid phase was adjusted until this value was achieved. Additional details pertaining to the exact experimental procedure used can be found in Appendix A.

The first system to be considered experimentally was the evaporation of n-pentane from the n-tridecane solvent. The gas (N_2) flow was fixed at a value of 166 cm^3/sec, corresponding to a gas phase Reynolds number of 286. The liquid flow rate was maintained at a value of 0.400 gpm, which corresponds to a liquid phase Reynolds number of approximately 500 for low concentrations of n-pentane (this value increases to nearly 1000 for $XL_A = 0.50$ in the n-pentane/tridecane system due to the large change in liquid phase viscosity). The interfacial temperature was maintained at 20 ± 0.1°C, corresponding to a vapor pressure of 0.572 atm for pure n-pentane.

The first series of experiments was carried out with the pentane concentration in the range of $XL_A \tilde{=} 0.01$; these runs confirmed that the experimental data were in good agreement with the low flux prediction using Byers' numerical technique. The pentane concentration in the liquid phase was consequently increased to a higher value ($XL_A \tilde{=} 0.10$) and the runs repeated. At this level of concentration the experimental fraction saturation of the gas phase had increased somewhat more than predicted by the theoretical calculations; and as the liquid phase concentration level was subsequently increased the discrepancy between the experimental results and those predicted by the theoretical approach outlined earlier became even greater.

The experimental results which were obtained for the n-pentane/tridecane system are presented in Fig. 21 in the form of F_s, the fraction saturation of the gas phase, versus liquid phase concentration, XL_A.

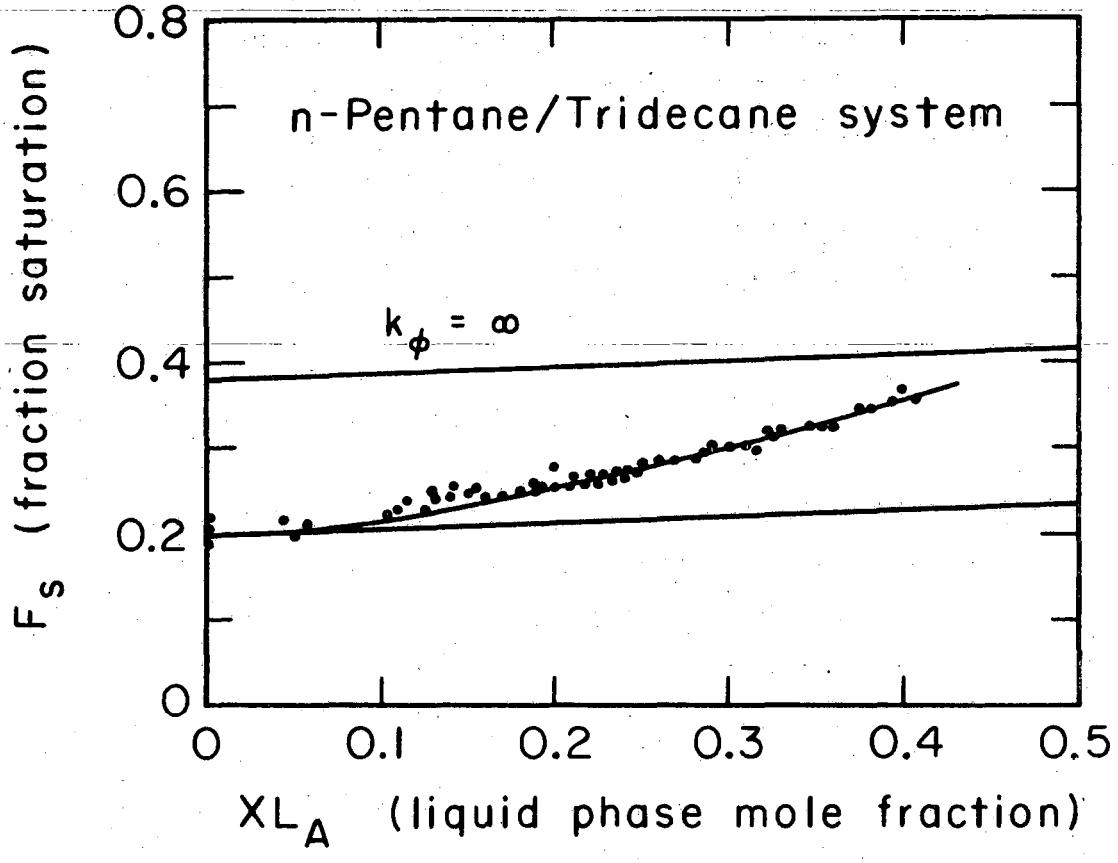

Fig. 21. Gas phase fraction saturation (cup mixing) as a function of bulk liquid phase mole fraction, for the system, n-pentane/tridecane evaporating into nitrogen. • ... indicates experimental data, the lower solid line represents the predicted behavior using the high flux addition of resistances approach.
Interfacial temperature = 20 ± 0.1°C

The lower solid line represents the functionality that is predicted using the addition of resistances principle outlined in Sec. 6(A)-1. The upper line, which is labled $k_\phi = \infty$, represents the predicted behavior for the system under the assumption of zero liquid phase resistance.

The theoretical calculations carried out for this system indicated that the mass transfer resistances in the liquid and gaseous phases were approximately equal; this fact was confirmed during the low concentration level runs by the excellent agreement between the theoretical predictions and the experimental results. From the data presented in Fig. 21 it can be seen that some mechansim seems to be operating which is substantially reducing the resistance to mass transfer. The most likely possibility for producing such behavior is some form of natural or cellular convection. Under close visual examination of the liquid in the surface region, small streamers could be seen which were moving in a vertical direction as they were swept along by the fluid motion.

Further confirmation of these vertical flow aberrations was obtained from the thermocouple probes which were used to obtain temperature profiles in the test section. Under the low concentration level, low flux level conditions the output from these probes had been quite steady as a function of time, and changed only when the tip was moved to a new vertical position. The typical form of the output at the high concentration levels can be seen in Fig. 22. Here the thermocouple output voltage trace is given as a function of time for the inlet and exit temperature probes at various vertical positions. As can be seen, the trace obtained at 0.550 in. from bottom of the channel (in the gas phase) is nearly constant, however, as the exit probe is placed into the liquid phase (0.500 and below) the output becomes quite erratic, indicating that fluid streamers with varying values of temperature were flowing past the probe. Since the interfacial temperature was several degrees cooler than the bulk fluid due to the evaporative heat flux; the flow of alternate streamers of fluid having interfacial and bulk conditions could produce such a behavior. This hypothesis is further confirmed by the fact that as the probe was placed deeper into the fluid the output became less erratic, finally reaching a constant value equal to the bulk temperature at depths of 0.300 in. and below.

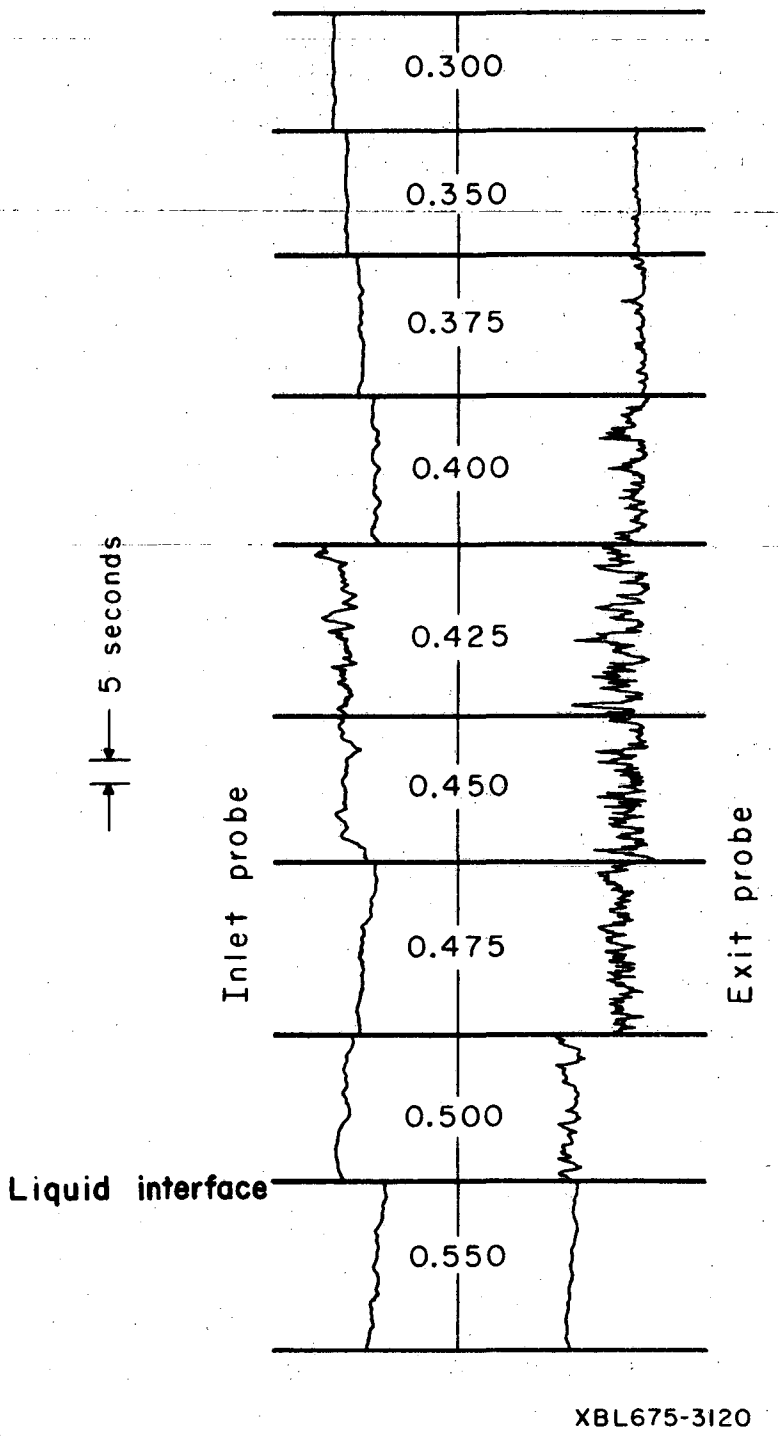

Fig. 22. Output from thermocouple probes showing oscillation of liquid phase temperature as a function of time for various vertical positions.

Also, as can be seen in Fig. 22, the inlet probe exhibited only very slight oscillatory behavior, which would be consistent with the theory of cellular convection, as the cells would not have grown very much after only 1/2 in. of exposure.

A final confirmation that the anomalous mass transfer behavior was caused by a liquid phase phenomenon is given in Fig. 23, which represents an experimentally obtained concentration profile under the high concentration level conditions. As can be seen, the experimental profile is at an intermediate position between the predicted profile and the profile for $k_\phi = \infty$, which again indicates that the liquid phase mass transfer coefficient is much higher than its predicted value, while the gas phase mass transfer is behaving in the manner predicted. Using the experimental value of x_{Ao} and F_s we can calculate a value of $k_\phi(EXP)/k_\phi(Theory) = 1.4$; whereas $k_x(EXP)/k_x(Theory)$ was found to be 0.921, which is within the experimental error of x_{Ao} and F_s.

After concluding that the increased liquid phase mass transfer coefficient was caused by cellular convection, it was next necessary to ascertain which of the four possible driving forces was producing the flow instability. These four mechanisms, which were presented earlier, can be written in brief form as: 1) surface tension-driven, temperature-induced; 2) surface-tension-drive, concentration-induced; 3) density-driven, temperature-induced; and 4) density-driven, concentration-induced. Since each of these mechanisms can be associated with an appropriate form of the Thompson or Rayleigh number, it was decided that an approximate estimate of the value of these numbers might aid in deciding which was the most important one of the four for the situation at hand.

A qualitative analysis of the situation shows that any of the above four mechanisms could have been responsible for the observed cellular convection, since all of the driving forces were in the direction leading to a possibly unstable situation. Thus, an attempt was next made to assign a rough numerical value to Th or R for each situation. In order to do this a number of assumptions were necessary, because of the large differences between the flow situation at hand and the theoretical situation for which the Thompson and Rayleigh numbers were originally devised.

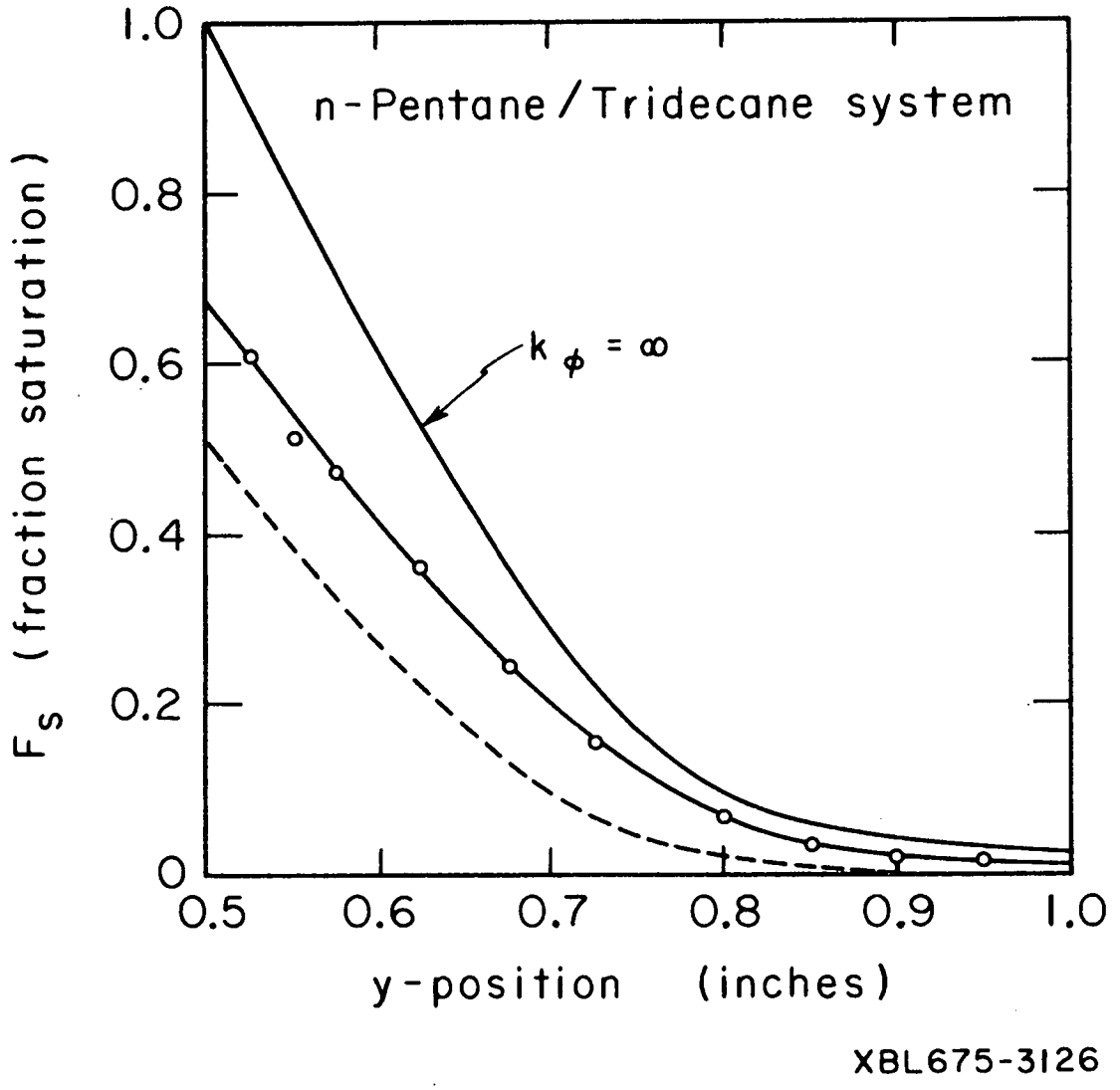

Fig. 23. Gas phase concentration profile from Run # 58; evaporation of n-pentane from tridecane into nitrogen. o ... indicates experimental data, the solid line through the data is a best fit to the points. The dashed line indicates the predicted profile in the absence of cellular convection.

1) The surface tension and density were assumed to be linear functions of concentration and temperature. For the systems which were ultimately used in this study, this assumption can be shown to be fairly good (see Appendix D). The worst error is on the order of 20% for one surface tension-concentration system; i.e. ethyl ether/tridecane.

2) The concentration and temperature profiles used for calculating values of h, $\partial C_A/\partial y$, and $\partial T/\partial y$ were calculated using the standard penetration approach for the liquid phase, ignoring the presence of the cells; see Appendix E for details.

3) All the important physical parameters, i.e. D_{AB}, α, μ, ρ, were assumed constant, at the values associated with the interfacial conditions.

4) The value of the interfacial concentration was assumed to be the same as that obtained by using the interphase numerical Graetz solution carried out by Byers.[13] Note that this value will be higher than the experimental value, due to the mixing of the liquid phase caused by the existance of any cellular convection.

There are two valid reasons for using the theoretical value in the absence of cells rather than the experimental value of interfacial concentration. The most important of the two reasons is that one would prefer to determine the influence of the cellular convection from a direct and non-iterative calculation based upon known or easily predicted quantities. The second reason is based upon the assumption that the magnitude of the cellular convection (and hence the experimental value of interfacial concentration) is a function of the driving force, or distance that the system lies from the point of critical stability. If this is a correct assumption, then it is only necessary to employ an interfacial concentration uniquely related to the true value. The proposed method is a convenient approach for obtaining such a value.

A sample calculation of the concentration dependent Thompson number based on the above assumptions is given in Appendix E. Upon calculation of the Thompson or Rayleigh numbers for each of the four possible situations, it was discovered that the surface tension-driven, concentration-dependent mechanism yielded a value of the Thompson number which was

two orders of magnitude larger in relation to the critical Th or R, than occurred for the other mechanisms. To illustrate the values of the four situations, the results of a sample calculation carried out for n-pentane/tridecane at a pentane mole fraction of 0.05 are given below:

1) For the concentration driven case

$$Th_{avg} = 13,900$$

$$R_{avg} = 26$$

2) For the temperature driven situation

$$Th_{avg} = 93$$

$$R_{avg} = 155$$

Of the four mechanisms, two tend to predominate, the concentration-dependent Marangoni cells and the temperature-dependent Benard cells. This is primarily due to the exponent on h, which is h^2 in Th and h^4 in R. Because of the extremely low value of the liquid phase diffusivities, h tends to be quite small for the concentration profile; thus the value of Th tends to be much larger than the value of R for the concentration dependent situation. If we consider the temperature dependent forms, the reverse is generally true. The penetration depths for the temperature profiles tend to be fairly large, making the density driven situation relatively more important than the surface tension driven one.

In order to confirm the above assumptions several other systems were devised, with physical properties which varied enough to provide a strong test of the four different possibilities. These systems were:

1) n-pentane/tridecane (discussed above)
2) cyclopentane/tridecane
3) ethyl ether/tridecane
4) carbon disulfide/tridecane

The experimental results for each of the remaining three systems are given in Figs. 24, 25, and 26 in a form similar to that used in Fig. 21 for the n-pentane/tridecane system. From Appendix D, we see that the $CS_2/n\text{-}C_{13}$ system should not exhibit concentration-induced cellular convection, as both the density and surface tension of CS_2 lie in the wrong

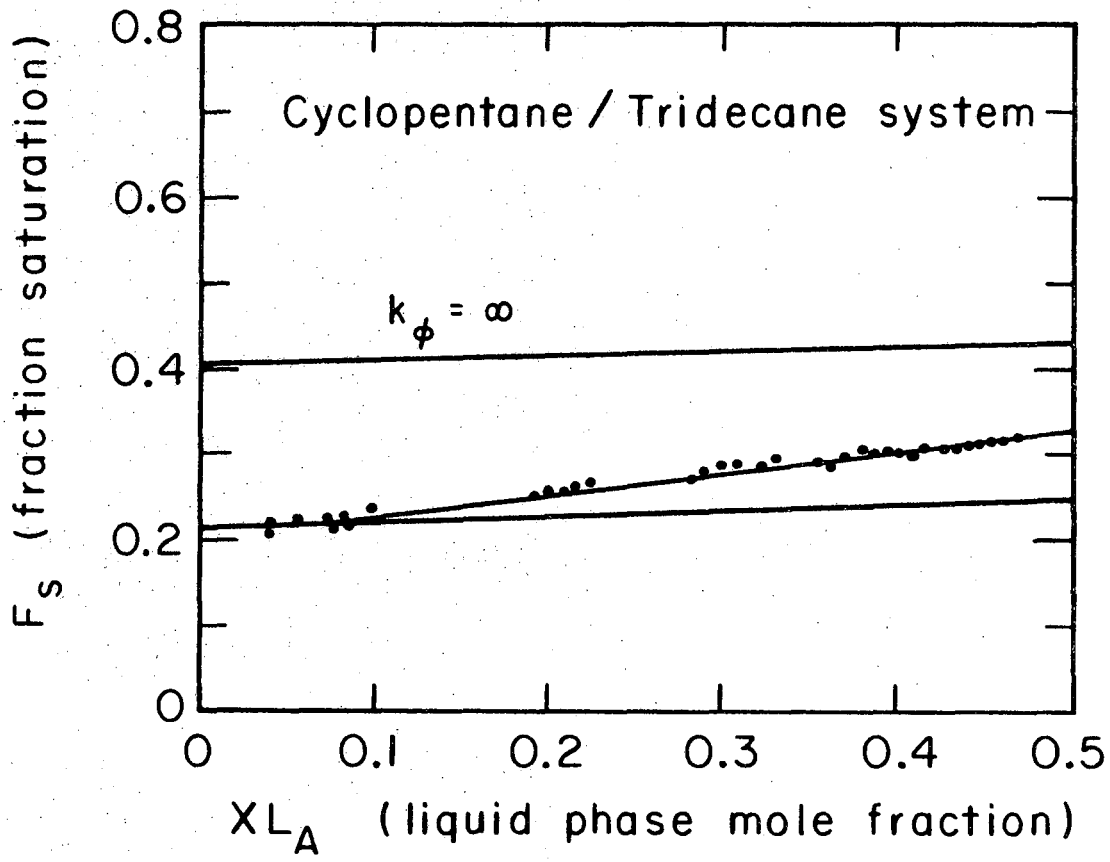

Fig. 24. Gas phase fraction saturation (cup mixing) as a function of liquid phase mole fraction (bulk), for the system; cyclopentane/tridecane evaporating into nitrogen. • ... indicates experimental data, the lower solid line represents the predicted behavior using the high flux addition of resistances approach.
Interfacial temperature = 25 ± 0.1°C

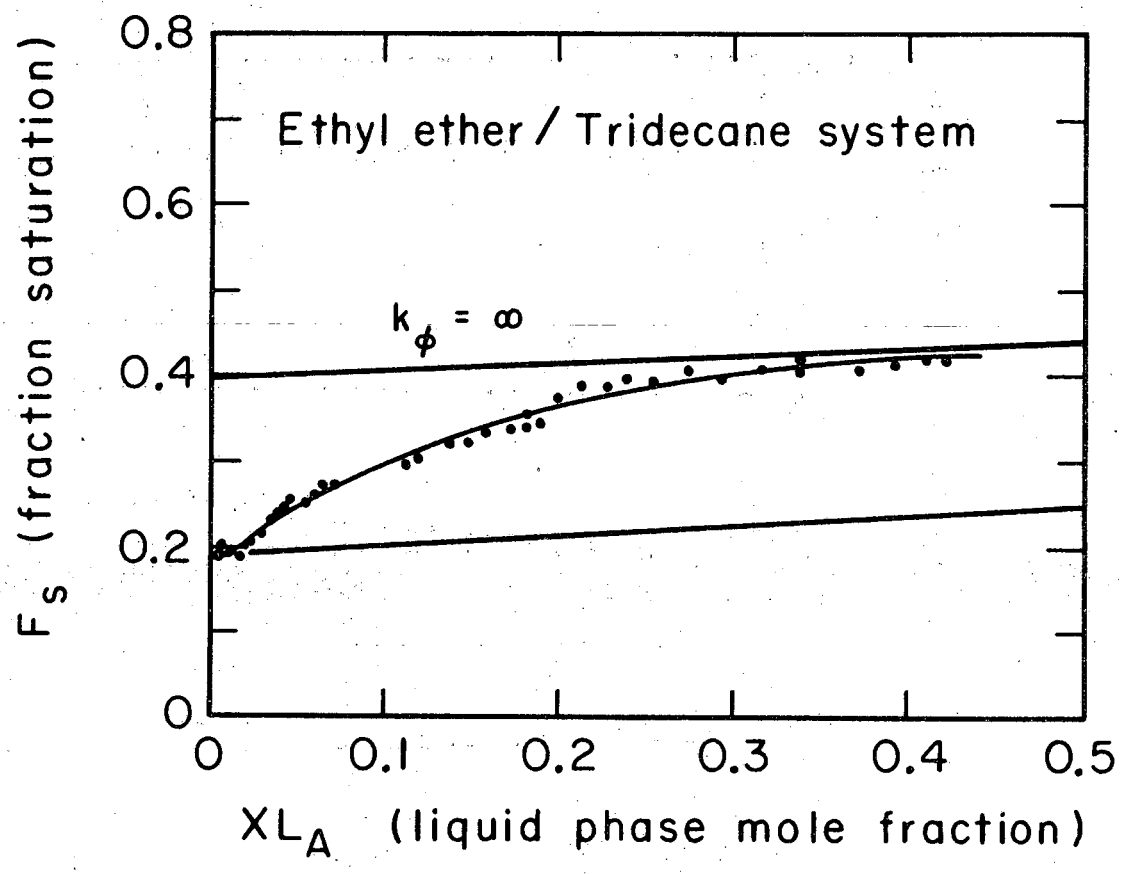

Fig. 25. Gas phase fraction saturation (cup mixing) as a function of liquid phase mole fraction (bulk), for the system; ethyl ether/tridecane evaporating into nitrogen. • ... indicates experimental data, the lower solid line represents the predicted behavior using the high flux addition of resistances approach.
Interfacial temperature = 25 ± 0.1°C

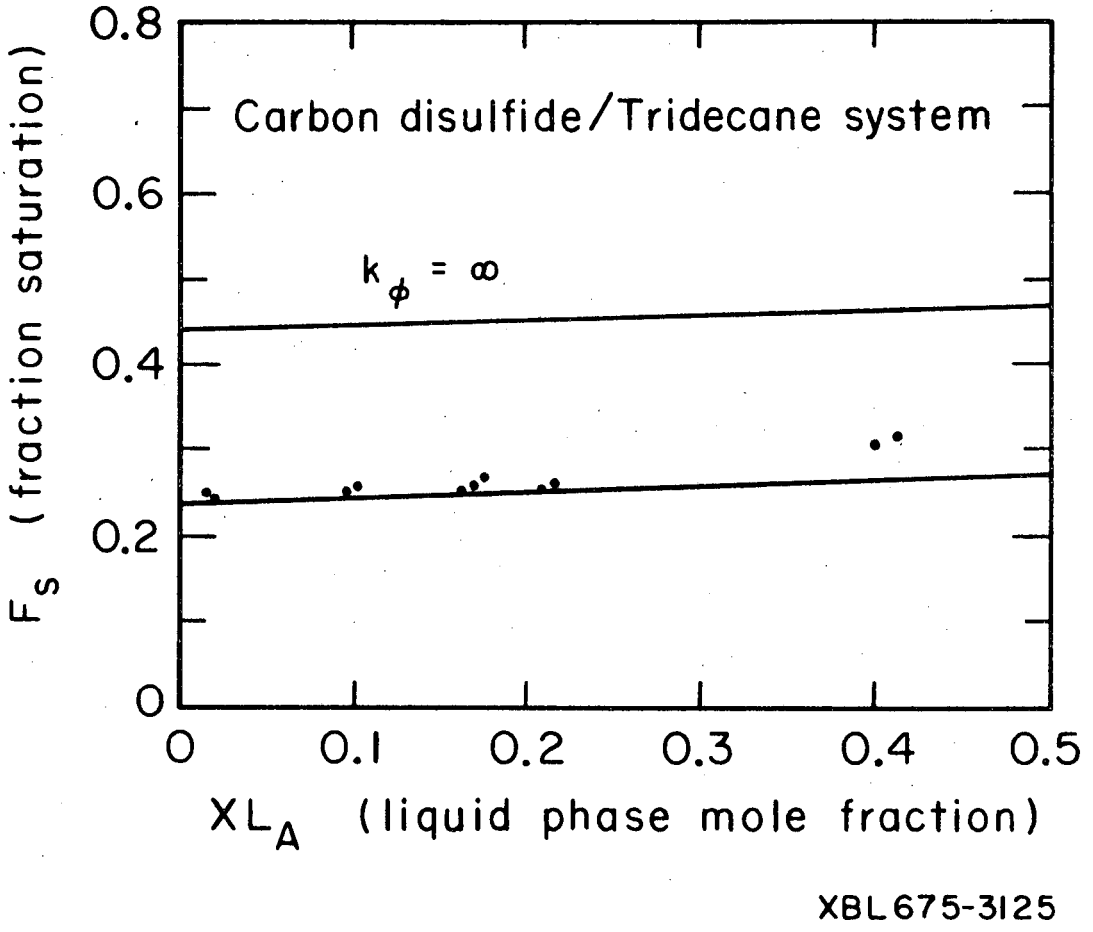

Fig. 26. Gas phase fraction saturation (cup mixing) as a function of liquid phase mole fraction (bulk), for the system; carbon disulfide/ tridecane evaporating into nitrogen. • ... indicates the experimental data, the lower solid line represents the predicted behavior using the high flux addition of resistances approach.
Interfacial temperature = 30 ± 0.1°C

direction from that of tridecane. The results for this system, which are shown in Fig. 26, support this fact with the agreement between experiment and interphase theory remaining quite good at values of XL_A up to 0.30 or more. The deviation which finally begins to occur at the high concentration levels can be attributed to temperature-induced, density-driven cells. This assumption is supported by the calculated value of the Rayleigh number for these conditions, which was $R_{avg} = 1600$; a value which is significantly larger than the theoretical critical value of approximately 650. To show that the cellular convection in the three other experimental systems was apparently not strongly influenced by density driven cells, the values of XL_A which yield a calculated value of $R_{avg} = 1600$ are: for n-pentane/tridecane $XL_A = 0.24$, for cyclopentane/tridecane $XL_A = 0.27$, and for ethyl ether/tridecane $XL_A = 0.22$.

Since the majority of the cellular convection appeared to be attributable to the concentration driven Marangoni effect, an effort was next made to correlate the mass transfer behavior of the liquid phase with the physical parameters which lead to this type of cellular convection.

C. Correlation of Results and Prediction of Cellular Convection

At present the most promising theoretical approach towards predicting the effect of surface tension driven cellular convection upon the mass transfer behavior of a system appears to lie in the solution of the non-linear flow equations. An approach similar to the one used by Malkus and Veronis[49] or that due to Kuo[40] should at least predict the behavior in the region near the critical point for low instability. Unfortunately, as was pointed out earlier, such a solution does not presently exist. An alternative procedure is to use the approach of dimensional analysis, which leads to the following expressions:

$$Sh = fn(Th, Sc, N_{Re}) \qquad (6\text{-}22)$$

and

$$Sh_{cr} = fn(Sc, N_{Re}) \qquad (6\text{-}23)$$

From the above two expressions, and in view of the results obtained by Kuo and others for the somewhat analogous heat transfer problem, we conclude that a resonable form for correlation of the experimental data should be

$$k'_{\phi}/k'_{\phi,cr} = fn\left(\frac{Th}{Th_{cr}}, Sc, N_{Re}\right) \qquad (6\text{-}24)$$

The variable $k'_{\phi,cr}$ is the value of the liquid phase mass transfer coefficient which is predicted theoretically (i.e. the value at the point where the flow instability is first observed, with concentration, flux and physical property corrections to the actual concentration level taken into account.) For this work it was found that a single value of $Th_{cr} = 8000$ was sufficient to predict the point of instability of all the experimental systems studied. A table of the values of XL_A which corresponds to $Th = 8000$ is given below:

n-pentane/tridecane ..... $XL_{A,cr} = 0.029$
ethyl ether/tridecane ..... $XL_{A,cr} = 0.014$
cyclopentane/tridecane ..... $XL_{A,cr} = 0.071$

A correlation of the type given by Eq. (6-24) has the advantage of giving the increase in mass transfer due to the Marangoni effect alone; i.e. $k'_{\phi}/k'_{\phi,cr}$ is determined as a function of the parameters which enter into the Thompson number. Thus the effect due to Marangoni circulation is obtained by simply multiplying the expected mass transfer rate by a correction factor to obtain the final mass transfer rate.

The experimental results of this study are shown in Fig. 27, plotted in the form suggested by Eq. (6-23). As can be seen, the agreement between the three widely differing systems—n-pentane, cyclopentane, and ethyl ether—is quite good when placed on this basis. It is interesting to note that this effect can be quite large for some systems, such as the ethyl ether/tridecane mixture, where the observed value of $k_{\phi,avg}$ was 10 to 20 times the expected value. Another fact which was observed from putting the data in the form given in Fig. 27, was that the initial slope was approximately the same as indicated by the nonlinear heat transfer analysis for density-driven cells, i.e., a 1/4 power dependence upon the Thompson (or Rayleigh) number ratio.[40] The dashed straight line on Fig. 27

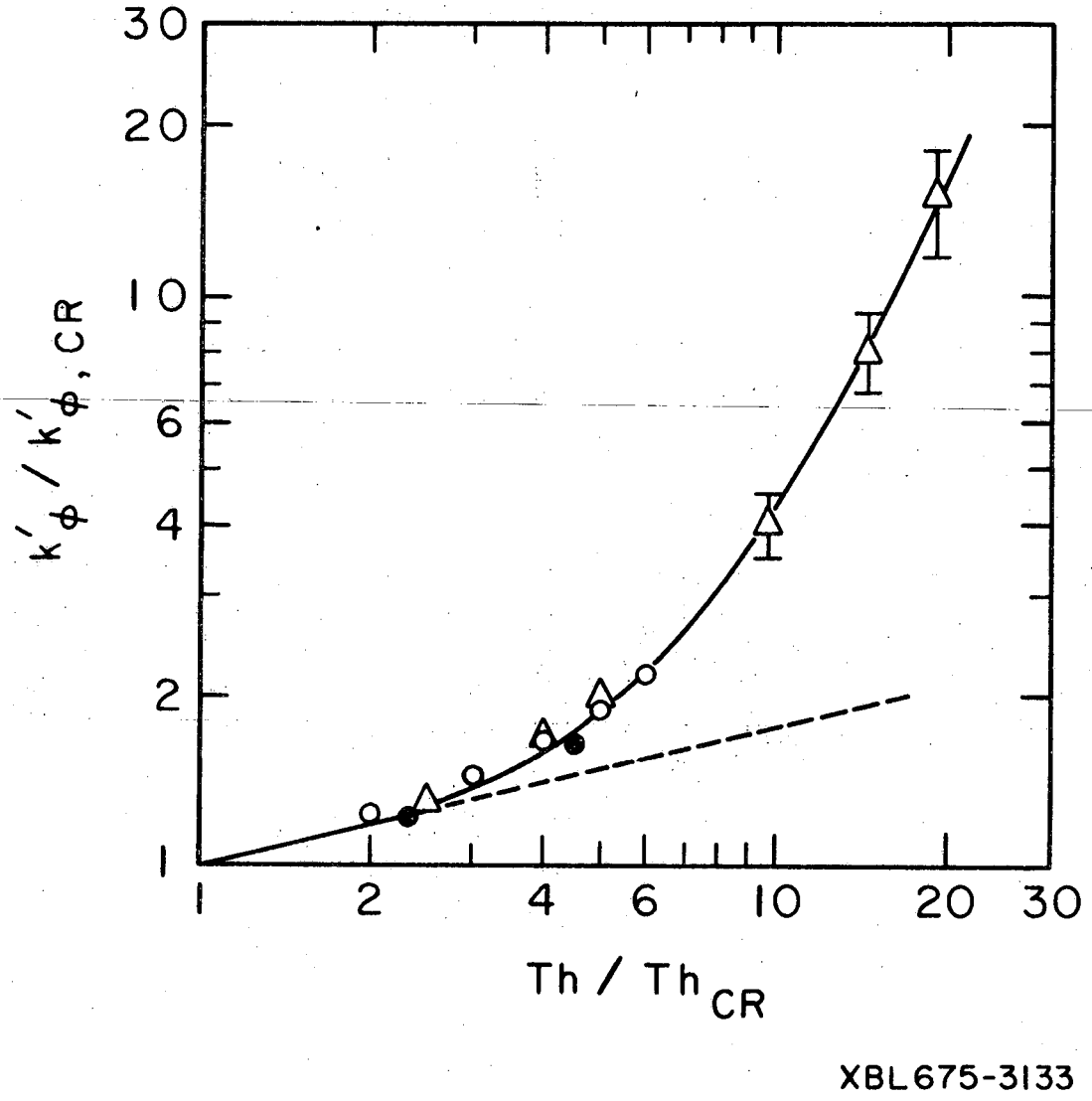

Fig. 27. Correlation of the effect of surface tension driven cellular convection upon liquid phase mass transfer coefficients.

- ● experimental results for the system cyclopentane/tridecane
- o experimental results for the system n-pentane/tridecane
- Δ experimental results for the system ethyl ether/tridecane

Dashed line indicates behavior assuming a 1/4 power dependence of ratio of coefficients on ratio of the Thompson numbers.

indicates the 1/4 power dependence, and can be seen to be tangent to the results obtained experimentally in the vicinity of the critical value of the Thompson number.

It should be noted that due to the similar physical constants of the liquid systems involved, the Sc variation was not large, and therefore the effect of Schmidt number, if any, could not be determined. Also, the effect of different liquid phase Reynolds numbers was not explored in this work. Further experimental work with more diverse systems at widely different flow rates should be carried out to define the above two effects, if they exist. If we examine the quantities entering into the correlation given by Fig. 27, we find that this is essentially a plot of $k'_{\phi}/k'_{\phi,cr}$ versus $\Delta\phi/\Delta\phi_{cr}$; since the other quantities in the Thompson number are only weak functions of concentration.

There are several other factors which need to be explored in more detail experimentally and theoretically. Among these are the effect of the ratio of gas phase to liquid phase mass transfer coefficient, k_x/k_{ϕ}, which was varied only slightly during this work. Substantial changes in this ratio could invalidate the procedure used to calculate $\phi_{A\infty} - \phi_{Ao}$ for use in the Thompson number. A second point is that the liquid depths utilized in this study were rather large; therefore any application of these results to systems having very small liquid depths, or radically different flow characteristics, should be made with caution. Finally, minute concentrations of surface active impurities could radically affect the flow characteristics of the surface tension driven cellular convection. This type of situation would be most likely to occur in an aqueous system, usually bringing about a large reduction in the quantity of cellular convection from that which would be predicted for such a system.

ACKNOWLEDGMENTS

The authors wish to express their appreciation to R. J. Ayen and R. A. Seban for their many helpful suggestions, and to G. G. Young and J. Byce for their aid in the design and construction of the experimental equipment.

The work described was performed in the Lawrence Radiation Laboratory under the auspices of the U. S. Atomic Energy Commission.

APPENDIX A

Experimental Procedures

Due to the large number of variables which had to be monitored during the course of an experimental run, a consistant routine was followed throughout this work, with only slight alterations depending upon the information desired. This experimental routine consisted of the following sequence of steps:

1) The desired concentration level of the solute in the tridecane solvent was selected, and sufficient solute was added to the liquid system to obtain the approximate level of bulk liquid concentration.

2) The liquid re-circulation pump was started, and the liquid was circulated through the system, by-passing the test-section. During this period of time, approximately 1 to 2 hrs, the liquid temperature was adjusted to the desired value by the use of the heater and cooler indicated in Fig. 7. Also, this practice allowed the solute concentration to become constant throughout the liquid system.

3) The liquid was slowly introduced into the test-section, and the by-pass was closed. After the desired liquid flow had been established through the test-section the liquid level was slowly adjusted by admitting air into the lower hold-up tank. If the liquid level was too high, it could be lowered by applying a slight vacuum to the lower hold-up tank.

4) After the liquid flow and level had been established, the gas was admitted from the supply cylinders, and the desired gaseous flowrate was established.

5) Usually at this point the bulk liquid temperature was adjusted slightly to yield the actual interfacial temperature for the particular run conditions. (Note that the interfacial temperature was maintained at a pre-determined value for all runs carried out with a given solute system.

6) The electric timer was started, and all subsequent data taken logged with respect to this timer.

7) Bulk liquid concentration samples were withdrawn using a hypodermic syringe and the sampling probe labled C_1 in Fig. 1. These samples were usually taken between 40 and 60 min apart, since the liquid concentration level changed rather slowly with respect to time.

8) The desired gas stream (either cup mixing or a profile probe) was continuously passed through the chromatograph, and at periodic intervals the gas phase mole fraction was determined.

9) Temperature profiles were also taken at periodic intervals, and the liquid and gas temperature adjusted when necessary. Usually it was possible to maintain the liquid temperature within 0.1 to 0.2 °C of the desired value.

10) Throughout the run, it was necessary to pay constant attention to the liquid level within the test-section, with adjustments usually being made every two or three minutes. With constant manipulation of this type, the level could be maintained within 0.010 in. of the prescribed value.

11) After the conclusion of the run, the liquid samples were analyzed with the chromatograph, and the data placed in the form illustrated by Figs. 28, 29, and 30; i.e., a plot of liquid phase concentration versus run time. From this graph the liquid phase concentration could be obtained for the time interval over which a set of gas phase chromatograms had been taken. Since the liquid concentration did not change appreciable over this time interval, it was considered constant at the value obtained from the graph (see Figs. 28, 29, 30).

The experiments involving the evaporation of pure liquids were run in a similar manner, except they did not require the liquid sampling procedure. Unfortunately, due to the rapid rates of evaporation involved in these experiments, it was impossible to maintain the test-section liquid level using the techniques outlined previously. Consequently, it was necessary to constantly add a stream of liquid from the make-up system (see Fig. 7). Even using this procedure the control of the liquid level was considerably more difficult than in the interphase experiments. This can be seen from the fact that the iso-pentane runs frequently involved liquid losses in excess of 1000 cc/hr.

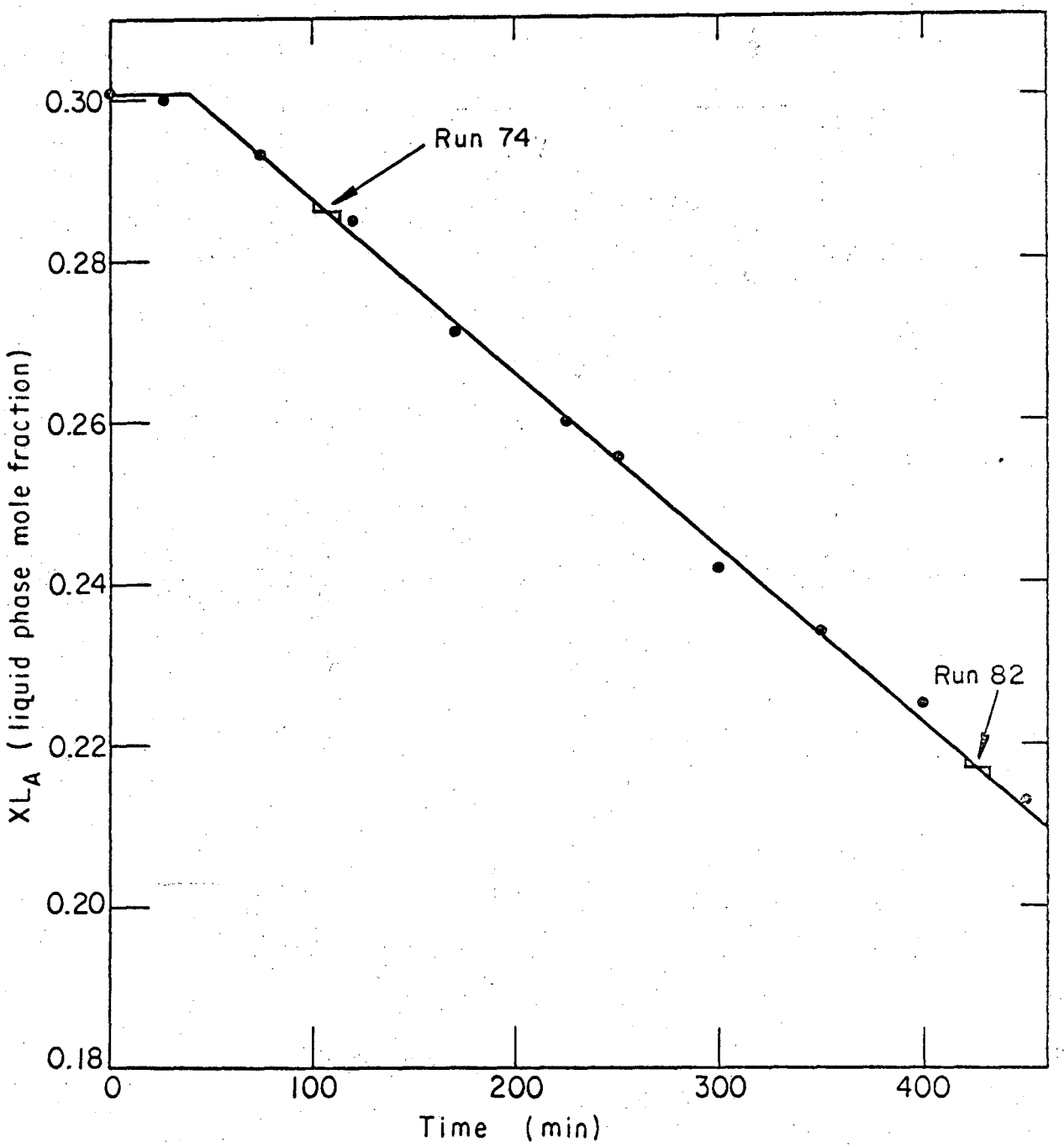

Fig. 28. Behavior of liquid phase concentration with respect to time.
System n-pentane/tridecane
Time for gas sample = 12.5 minutes
Runs # 71 to 83..

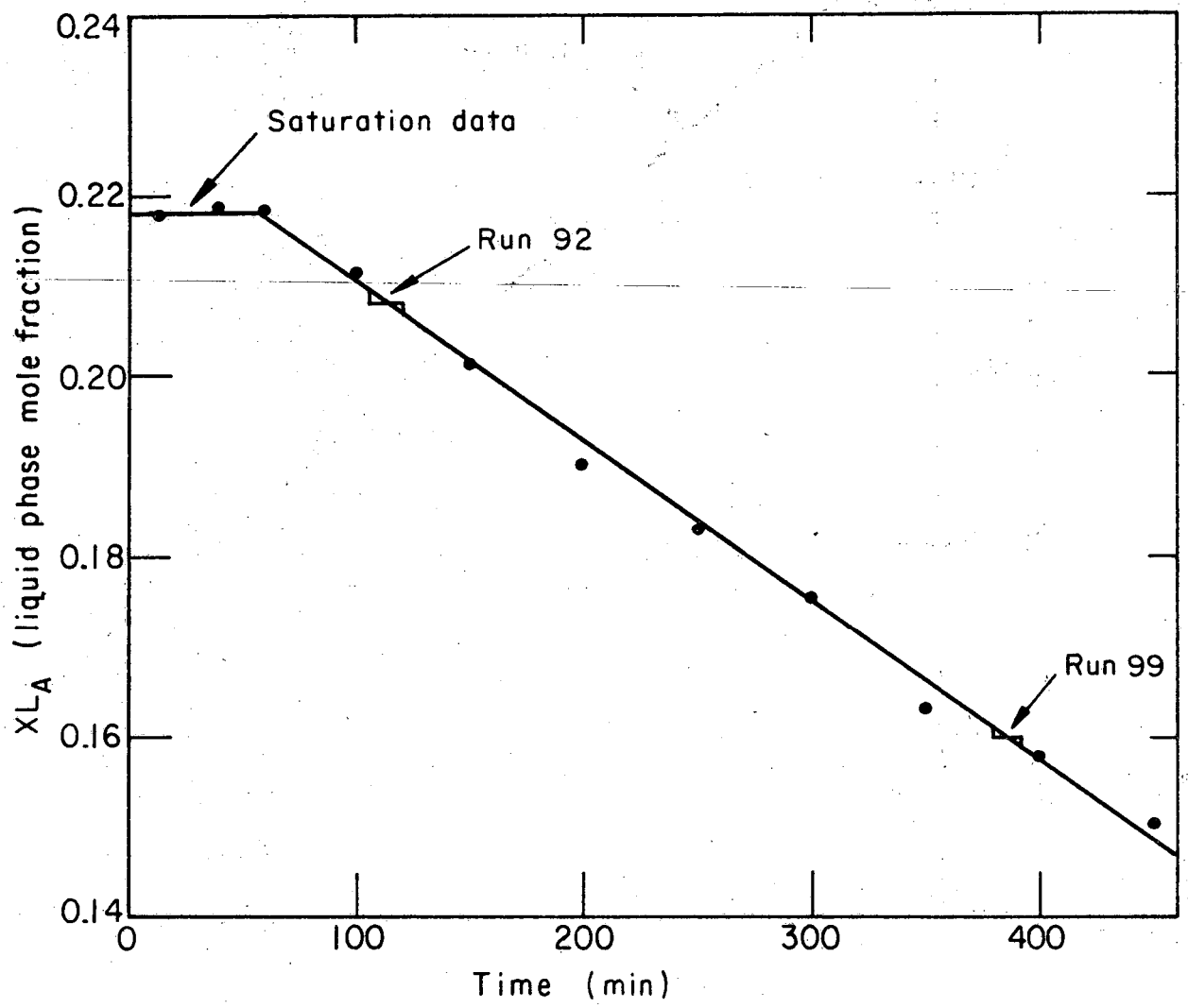

Fig. 29. Behavior of liquid phase concentration with respect to time.
System n-pentane/tridecane
Time for gas sample = 12.5 minutes
Runs # 90 to 100.

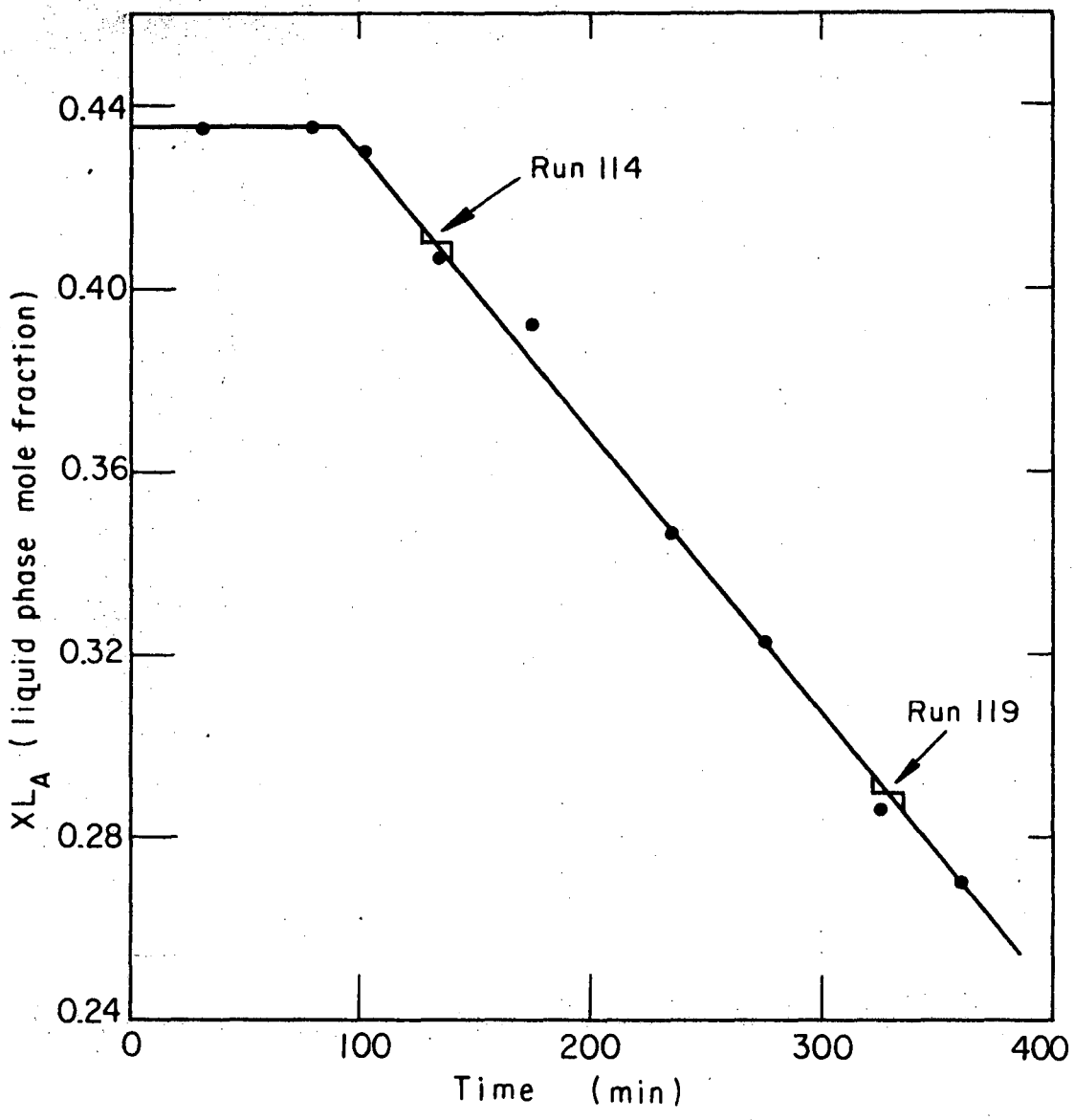

Fig. 30. Behavior of liquid phase concentration with respect to time.

System ethyl ether/tridecane
Time for gas sample = 12.5 minutes
Runs # 112 to 120.

APPENDIX B

Experimental Results

This section is devoted primarily to furnishing additional information about the experimentally obtained results. Included are tabulated results for a large number of runs. Where appropriate, results are also given in graphical form.

Gas-Liquid Heat Transfer Results

Run #	N_{Re} (gas)	N_{Re} (liquid)	gas	T_{in} (gas)	T_{in} (liquid)
14	1200	500	air	33.3 °C	19.8 °C
15	1200	1010	air	33.5	19.4
16	850	440	air	33.8	19.5
17	850	1010	air	33.5	19.2
18	850	735	air	33.5	19.4
19	515	670	air	32.6	19.5
20	520	990	air	33.0	19.1
21	285	990	air	33.0	19.1
22	320	250	air	30.1	20.9
23	155	450	helium	30.4	20.6
24	270	450	helium	32.4	20.8
25	290	370	helium	30.5	21.7
26	83	370	helium	28.5	20.9

See Table I for results of these runs.

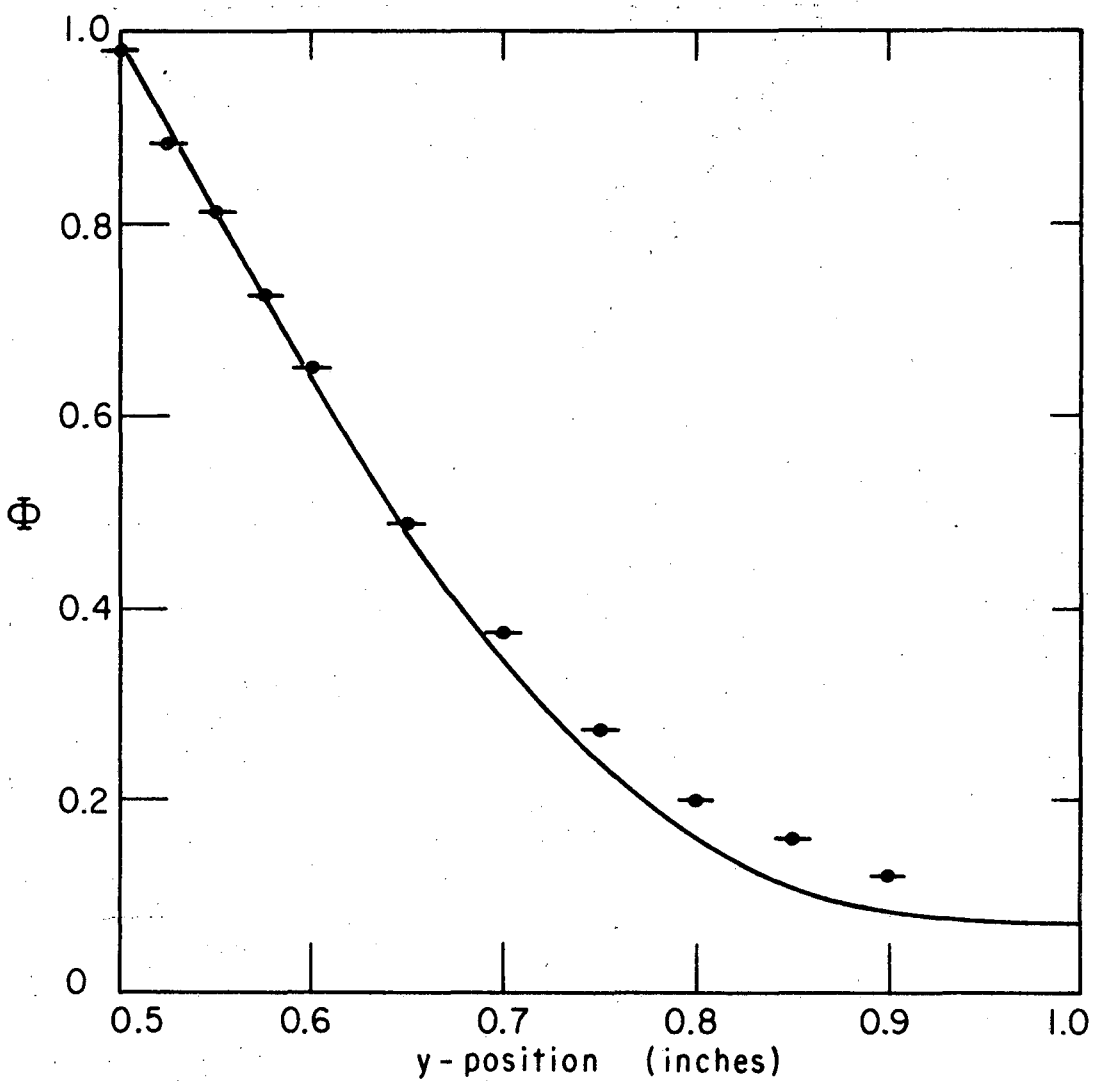

Fig. 31. Dimensionless experimental temperature profile taken at 17.5 in. from the test section inlet; QG = 493 cm^3/sec, QL = 0.810 gpm. Run # 17, System: air/tridecane

● = experimental data
— = theoretically predicted curve

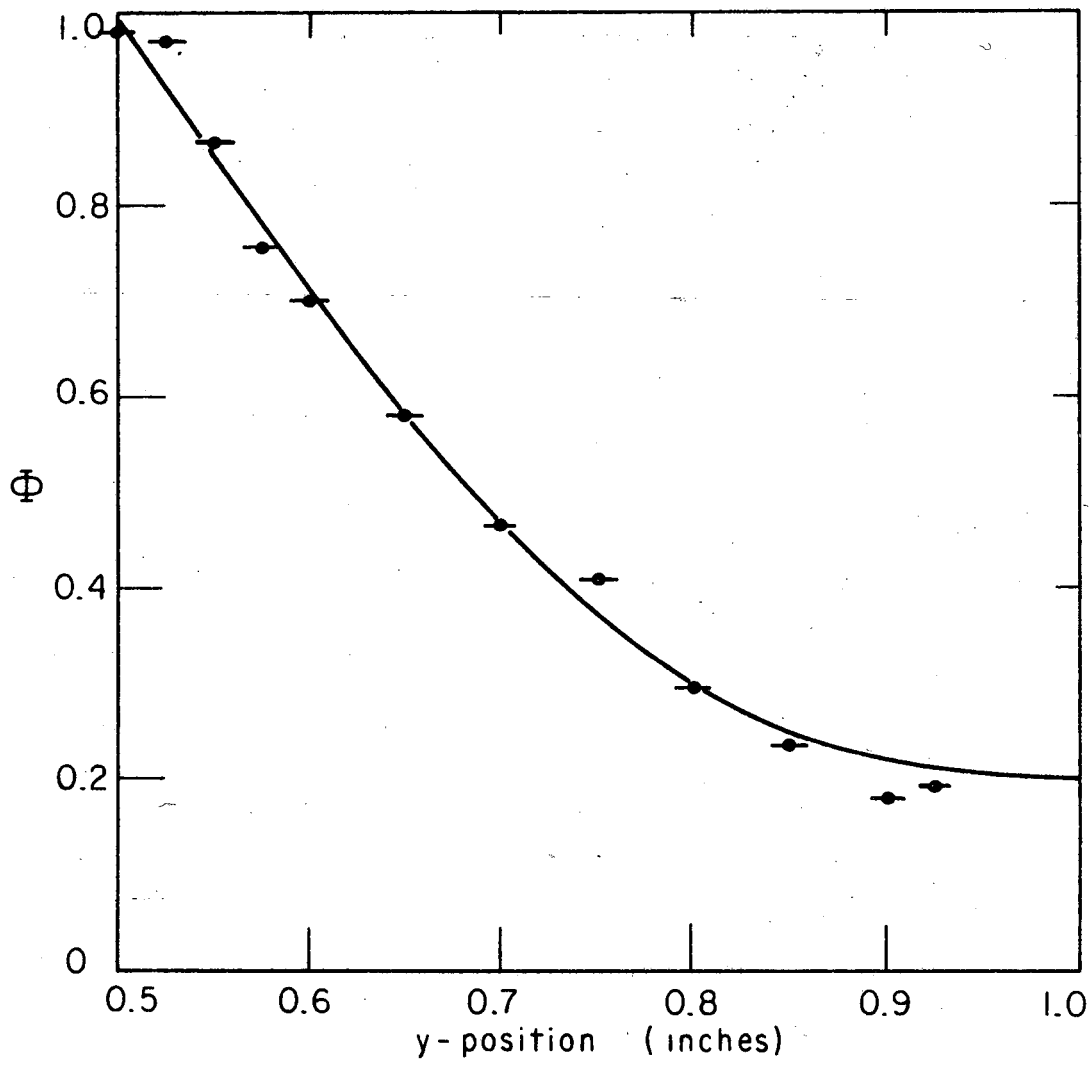

Fig. 32. Dimensionless experimental temperature profile taken at 17.5 in. from the test section inlet; QG = 300 cm^3/sec, QL = 0.795 gpm. Run # 20, System: air/tridecane.

●— = experimental data
— = theoretically predicted curve

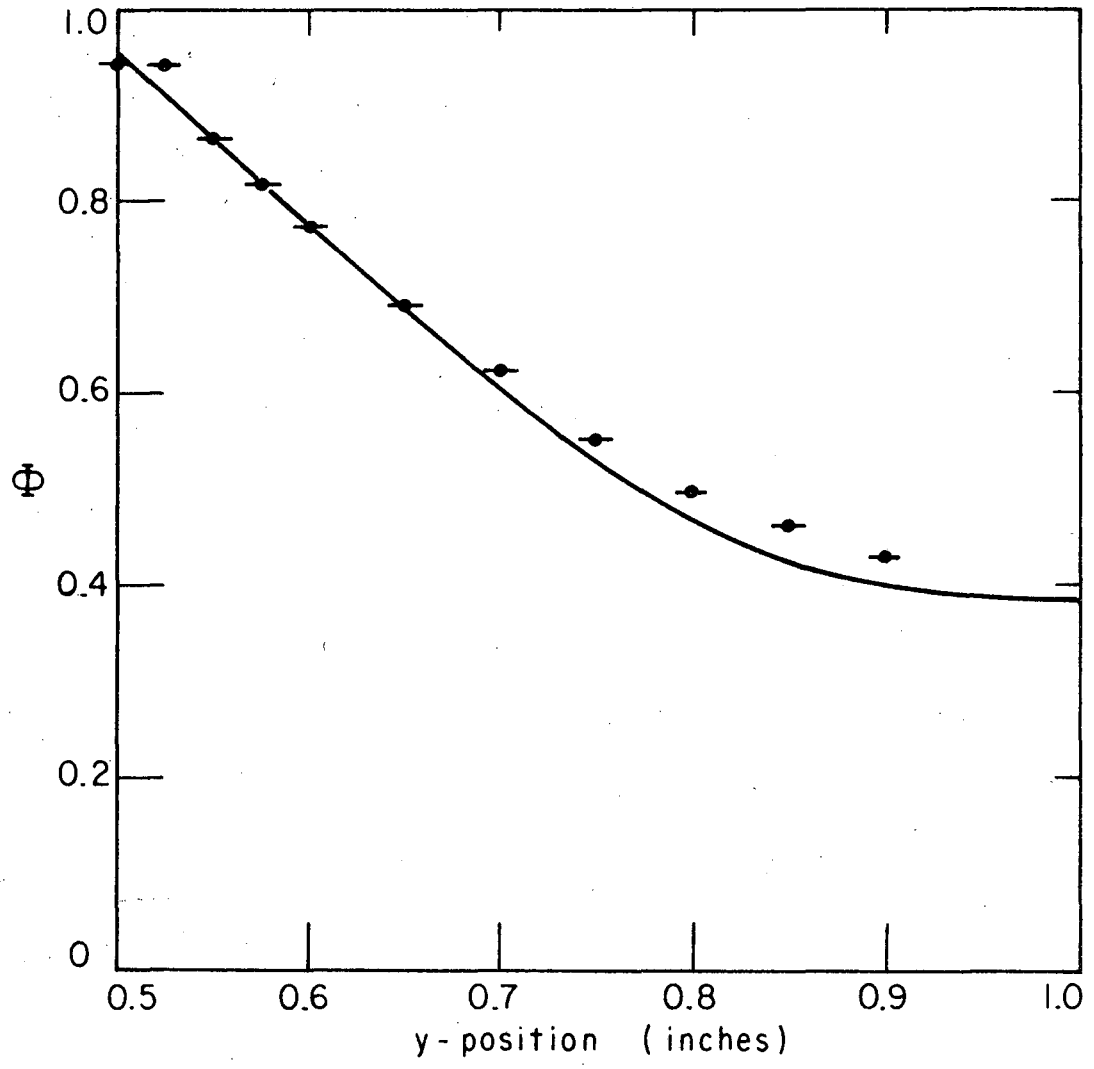

Fig. 33. Dimensionless experimental temperature profile taken at 17.5 in. from the test section inlet; QG = 1540 cm^3/sec, QL = 0.300 gpm. Run # 25, System: helium/tridecane.

● = experimental data
— = theoretically predicted curve

Low Flux Mass Transfer

Run #	QG(cm^3/sec)	QL(cm^3/sec)	T_{int}(°C)	F_s expt'l cup mixing	F_s theory
28	166	24.2	20.6	0.213	0.213
29	100	29.3	20.7	0.310	0.299
30	235	29.3	20.6	0.162	0.146
31	397	29.3	20.6	0.085	0.090
32	166	24.2	20.8	0.220	0.213
33	235	29.3	20.7	0.169	0.146
34	397	29.3	20.7	0.103	0.090

All of the above runs were made with the system:

n-pentane/tridecane – Nitrogen,

where the n-pentane concentration in the liquid phase was in the neighborhood of XL_A = 0.01 for all runs.

Interphase Mass Transfer Data

System: n-pentane/tridecane liquid evaporating into nitrogen

Interfacial Temperature maintained at 20 °C ± 0.2 °C

QG = 166 cm^3/sec QL = 0.400 gpm

Run #	XL_A(bulk)	F_s(cup mixing) (experimental)
58	0.195 to 0.175	0.260 **
59	0.1547	1.0000*
60	0.1515	0.255
61	0.1445	0.258
62	0.1376	0.250
63	0.1320	0.249
64	0.1273	0.240
65	0.1225	0.231
66	0.1184	0.235
67	0.1139	0.228
68	0.1100	0.224
69	0.1054	0.224
70	0.1031	0.971 *
71	0.3005	1.000 *
72	0.298	0.308
73	0.291	0.309
74	0.285	0.299
75	0.277	0.293
76	0.268	0.291
77	0.258	0.290
78	0.249	0.279
79	0.240	0.278
80	0.234	0.273
81	0.226	0.269
82	0.217	0.268
83	0.209	0.264

n-pentane/tridecane system (continued)

Run #	XL_A(bulk)	F_s(cup mixing) (experimental)
90	0.2182	1.000 *
91	0.2165	0.261
92	0.2090	0.258
93	0.2013	0.257
94	0.1930	0.253
95	0.1855	0.247
96	0.1785	0.249
97	0.1732	0.248
98	0.1665	0.250
99	0.1595	0.243
100	0.1530	0.249
101	0.400	1.000 *
102	0.395	0.358
103	0.383	0.344
104	0.373	0.344
105	0.361	0.327
106	0.351	0.322
107	0.341	0.323
108	0.330	0.317
109	0.322	0.304
110	0.313	0.298
111	0.304	0.300

* Data taken at very low gas flow rate to determine equilibrium between the gas and liquid phases.

** Experimental profile integration.

System: ethyl ether/tridecane liquid evaporating into nitrogen

Interfacial temperature maintained at 25°C ± 0.2°

QG = 166 cm^3/sec QL = 0.400 gpm

Run #	XL_A(bulk)	F_s(cup mixing)
112	0.435	1.000 *
113	0.421	0.420
114	0.410	0.422
115	0.391	0.417
116	0.372	0.409
117	0.336	0.406
118	0.314	0.409
119	0.291	0.399
120	0.272	0.404
121	0.267	1.000 *
123	0.252	0.399
124	0.237	0.401
125	0.226	0.391
126	0.212	0.390
127	0.198	0.377
128	0.193	1.000 *
129	0.188	0.346
130	0.181	0.344
131	0.171	0.341
132	0.164	0.353
133	0.154	0.333
134	0.144	0.327
136	0.127	0.327
138	0.119	0.306
141	0.0970	0.304
142	0.0920	0.327
143	0.0865	0.314

ethyl ether/tridecane system (continued)

Run #	XL_A(bulk)	F_s(cup mixing)
152	0.0720	1.000 *
153	0.0700	0.279
154	0.0665	0.277
155	0.0625	0.276
156	0.0585	0.270
157	0.0542	0.267
158	0.0505	0.264
159	0.0463	0.264
160	0.0425	0.264
161	0.0426	0.270
162	0.0408	0.254
165	0.0347	0.240
166	0.0308	0.234
167	0.0278	0.247
168	0.0248	0.236
169	0.0235	0.216
170	0.0220	0.215
171	0.0206	0.202
172	0.0182	0.199
173	0.0170	0.192
174	0.0158	0.200

System: cyclopentane/tridecane evaporating into nitrogen
Interfacial temperature maintained at 25°C ± 0.2°
QG = 166 cm^3/sec QL = 0.400 gpm

Run #	XL_A(bulk)	F_s(cup mixing)
175	0.476	1.000 *
176	0.469	0.315
177	0.463	0.316
178	0.457	0.316
179	0.451	0.312
180	0.443	0.309
181	0.437	0.308
182	0.429	0.304
184	0.417	0.303
185	0.409	0.299
186	0.4080	1.000 *
187	0.4030	0.300
188	0.3965	0.301
189	0.3885	0.301
190	0.3785	0.303
191	0.3710	0.297
192	0.3630	0.285
193	0.3570	0.290
194	0.3360	1.000 *
195	0.3325	0.293
196	0.3215	0.289
197	0.3100	0.289
198	0.3010	0.284
199	0.2925	0.281
200	0.2860	0.276

cyclopentane/tridecane system (continued)

Run #	XL_A(bulk)	F_s(cup mixing)
201	0.2260	1.000 *
202	0.2240	0.268
203	0.2185	0.261
204	0.2110	0.257
205	0.2025	0.255
206	0.1965	0.254
207	0.1000	1.000 *
208	0.0990	0.231
209	0.0952	0.229
211	0.0870	0.224
213	0.0790	0.208
215	0.0742	0.219
217	0.0623	0.215
219	0.0572	0.220
220	0.0550	0.215
221	0.0528	0.218
222	0.0515	0.213
223	0.0424	0.210
224	0.0417	0.203
225	0.0407	0.202

APPENDIX C

Computer Programs

A number of computer programs were used during the course of this work. Some of these were quite complex, such as in the solution of the partial differential equations of convective transport; others were written simply to carry out repetitive, but necessary calculations. All of the important programs used in the work are given in this section along with a brief description of their usage. The programs are written in Fortran IV, and all calculations were carried out utilizing the CDC 6600 digital machine at the Lawrence Radiation Laboratory. The control cards have been omitted since they vary from one location to the next.

GCCALC

The bulk of the experimental data taken were in the form of chromatograms from an Aerograph, Model A-90P2 Gas Chromatograph. Since several thousand readings were taken, these data were recorded on IBM cards, and the necessary calculations carried out by the above program. The calculations involved simply convert the experimentally determined peak areas to solute mole fraction. A number of chromatograms (5 to 10) were taken for each run condition; these were averaged before the calculation of the mole fraction for each run.

The input data are: N, the number of chromatograms for a given run; B(I), the solute peak area in MV-sec; A(I), the nitrogen peak area in MV-sec; No, the experimental run number; R2, the solute peak attenuation factor from the chromatograph; and R1, the nitrogen peak attenuation factor. The calculations are then carried out based on the following equations:

$$AR(I) = A(I)*R1$$

$$BR(I) = B(I)*R2*(F_r)$$

$$RAT(K) = BR(K)/AR(K)$$

where F_r is a calibration factor which relates the mole ratio of the solute to solvent (nitrogen) with the ratio of the respective peak areas. This factor had to be experimentally determined for each system, usually by taking readings on a sample with a know mole ratio. A brief table of the values for several solutes is given below:

solute (nitrogen = solvent)	F_r
n-pentane	0.509 to 0.542
ethyl ether	0.620
cyclopentane	0.682
iso-pentane	0.570

The value of F_r was dependent upon the Chromatograph conditions, and was therefore re-evaluated from time to time, particularly when the conditions were altered. The calculated values of the mole ratios for all the chromatograms taken during a given run are then averaged by the program and an average value of the mole fraction calculated.

The program then procedes to a package of liquid phase data which have the exact same format as the gas phase calculations outlined above. The calculations are carried out in an analogous manner to yield the liquid phase mole fraction for the solute/Tridecane systems. It should be noted that both the liquid and gas calculations are made by referring the solute to the solvent peak areas, rather than attempting to maintain a known sample volume and using this as a basis.

TOHETR

Since all of the experimental heat transfer data were taken in the form of temperature profiles, it was necessary to integrate these profiles in order to obtain the experimental cup mixing temperature. This was done using the relationship,

$$T_{\text{cup mixing}} = \int_0^b \frac{T(y)\ u_x(y)\ dy}{b\ U_{avg}}$$

```
      PROGRAM GCCALC (INPUT,OUTPUT,TAPE2=INPUT, TAPE3=OUTPUT)
      DIMENSION C(20), D(20), CR(20), DR(20), BAT(20)
      DIMENSION A(20), B(20), AR(20), BR(20), RAT(20)
      WRITE (3,114)
  114 FORMAT (31H0 EXPERIMENTAL GLC CALCULATIONS)
   30 READ(2,31) NO
   31 FORMAT(I3)
      IF (NO) 50, 200,50
   50 READ(2,10)N, ((A(I), B(I)), I=1,N)
   10 FORMAT (I2/(F3.1,F3.1))
      READ (2,101) R1,R2
  101 FORMAT(2F3.0)
      DO 103 I=1,N
      AR(I) = A(I)*R1
  103 BR(I) = B(I)*R2*.509
      SUM = 0.0
      DO 104 K=1,N
      RAT(K) = BR(K)/AR(K)
  104 SUM = SUM + RAT(K)
      XX = SUM/FLOAT(N)
      XG = XX/(1.0 + XX)
      WRITE (3,105) NO, XG
  105 FORMAT(12H RUN NUMBER ,I3, 23H       GAS PHASE CONC.= ,F5.4//)
      WRITE (3,106) (RAT(K), K=1,N)
  106 FORMAT (25X,F5.4)
      WRITE (3,111)
  111 FORMAT (1H0)
      GO TO 30
  200 CONTINUE
      WRITE (3,107)
  300 READ(2,301) NB
  301 FORMAT(I2)
      IF (NB) 302, 400, 302
  302 READ (2,303) M,((C(I), D(I)), I= 1,M)
  303 FORMAT (I2/(F3.1,F3.1))
      READ (2,305) R3, R4
  305 FORMAT (2F3.0)
      DO 307 I = 1,M
      CR(I) = C(I)*R3*2.277
  307 DR(I) = D(I)*R4
      BUM = 0.0
      DO 309  J= 1,M
      BAT(J) = CR(J)/DR(J)
  309 BUM = BUM + BAT(J)
      XY  = BUM/FLOAT(M)
      XL  = XY/(1.0 + XY)
      WRITE (3,311) NB, XL
  311 FORMAT (13H SAMPLE NO.  ,I2, 21H     LIQUID CONC. =  ,F4.3//)
      WRITE(3,312) (BAT(J) , J= 1,M)
  312 FORMAT (25X, F5.4)
      WRITE (3,111)
      GO TO 300
  400 STOP
      END
```

```
      PROGRAM TOHETR (INPUT,OUTPUT,TAPE2=INPUT, TAPE3=OUTPU3)
C  GAS LIQUID VELOCITY PROFILES (CM/SEC) AND EXPTL TOTAL HEAT TRANSFER CALC
      DIMENSION TL(25),VG(25), VL(25), YL(25), TG(25), YG(25)
      DIMENSION TLVL(25), TGVG(25)
  100 READ(2,101) QG, QL, VISCL, VISCG
  101 FORMAT (4F10.0)
   20 READ(2,201) TG(1), TG(2), TG(3), TG(4), TG(5), TG(6), TG(7)
   21 READ(2,201)TG(8),TG(9),TG(10),TG(11),TG(12),TG(13),TG(14)
   22 READ(2,201)TG(15),TG(16),TG(17),TG(18),TG(19),TG(20),TG(21)
      READ(2,201)TL(1),TL(2),TL(3),TL(4),TL(5),TL(6),TL(7)
      READ(2,201)TL(8),TL(9),TL(10),TL(11),TL(12),TL(13),TL(14)
      READ(2,201)TL(15),TL(16),TL(17),TL(18),TL(19),TL(20),TL(21)
  201 FORMAT (7F10.0)
      READ (2,25) CPG, CPL
   25 FORMAT (2F10.0)
      B=1.27
      W = 7.62*.915
      C3=(1.5/(W*B))*(QG + QL*(VISCL/VISCG))/(1.0 + VISCL/VISCG)
      C2G=(1.0/B**2)*(4.0*B*C3 - 6.0*QL/W)*(VISCL/VISCG)
      C2L= C2G*(VISCG/VISCL)
      C1G=-(C2G*B + C3)/B**2
      C1L= (B*C2L - C3)/B**2
C DEFINE YL(1)  AS THE INTERFACE,  THUS THE WALL POSITION IS YL(21)
      YL(1) = 0.0
      DO 103 I=1,21
      VL(I) = C1L*YL(I)**2 + C2L*YL(I) + C3
  103 YL(I+1) = YL(I) -B/20.0
      YG(1) = 0.0
      DO 104 I = 1,21
      VG(I) = C1G*YG(I)**2 + C2G*YG(I) + C3
  104 YG(I + 1) = YG(I) + B/20.0
      DO 105 I=1,21
  105 TLVL(I) = TL(I)*VL(I)
      ODD = 0.0
      EVEN = 0.0
      DO 106 I=2,18,2
  106 EVEN = EVEN + TLVL(I)
      DO 107 I=3,19,2
  107 ODD= ODD + TLVL(I)
      DELY = 0.0635
     OSUML=(DELY/3.0)*(TLVL(1) +4.0*EVEN +2.0*ODD + TLVL(20))
     1  + (DELY/2.)*(TLVL(20) + TLVL(21))
      HTL = W*CPL*SUML
      DO 108 I=1,21
  108 TGVG(I) = TG(I)*VG(I)
      UGH = 0.0
      EBE = 0.0
      DO 109 I=2,18,2
  109 EBE = EBE + TGVG(I)
      DO 110 I=3,19,2
  110 UGH = UGH + TGVG(I)
      SUMG = (DELY/3.0)*(TGVG(1) + 4.0*EBE + 2.0*UGH + TGVG(20))
      HTG = W*CPG*SUMG
      WRITE (3,400)
  400 FORMAT (33H LIQUID AND GAS VELOCITY PROFILES///)
```

```
      WRITE (3,401) (YL(I), VL(I), I=1,21)
  401 FORMAT (4H YL= 1PE16.7, 5H  VL= E16.7)
      WRITE (3,402) (YG(I), VG(I), I=1,21)
  402 FORMAT (4H YG= 1PE16.7, 5H  VG= E16.7)
      WRITE (3,408) QG, QL
  408 FORMAT (5H QG=  1PE16.7, 5H QL= E16.7)
      WRITE (3,405) QG, HIG
  405 FORMAT(4H QG= 1PE16.7, 6H  HTG= E16.7)
      WRITE (3,406) QL, HTL
  406 FORMAT(4H QL= 1PE16.7, 6H  HTL= E16.7)
C  END OF EXPTL HEAT TRANSFER CALCULATIONS, NOW TO CALC. THE BEEK AND
C  BAKKER GROUP, AND THE VALUE OF THEORETICAL AVGK
  500 READ(2,501) DIFFG
  501 FORMAT (F10.0)
        XO=17.0625 * 2.54
      GRP = (C2G**2)*DIFFG*XO/C3**3
      GUMP = C3**3/(C2G*C2G*DIFFG)
      STAR = C2G*DIFFG/(XO*C3)
      IF (GRP - 0.1) 503,503,504
  503 AVGK = STAR*((4.0/3.1416)**.5*XO**.5*GUMP**.5 + XO/4.0)
      GO TO 515
  504 IF (GRP - 10.0)505,505,506
 5050 AVGK = (C3*DIFFG/XO)**.5*(1.2036 + .0616*GRP - .00787*GRP**2
     1 + .00037*GRP**3)
      GO TO 515
  506 DG=DIFFG
      AVGK=(C3*DG/XO)**.5*(1.615*GRP**.1667*(.5+.375/(GRP**.333))-.193)
  515 CONTINUE
      CHB = AVGK*(XO/(C3*DIFFG))**0.5
      WRITE(3,516) DIFFG, C2G, C3
  516 FORMAT(7H DIFFG= 1PE16.7, 6H  C2G= E16.7, 5H  C3= E16.7)
      WRITE(3,517) GRP, CHB, AVGK
  517 FORMAT(5H GRP= 1PE16.7, 6H  CHB= E16.7, 7H  AVGK= E16.7, 1H ///)
      WRITE (3,403)
  403 FORMAT (1H1)
      GO TO 100
      STOP
      END
```

This integration was carried out numerically using a total of 20 points in the y-direction (corresponding to a Δy of 0.025 in.).

The input data are: QG, the gas flow rate in cm^3/sec; QL, the liquid flow rate in cm^3/sec; VISCL, the liquid viscosity in centipoise; VISCG, the gas viscosity in centipoise; TG(I), the gas temperature matrix, starting at the upper wall and proceeding downward to the liquid interface; TL(I), the liquid temperature matrix, starting at the gas-liquid interface and proceeding downward to the bottom of the channel. Also necessary are CPG; the gas heat capacity in cal/mole °C, and CPL; the liquid heat capacity in the above units. The program first generates exact velocity profiles for the gas and liquid phases. Then these are put in matrix form, multiplied by the appropriate temperature matrix, and the resulting matrix integrated using a Simpson's rule integration technique. For comparison, the input experimental run conditions are also fed into the appropriate equations for calculating average heat transfer coefficients (AVGK) using the theoretical approach outlined by Beek and Bakker. Provision is also made for printing the calculated velocity profiles as functions of the vertical distance parameters YL, and YG.

PROINT

Several experimental concentration profiles were obtained in the gas phase; thus it was desirable to have a method for integrating these to obtain cup mixing concentrations. This calculation was carried out by the program PROINT. The input data consisted of: QG, QL, VISCL, and VISCG, all defined as in the prior discussed program TOHETR. Additional input data are: IRUN, the experimental run number; and CG(I), the experimentally determined concentration profile which was usually expressed as gas phase mole fraction. The calculational procedure is very similar to that used in TOHETR; with the integration of the concentration-velocity matrix again being carried out by a Simpson's procedure.

```
      PROGRAM PROINT (INPUT,OUTPUT,TAPE2=INPUT, TAPE3=OUTPUT)
      DIMENSION       VG(25), VL(25), YL(25), CG(25), YG(25),CGVG(25)
  100 READ(2,101) QG, QL, VISCL, VISCG
  101 FORMAT (4F10.0)
      IF (QG)20,600,20
      READ(2,59) IRUN
   59 FORMAT(I3)
   20 READ (2,201)(CG(I), I=1,21)
  201 FORMAT (21F3.1)
      B=1.27
      W = 7.62*.915
      DELY = 0.0635
      C3=(1.5/(W*B))*(QG + QL*(VISCL/VISCG))/(1.0 + VISCL/VISCG)
      C2G=(1.0/B**2)*(4.0*B*C3 - 6.0*QL/W)*(VISCL/VISCG)
      C2L= C2G*(VISCG/VISCL)
      C1G=-(C2G*B + C3)/B**2
      C1L= (B*C2L - C3)/B**2
C DEFINE YL(1)  AS THE INTERFACE,  THUS THE WALL POSITION IS YL(21)
      YL(1) = 0.0
      DO 103 I=1,21
      VL(I) = C1L*YL(I)**2 + C2L*YL(I) + C3
  103 YL(I+1) = YL(I) -B/20.0
      YG(1) = 0.0
      DO 104 I = 1,21
      VG(I) = C1G*YG(I)**2 + C2G*YG(I) + C3
  104 YG(I + 1) = YG(I) + B/20.0
      DO 108 I=1,21
  108 CGVG(I) = CG(I)*VG(I)
      UGH = 0.0
      EBE = 0.0
      DO 109 I=2,18,2
  109 EBE = EBE + CGVG(I)
      DO 110 I=3,19,2
  110 UGH = UGH + CGVG(I)
     OSUMG = (DELY/3.0)*(CGVG(1) + 4.0*EBE + 2.0*UGH + CGVG(20))
     1 + (DELY/2.)*(CGVG(20) + CGVG(21))
       CAVG = SUMG*W/QG
      WRITE(3,77)
   77 FORMAT(53H  INTEGRATION OF CONCENTRATION PROFILE TO GET CMC      )
      WRITE(3,78)  IRUN
   78 FORMAT(///13H RUN NUMBER    I3)
      WRITE (3,408) QG, QL
  408 FORMAT (5H QG=  3PE16.2, 5H QL= 2PE16.2//)
      WRITE (3,700) CAVG
  700 FORMAT(16H AVERAGE CONC. = E16.7///)
      WRITE (3,400)
  400 FORMAT (33H LIQUID AND GAS VELOCITY PROFILES//)
      WRITE (3,401) (YL(I), VL(I), I=1,21)
  401 FORMAT (4H YL= 1PE16.7, 5H  VL= E16.7)
      WRITE (3,402) (YG(I), VG(I), I=1,21)
  402 FORMAT (4H YG= 1PE16.7, 5H  VG= E16.7)
  600 STOP
      END
```

VARDIF

The major purpose of this program was to ascertain the effect of allowing the liquid phase diffusivity to vary as a function of liquid phase concentration. The program is essentially an extension of an earlier program, GRAGRA, written by Byers. A detailed description of GRAGRA can be found in Byers' Ph.D. Thesis,[13] and thus will not be repeated here. The major changes which are employed in VARDIF fall into three categories. The first is that an exact velocity profile was inserted for both the gas and liquid phases. The older program due to Byers used parabolic profiles in both phases; however, it neglected the small effect of acceleration of the liquid interface due to the gas phase drag.

The second, and most important, change in the calculational procedure is that the liquid phase diffusivity is allowed to vary with liquid phase concentration in VARDIF. This was carried out in the following manner: First, a functional dependence of the diffusivity, DIFFL, upon liquid phase concentration was determined (see Appendix D). The solution of the partial differential equations was carried out by marching one step at a time in the Z direction, using the matrix of concentrations from the previous Z step to calculate the next step. This means that one always has available the values of liquid phase concentration as a function of Y from the prior Z step. This matrix of concentrations was used to calculate a matrix of diffusivities, using the previously mentioned functionality. This diffusivity matrix could now be inserted into the calculational procedure where the constant value of diffusivity had formerly been used, and the resulting set of equations solved in the same manner as before, with a value of D_L 1/2 step out of line. This procedure was then repeated for each step down the channel in the Z direction. The calculations are carried out subject to the assumptions of low flux and concentration level.

The third, and least important change from GRAGRA was the form of the input data. This was necessitated by the insertion of the exact velocity profile, which requires several physical variables not required by Byers' earlier version. These input variables were QG, QL, VISCG, VISCL,

```
0
      PROGRAM VARDIF (INPUT,OUTPUT,TAPE2=INPUT, TAPE3=OUTPUT)
      DIMENSION S(500),T(0500),XR(0500),XTS(0500)
      DIMENSION UL(500), X(500), A(500), B(500), C(500), VAR(500)
      DIMENSION G(500), O(500), Q(500), XNU(500), W(500)
      DIMENSION YD(500) ,DFL(500),BET(500)
C     GAS LIQUID MASS TRANSFER IN CONFINED COCURRENT FLOW
   50 READ(2,1) K,M,N ,IND,JELL,TOL,JS
    1 FORMAT(5I5,F6.3,I2)
C CALCULATION OF VELOCITIES WITH INTERFACIAL DRAG INCLUDED
   71 READ(2,107) QG, QL
  107 FORMAT (2F12.6)
      READ (2,108) XIN  , DIFFG, XLONG, HNCON, VISCL, VISCG
  108 FORMAT(6F12.6)
C      CALCULATION OF DIFFL (FOR PENTANE TRIDECANE SYSTEM ONLY)
      DIFFL =.00001* (2.11 - 1.22*XIN)/(1.92 - 2.74*XIN + 1.06*XIN*XIN)
      AA = 1.27
      BB = 1.27
      WW = 7.62*.915
      UINT =(1.5/(WW*BB))*(QG+QL*(VISCL/VISCG))/(1.0+VISCL/VISCG)
      C2G = (1.0/BB**2)*(4.0*BB*UINT - 6.*QL/WW)*(VISCL/VISCG)
      C2L = C2G*(VISCG/VISCL)
      C1G = -(C2G*BB + UINT)/(BB*BB)
      C1L =  (BB*C2L - UINT)/(BB*BB)
      GP = ((DIFFL*XLONG)/(UINT*BB*BB))* .01
      R = ((DIFFG*XLONG)/(UINT*BB*BB))* .01
      F = DIFFL/(DIFFG*HNCON)
C NOTE THAT VAV IS CORRECTED AT THIS POINT FOR THE VELOCITY SIDE CORRECTIONS
      VAV = QG/(BB*WW*UINT)
      CON=(GP/R)**0.5/F
      WRITE(3,67)
   67 FORMAT(53H1RESULTS OF GRAETZ SOLUTION WITH INTERFACIAL VELOCITY)
      WRITE (3,80)
   80 FORMAT (28H AND LIQUID PHASE RESISTANCE //)
      WRITE (3,455) JS
  455 FORMAT (10H RUN NO.    , I2)
      WRITE(3,104) F,R,GP
  104 FORMAT (3H F=,F10.3,3H R=,F10.6,4H GP=,F10.6)
      H1=1./(FLOAT(K)*TOL)
      KRUMB=M-K
      H2=1./FLOAT(KRUMB)
      P=1./FLOAT(N)
      WRITE(3, 4 ) H1,H2
    4 FORMAT(F6.4,19H LIQUID Y INCREMENT,F6.4,17H GAS Y INCREMENT    )
      WRITE(3, 5 ) P
    5 FORMAT(F6.4,22H X DIRECTION INCREMENT    )
      WRITE(3,110)   VAV,AA,BB
  110 FORMAT( 7H VAV = ,F10.5,4H AA=,F10.5,5H BB= ,F10.5)
      RAG=R/VAV
      WRITE (3,91)  CON
   91 FORMAT(10H SIGMA*H= ,E10.4)
      CON=F  *H2/H1
      DIV=1.0
      MD=1
```

```
      TR=1./TOL
      II=0
      KO=K+1
      KO1=KO+1
      L=M+1
      MR=1
      DO  15  J=1,K
   15 X(J)=1.0
      DO 81 J=KO,L
   81 X(J)=0.0
      ALP=(H2*H2)/(R*P)
      DO 401 J=1,K
      DFL(J) = .00001*(2.11 - 1.22*X(J)*XIN)/
     1 (1.92 - 2.74*X(J)*XIN + 1.06*X(J)*X(J)*XIN*XIN)
  401 BET(J)=(H1*H1)/(P*.01*(DFL(J)*XLONG)/(UINT*BB*BB))
     *  CON = (DFL(K)/(DIFFG*HNCON))*H2/H1
      X(K+1)=(BET*CON)/(BET*CON+ALP)
      VEX=X(K+1)
      XNUI=(1.0-VEX)/H1
   18 ALP=(H2*H2)/(R*P)
      DO 402 J=1,K
      DFL(J) = .00001*(2.11 - 1.22*X(J)*XIN)/
     1 (1.92 - 2.74*X(J)*XIN + 1.06*X(J)*X(J)*XIN*XIN)
  402 BET(J) = (H1*H1)/(GP*DFL(J)*P/DIFFL)
      CARL=0.5*BET(1)*((1.-TR*TR)-TR*H1/2.0-H1*H1/12.)
      CARG=ALP*0.25*H2*(3.*VAV-1.+H2/2.-VAV*H2)
      WRITE(3,60)  ALP,CARG,CARL  ,BET(1)
   60 FORMAT(6H ALP=  ,F10.5,6H CARG= ,E10.4,6H CARL= ,E10.4,6H BET= ,E1
     10.4//)
      DO 19 I=MR,N
       DO 403 J=1,K
      DFL(J) = .00001*(2.11 - 1.22*X(J)*XIN)/
     1 (1.92 - 2.74*X(J)*XIN + 1.06*X(J)*X(J)*XIN*XIN)
  403 BET(J) = (H1*H1)/(GP*DFL(J)*P/DIFFL)
      CARL=0.5*BET(1)*((1.-TR*TR)-TR*H1/2.0-H1*H1/12.)
      CON = (DFL(K)/(DIFFG*HNCON))*H2/H1
      A(1)=-(1.+4.*CARL/3.)
      YD(L)=1.0
      YD(1)=-  TR
      YD(KO)=0.0
      B(1) =1.-2.*CARL/3.
      DO 8 J=2,K
      YL    =H1*(FLOAT(J)-FLOAT(KO))
      YD(J)=TR* YL
      UL(J) = C1L*BB*BB*YL*YL/UINT + C2L*BB*YL/UINT + 1.0
      A(J) =-(1.+ BET(J)*UL(J))*2.0
      C(J  ) = 1.
    8 B(J) = 1.
      A(K+1)=-(CON*(1.+BET(K))+    (1.+ALP))
      B(K+1)=1.
      C(K+1)=CON
      DO 9 J=KO1,L
      J1=J-KO
      Z=H2*FLOAT(J1)
      YD(J)=Z
```

```
      VAR(J)=(C1G*BB*BB*Z*Z/UINT + C2G*BB*Z/UINT + 1.0    )*ALP
      A(J)=-(1.+VAR(J))*2.0
      C(J)=1.
    9 B(J)=1.
      C(L)=1.-2.*CARG/3.
      A(L)=-(1.+4.*CARG/3.)
      O(1)=A(1)
      DO 10 J=2,L
      Q(J-1)=B(J-1)/O(J-1)
   10 O(J)=A(J)-C(J)*Q(J-1)
      II=II+1
      G(1)=((1.-4.*CARL/3.)*X(1)-(1.+2.*CARL/3.)*X(2))/O(1)
      DO 31 J=2,K
      W(J)=X(J)
   31 G(J)=(-X(J-1)-X(J+1)+2.*(1.-BET(J)*UL(J))*X(J)-C(J)*G(J-1))/O(J)
      G(K+1)=(-CON*X(K)-X(KO1)+(CON*(1.-BET(K))+(1.-ALP))*X(K+1)-
     1C(KO)*G(K))/O(KO)
      DO 12 J=KO1,M
      W(J)=X(J)
   12 G(J)=(2.*(1.-VAR(J))*X(J)-X(J-1)-X(J+1)-C(J)*G(J-1))/O(J)
      G(L)=((1.-4.*CARG/3.)*X(L)-(1.+2.*CARG/3.)*X(M)-C(L)*G(M))/O(L)
      W(K+1)=X(K+1)
      W(1)=X(1)
      W(L)=X(L)
      X(L)=G(L)
      DO 13 J=1,M
      J1=L-J
      J2=J1+1
   13 X(J1)=G(J1)-Q(J1)*X(J2)
      DO 75 JO=1,JELL
      SET=X(1)
      X(1)=1.25*((1.-2.*CARL/3.)*X(2)-(1.-4.*CARL/3.)*W(1)+(1.+.667*CARL
     1)*W(2))/(1.+4.*CARL/3.)-0.25*SET
      S(1)=ABS(X(1)-SET)
      DO  32 J=2,K
      SET=X(J)
      X(J)=-1.25*(X(J+1)+X(J-1)-2.*(1.-BET(J)*UL(J))*W(J)+W(J+1)+W(J-1))
     1/A(J) - 0.25*SET
   32 S(J)=ABS(X(J)-SET)
      SET=X(K+1)
      X(KO)= -1.25*(X(K)*CON+X(KO1)+W(K)*CON-(CON*(1.-BET(K))+(1.-ALP))
     1*W(KO)+W(KO1))/A(KO )-0.25*SET
      S(KO )=ABS(X(K+1)-SET)
      DO 79 J=KO1,M
      SET=X(J)
      X(J)=-(X(J+1)+X(J-1)-2.*(1.-VAR(J))*W(J)+W(J+1)+W(J-1))/A(J)*1.25-
     10.25*SET
   79 S(J)=ABS(X(J)-SET)
      SET=X(L)
      X(L)=-(X(M)*C(L)-(1.-4.*CARG/3.)*W(L)+(1.+2.*CARG/3.)*W(M))/A(L)
     1*1.25-0.25*SET
      S(L)=ABS(X(L)-SET)
      DO 33 JOKE= 1,L
      IF(S(JOKE)-0.0001)  33,33,75
   33 CONTINUE
```

```
      GO TO 34
   75 CONTINUE
   34 CONTINUE
      DO 11 J=1,L
      IF(X(J)-1.0)    11,11,40
   40 X(J)=1.00
   11 CONTINUE
      Y=P*FLOAT (I)    *DIV*RAG
      WRITE(3, 14)  Y
   14 FORMAT(16H GRAETZ NUMBER= ,F9.5    )
      T(II)=Y
      XN=(19.*X(KO) -30.*X(KO1) +18.*X(K+3)-10.*X(K+4) +3.*X(K+5)) /
     1(12.*H2)
      XS2=X(K+1)
      IF( MOD (I,IND))20,42,20
   42 WRITE (3,38) (X(J) , J=1,K,5)
   38 FORMAT(25X,F10.6)
      WRITE(3, 35)  XS2
   35 FORMAT(30H INTERFACIAL CONCENTRATION IS F7.5///)
      WRITE(3,22 )
   22 FORMAT(//30X,3H P ,28H GAS PROFILE FROM INTERFACE //)
       WRITE(3,23)(X(J) , J=KO1,L,2)
   23 FORMAT(25X,F10.6)
   20 VEX=X(K+1)
      XNU(I)=XN
      WRITE(3,30)  XN ,JO
   30 FORMAT(5X,24H LOCAL NUSSELT NUMBER = ,E10.4,20H CONVERGENCE AT J =
     1 ,I3)
      SUM1=0.
      SUM2=0.
      DO 28 J=KO1,M,2
      SUM1=(VAR(J)/ALP)*X(J)+SUM1
   28 SUM2=(VAR(J+1)/ALP)*X(J+1)+SUM2
      CUP = H2 * (4.0 * SUM1 +2.*SUM2+XS2)/(VAV*3.00)
       XNS = CUP / Y
      WRITE (3,17)   CUP,XNS
   17 FORMAT(5X,25H CUP MIXING CONCENTRATION ,E12.6,16H AVG NUSSELT NO=,
     1E12.6//)
   19 CONTINUE
      READ (2,2)  LR,MD  ,IND
    2 FORMAT(2I2,I5)
      IF(LR)  3,6,3
    3 DI =FLOAT(MD)
      R=R*DI
      GP =GP*DI
      DIV=DIV*DI
      DO 41  I=1,N
      MO=I/MD
      IF(MOD(I,MD))   41,16,41
   16 XNU(MO)=XNU(I)
   41 CONTINUE
      MR=N/MD +1
      MR1=MR
      GO TO 18
    6 SUM1=0.
```

```
      SUM1=0.
      SUM2=0.
      NO=N-2
      DO 24 J=1,NO,2
      SUM1=XNU(J)+SUM1
   24 SUM2=XNU(J+1)+SUM2
      XNUSLT=P*(4.*SUM1+2.*SUM2+4.*XNU(N-1)+XNU(N)+XNUI) /3.
      WRITE (3,25) XNUSLT
   25 FORMAT(27H THE AVE NUSSELT NUMBER IS ,E10.4)
      SUM1=0.
      SUM2=0.
      SUM3=0.0
      SUM4=0.0
      DO 26 J=K01,M,2
      SUM1=(VAR(J)/ALP)*X(J)+SUM1
      SUM3=VAR(J)/ALP +SUM3
      SUM4=VAR(J+1)/ALP+SUM4
   26 SUM2=(VAR(J+1)/ALP)*X(J+1)+SUM2
      CUP1=H2*      (4.*SUM1+2.*SUM2+1.00)/(VAV*3.00)
      WRITE(3,27 )  CUP1
   27 FORMAT(//37H CUP MIXING CONC FROM EXIT PROFILE = ,E10.4    )
       VEL=XNUSLT*R/VAV
      WRITE(3,29 )  VEL
   29 FORMAT(43H CUP MIXING CONC FROM INTERFACIAL FLUXES = ,E10.4 )
      READ (2,449) LMN
  449 FORMAT(I2)
      IF (LMN) 82, 450, 82
   82 GO TO 50
  450 STOP
      END
```

and DIFFG, all of which have the same meaning as in the programs already described (see TOHETR). In addition, the variables XIN, or inlet liquid phase mole fraction; HNCON, which is the value of the Henry's law constant in dimensionless form; and XLONG, the overall exposure length in centimeters, were utilized. All other variables are described in Appendix D of Byers' Ph.D. Thesis.

LEVHIF

The purpose of this program was to carry out the numerical solution of Eq. (5-24), subject to the boundary conditions given by (5-25). As was mentioned earlier, the equation is first put into the Crank-Nicholson six-point implicit form; then the resulting tridiagonal matrix is solved using the Thomas method.

The input consisted of two cards; the first contained the variables DELX, the x-direction step size; DELY, the y-direction step size; M, the number of steps in the x-direction; and N, the number of steps in the y-direction. The second card contained the variables QG, the volumetric gas flow rate; DAB, the gas phase diffusion coefficient; and XAI, the interfacial mole fraction of component A. To increase the generality of the solution, the two physical variables, QG and DAB, could be replaced with the constants K_1 and K_2 from Eq. (5-24); and, since K_1 (CK1) and K_2 (CK2) are calculated from these variables within the program, this substitution would be quite simple. This would allow any desired physical system to be represented; however, the results as presented in Fig. 14 are in a general form and allow one to calculate the high flux correction factor from a knowledge of R_{AB} for any system.

The program listing is broken into a number of portions through the use of comment statements, and can be conveniently explained by using these as guides. The first portion is concerned with the calculation of the constants which arise in the difference equation representation of the partial differential equation.

The second section allows one to define any desired inlet concentration profile as an initial condition.

The third section had to be inserted due to stability problems which arose from the infinite flux at the start of the solution. This mathematical singularity arises because the flux, and hence v_{yo}, has been defined as being proportional to $x^{-1/3}$. Thus when $x = 0$, an infinite value of v_{yo} arises, which creates initial instabilities. The method chosen to remedy this situation was to calculate the first x-direction step using an analytic expression, derived from the low flux Leveque solution. While this procedure was not absolutely necessary, it did result in an accelerated convergence to the correct solution.

The remaining sections are concerned with the generation of several vectors (ALP, G, D, W) which are used in the course of the Thomas solution. The final values of the concentration profile, X(I,2), are then generated from the previous profile, X(I,1), and these vectors.

The concentration-velocity vector, Q(I), is then generated and integrated using a Simpson's rule subroutine, SIMPIN, to yield a value for the average mass transfer coefficient, FLIN.

The local mass transfer coefficient was also calculated (DRVT), using a five-point derivative subroutine (DERIV). The values calculated using this method tended to oscillate rather wildly at the start of the solution; therefore the calculation of DRVT was delayed until ten x-direction steps had been taken. The local transfer coefficients were then integrated starting at the fourteenth x-direction step to yield a second value of the average transfer coefficient (FLOP).

```
      PROGRAM LEVHIF (INPUT, OUTPUT, TAPE2=INPUT, TAPE3=OUTPUT)
      DIMENSION A1(4000),A2(100),X(4000,2),ALP(4000),W(4000),D(4000)
      DIMENSION G(4000), Q(4000), DRVT(100)
      EQUIVALENCE (ALP,D)
      EQUIVALENCE (Q,G)
      READ (2,101) DELX, DELY, M, N
  101 FORMAT(2F10.0, I4, I3)
      WRITE (3,1)
    1 FORMAT(1H1)
      READ (2,100) QG, DAB, XAI
  100 FORMAT (3F10.0)
      WRITE (3,4)
    4 FORMAT(51H SOLUTION OF THE LEVEQUE PROBLEM AT HIGH FLUX RATES///)
      WRITE (3,5) DELY, DELX
    5 FORMAT (11H DELTA Y = 1PE16.7, 15H      DELTA X = 1PE16.7)
      WRITE (3,6)M , N
    6 FORMAT(19H NO. OF Y POINTS = I4,23H      NO. OF X POINTS = I3//)
      WRITE (3,7) QG, XAI
    7 FORMAT ( 6H QG = F6.2, 9H    XAI = F5.4//)
C
C   CALCULATION OF NECESSARY CONSTANTS FOR THE DIFFERENCE EQUATIONS
C
       XLONG = 45.72
      C1 = 0.7114*QG
      FAT = 1.0 + 0.40*XAI - 0.0457*XAI**2 + .3714*XAI**3
      C2 =(.480*XAI*(QG*DAB**2)**(1./3.) )*FAT
      CK1 = 0.006117*C2/C1
      CK2 = DAB/(C1*2090.3)
      MP1 = M + 1
      MM1 = M - 1
      MM2 = M - 2
      DO 120 I=1,MP1
  120 A1(I) = 2.0*((FLOAT(I))*DELY**3)/(DELX*CK2)
      DO 121 J=1,N
  121 A2(J) = (CK1/CK2)*(2.0*DELY)/((FLOAT(J))*DELX)**(1./3.)
C
C     DEFINITION OF INITIAL CONCENTRATION PROFILE AT X=0
      DO 122 I=2,M
  122 X(I,1) = 0.0
C
C   DEFINITION OF CONCENTRATION PROFILE FOR FIRST STEP OF CALCULATIONS
C    USING THE LEVEQUE SOLUTION TO CALCULATE THE PROFILE
C
      DO 135 I = 1,M
      IM1 = I - 1
      XB = XLONG*FLOAT(IM1)*DELY*(C1/(9.*DAB*DELX*XLONG))**(1./3.)
      XBF = 1.0500*XB - .214*XB*XB - .0490*XB**3
      CHA = 2.0
      IF (XB.GE.CHA) GO TO 136
      BAA = 0.893
      IF (XBF.GE.BAA) GO TO 136
  135 X(I,1) = 1.0 - XBF/.893
  136 CONTINUE
C  CALCULATION OF PARAMETERS FOR APPLICATION IN THE THOMAS METHOD
      DO 123 I= 1,MM1
```

```
  123 ALP(I) = - (2.0 + A1(I))
      W(1) = ALP(1)
      DO 124 I = 2, MM1
  124 W(I) = ALP(I) - 1.0/W(I-1)
C
C  THE REMAINING PARAMETERS ( D(I), G(I)) ARE FNS OF X-POSITION (N)
      DO 150 J = 3,N
      JM1 = J - 1
      D(1)= (2.-A1(1) - A2(J-1))*X(2,1)+ (A2(J-1)-1.)*X(3,1) - 2.0
          DO 125  I=2,MM2
  125 D(I) = -X(I,1) + (2.-A1(I  )-A2(J-1))*X(I+1,1)+(A2(J-1)-1.0)*
     1 X(I+2,1)
      D(M-1) = -X(M-2,1) + (2. - A1(M-2)- A2(J-1))*X(M-1,1)
      G(1) = D(1)/W(1)
      DO 126 I=2,MM1
  126 G(I) = (D(I) - G(I-1))/W(I)
C
C  NOW WE CAN CALCULATE X(M,2) FROM X(M,1) AND G(I) , W(I)
      X(1,1) = 1.0
      X(1,2) = 1.0
      X(M,2) = 0.00
      X(M-1,2) = G(M-1)
      DO 127 I=2,MM2
  127 X(M-I,2) = G(M-I) - (1.0/W(M-I))*X(M-I+1,2)
C
C  CALCULATION FINISHED FOR THIS STEP, NOW TO PRINT THE RESULTS
C
      ZIP = DELX*FLOAT(JM1)
      WRITE(3,3) J, ZIP
    3 FORMAT (10X, 3H J=  I3,18H        Z-LENGTH = 1PE16.7,//)
      Q(1) = 0.00
      DO 129 I = 2,MM2
      IM1 = I - 1
  129 Q(I) = FLOAT(IM1)*X(I,2)
      EPSIL = .01
      DO 130 I = 1,M,40
      IM1 = I - 1
      YDIST = DELY*FLOAT(IM1)
      IF (X(I,2).LE.EPSIL) GO TO 131
      WRITE(3,2) X(I,2), I,YDIST
    2 FORMAT(13H   X(I,2) =  1PE16.7,8H   I =  I4,12H   Y-DIST = E16.7)
  130 CONTINUE
  131 CONTINUE
      FLIN= 32.525*QG*DELY*SIMPIN(Q,MM2,DELY)/(DELX*FLOAT(JM1))
      WRITE(3,10) FLIN
   10 FORMAT(/// 15H  KAVG (INT) = 1PE16.7)
      FLIP = AVGK(QG,DAB,JM1,DELX)
      WRITE (3,11) FLIP
   11 FORMAT(/// 15H  KAVG (LEV) = 1PE16.7)
C
C   PROCEDURE FOR THE CALCULATION OF KAVG FROM INTEGRATION OF FLUX(INT)
C
       JM10 = J - 10
      JDIV = J - 9
      IF (JM10) 299,202,202
```

```
  202 DRVT(JDIV) =(DAB*DERIV(X(1,2),X(2,2),X(3,2),X(4,2),X(5,2),DELY))/
     1(XLONG*(1.0 - XAI)*DELX*FLOAT(JDIV))
      WRITE(3,15) DRVT(JDIV)
   15 FORMAT(25X, 16H  DRVT(JDIV) =  1PE16.7)
      IF (JM10) 299,203,204
  203 ADCON = FLIP
  204 CONTINUE
       JEBE = (J/2 - (J + 1)/2)
      IF (JEBE) 299,206,206
  206 IF (J-14) 299,205,205
  205 CONTINUE
      FLOP = SIMPIN(DRVT,JDIV ,DELX) + ADCON
      WRITE(3,12) FLOP
   12 FORMAT(///18H  KAVG (DERIV) =  1PE16.7)
  299 CONTINUE
C
C      PUT THE NEW CONCENTRATION PROFILE IN PLACE OF THE OLD
C      AND PROCEED TO THE NEXT STEP IN THE Z-DIRECTION
C
      DO 128 I= 2,M
  128 X(I,1) = X(I,2)
      WRITE (3,1)
  150 CONTINUE
  200 STOP
       END
      FUNCTION  SIMPIN(ARG,NUMB,DELTA)
C       SIMPSON'S RULE INTEGRATION OF THE MATRIX (ARG), WITH
C       THE NO. OF ELEMENTS = NUMB, AND SPACING = DELTA
      DIMENSION  ARG(500)
      ODD = 0.0
      EVEN = 0.0
      NNN1 = NUMB - 1
      NNN2 = NUMB - 2
      DO 500 I = 2,NNN1,2
  500 EVEN = EVEN + ARG(I)
      DO 501 I = 3,NNN2,2
  501 ODD = ODD + ARG(I)
      SIMPIN = (DELTA/3.0)*(ARG(1) + 4.*EVEN + 2.*ODD + ARG(NUMB) )
      RETURN
      END
      FUNCTION DERIV(XY1, XY2, XY3, XY4, XY5, DELTA)
C
C  UNSYMETRICAL  FIVE-POINT DERIVATIVE FORMULA FOR FLUX EVALUATION
C  WHERE XY1 = INTERFACE (THAT IS POINT WHERE DERIV IS EVALUATED...)
      DERIV =(1.0/(12.0*DELTA))*(-25.*XY1 + 48.*XY2 - 36.*XY3 + 16.*
     1  XY4 - 3.*XY5)
      RETURN
      END
      FUNCTION  AVGK(QG, DAB, J, DELX)
C
C       CALCULATION OF KG AVERAGE USING THE LEVEQUE SOLUTION
      AVGK =.2013*((QG*(DAB**2))/(FLOAT(J  )*DELX))**(1./3.)
      RETURN
      END
```

APPENDIX D

Physical Properties

All the physical properties given in this section will be reported in cgs units. Since the experimental conditions were frequently non-isothermal, the properties which are temperature dependent will be presented as functions of temperature. Also, because of the extremely wide range of liquid concentrations which were used in the study, a number of properties will be presented in their concentration dependent forms.

The normal-tridecane which was utilized in this study was actually a "still cut" with the following composition:*

$n\text{-}C_{12}$ --- 16.0 mole %
$n\text{-}C_{13}$ --- 57.5 mole %
$n\text{-}C_{14}$ --- 25.0 mole %
$n\text{-}C_{15}$ --- 1.0 mole %

However, since the properties of normal alkanes are quite well-behaved as a function of chain length in this range, it was felt that the mixture could be handled by calculating it's properties from the properties of the above pure components, weighting each by it's particular mole fraction in the mixture. This method was experimentally confirmed in the case of both density and viscosity to better than 0.5% accuracy. It should also be pointed out that the most important properties to the study—density, diffusivity, and surface tension—are very weak functions of chain length between C_{12} and C_{15}. To illustrate the above method, we see that the density of the mixture, ρ_{mix}, can be calculated by:

$$\rho_{mix} = 0.16\rho_{12} + 0.575\rho_{13} + 0.25\rho_{14} + 0.015\rho_{15}$$

$$\rho_{mix} = 0.15(0.749) + 0.575(0.756) + 0.250(0.763) + 0.015(0.768)$$

$$\rho_{mix} = 0.757$$

---

*Composition was determined using temperature programmed gas chromatography.

This value compares quite well with the experimentally obtained value of 0.756 (all values taken at 25°C.) In a similar manner we can obtain an average molecular weight for the mixture:

$$MW_{mix} = 0.16(170.33) + 0.575(184.35) + 0.25(198.38) + 0.015(212.40)^{**}$$

$$MW_{mix} = 186.04$$

1. Molecular Weights and Critical Properties

The values of molecular weight and critical properties were obtained from two sources: Maxwell's "Data Book on Hydrocarbone"[51] for the alkanes, and the "Handbook of Physics and Chemistry"[31] for the remaining substances. Numerical values are listed in the following table:

Substance	Molecular Weight (gms/gm-mole)	Critical Temp. (°K)	Critical Pressure (atm)
n-Pentane	72.15	469.8	32.6
Cyclo pentane	70.13	512.0	44.6
Isopentane	72.15	460.6	32.4
Ethyl ether	74.12	466.9	35.5
Carbon disulfide	76.13	552	78.0
n-Tridecane	186.04	--	--
Nitrogen	28.0	126.2	33.5
Helium	4.00	5.2	2.26

2. Vapor Pressure and Surface Tension

a. Pure substances. There are two comprehensive works on organic chemical properties, both of which were used to obtain the vapor pressure and surface tension behavior of the substances of interest as function of temperature. These works are: "Physical Properties of Orangic Compounds", "Advances in Chemistry Series";[3] and "Physicochemical Properties of Pure Organic Compounds", by Timmermans.[79] The data reported in this section reflect the most recent given in the above two works, particularly when

Physical Properties of Normal Alkanes

Substance	Density (gm/ml) 25°C	Thermal Conductivity (cal/sec°Ccm)	Heat Capacity (cal/gm°C) 20°C	Normal Boiling Pt. (°C)	100 mm Vapor Press. (°C)	Viscosity (cp.) 20°C	Surface Tension (dynes/cm) 20°C
Pentane	0.626	0.000322	0.600	36.1	-20.2	0.239	16.0
Hexane	0.660	0.000329	0.550	68.7	15.8	0.314	18.4
Heptane	0.684	0.000335	0.530	98.4	41.8	0.409	19.3
Octane	0.704	0.000337	0.525	125.6	65.7	0.542	21.8
Nonane	0.718	0.000337	0.503	150.8	88.1	0.711	22.9
Decane	0.730	0.000335	0.522	174.1	108.6	0.861	23.9
Undecane	0.740	--	0.520	195.8	128.1	0.995	24.7
Dodecane	0.749	--	0.518	216.2	146.2	1.150	25.4
Tridecane	0.756	0.000345(est)	0.521	234.0	162.5	1.520	26.1
Tetradecane	0.763	--	0.519	252.5	178.5	2.22	26.6
Pentadecane	0.768	--	0.522	270.5	194.0	2.86	27.1

The most convenient and detailed source for the properties of normal alkanes was found to be: "Physical Properties of Organic Compounds", Advances in Chemistry Series, Vol. II.[3]

there was any disagreement between the experimenters that contributed to the above compilations. Since the vapor pressure was frequently desired to an accuracy of 0.10% for a variety of interfacial temperatures; the procedure used was the following: First the existing data were used to calculate the constants in an equation of the form,

$$\mathrm{Log}_{10}(VP) = A + B/T \quad .$$

Then a short computer routine was written to calculate values of vapor pressure as a function of temperature for the range of temperature from 0°C to the boiling point of the substance in question. These values were printed out for temperature steps of 0.1°C, which was the accuracy to which the interfacial temperature could be determined with the experimental apparatus. Values of vapor pressure versus temperature are tabulated below for all of the substances of interest.

Vapor pressures of Pure Substances in mm Hg

Substance	-10°	0°	10°	20°	30°
n-Pentane	--	173.8	279.6	418.8	610.9
Cyclopentane	--	--	171.0	259.2	382.3
Isopentane	--	255.4	387.2	570.6	27.85°BP
Ethyl Ether	112.3	185.3	291.7	442.2	647.3
Carbon disulfide	72.2	130.0	207.5	307.0	426.4
Tridecane	(Vapor Pressure = 1.0 mm Hg at 66.3°C).				

The surface tension data for the above substances are given in the following table. For accurate interpolation between given temperatures, the formula,

$$\gamma_1/\gamma_2 = ((T_c - T_2)/(T_c - T_1))^{1.2}$$

can be utilized,[66] where T_c is the critical temperature of the substance.

Surface Tensions of Pure Substances in dynes/cm

Substance	15°	20°	25°	30°
n-Pentane		16.00		
Cyclopentane	23.16	22.57		21.17
Isopentane		15.0		13.93
Ethyl Ether	17.62	17.06		15.95
Carbon Disulfide		33.07		32.25
Tridecane		26.1		25.2

b. Mixtures. There are a number of methods for the prediction of the variation of surface tension and vapor pressure of a binary liquid mixture with composition. In this work the vapor pressure behavior was determined experimentally by using a very low flow rate of N_2 within the channel and analyzing the exit gas stream until it reached an equilibrium value with respect to time. The experimental results agreed somewhat better with a simple Raoult's law assumption than with the more complex theory due to Chao and Seader.[19] This is not too surprising, since the latter is based on Regular Solution Theory, and this tends to break down when the two species have greatly differing molecular weights, as was the case here. Thus all the final calculations were carried out using the experimentally obtained vapor pressure relationships. Figures 34, 35 and 36, show the experimental data in the form of gas phase partial pressure versus liquid phase mole fraction for the solutes n-pentane, cyclopentane, and ethyl ether, with n-tridecane the solvent in all cases.

Reid and Sherwood[66] have presented several correlations for predicting the surface tension of non-aqueous mixtures. The most accurate method, and the one they recommend is

$$\gamma_{mix} = \sum_j x_j \gamma_j \quad .$$

This equation reduces to the assumption of linear behavior between the pure component values for a binary mixture.

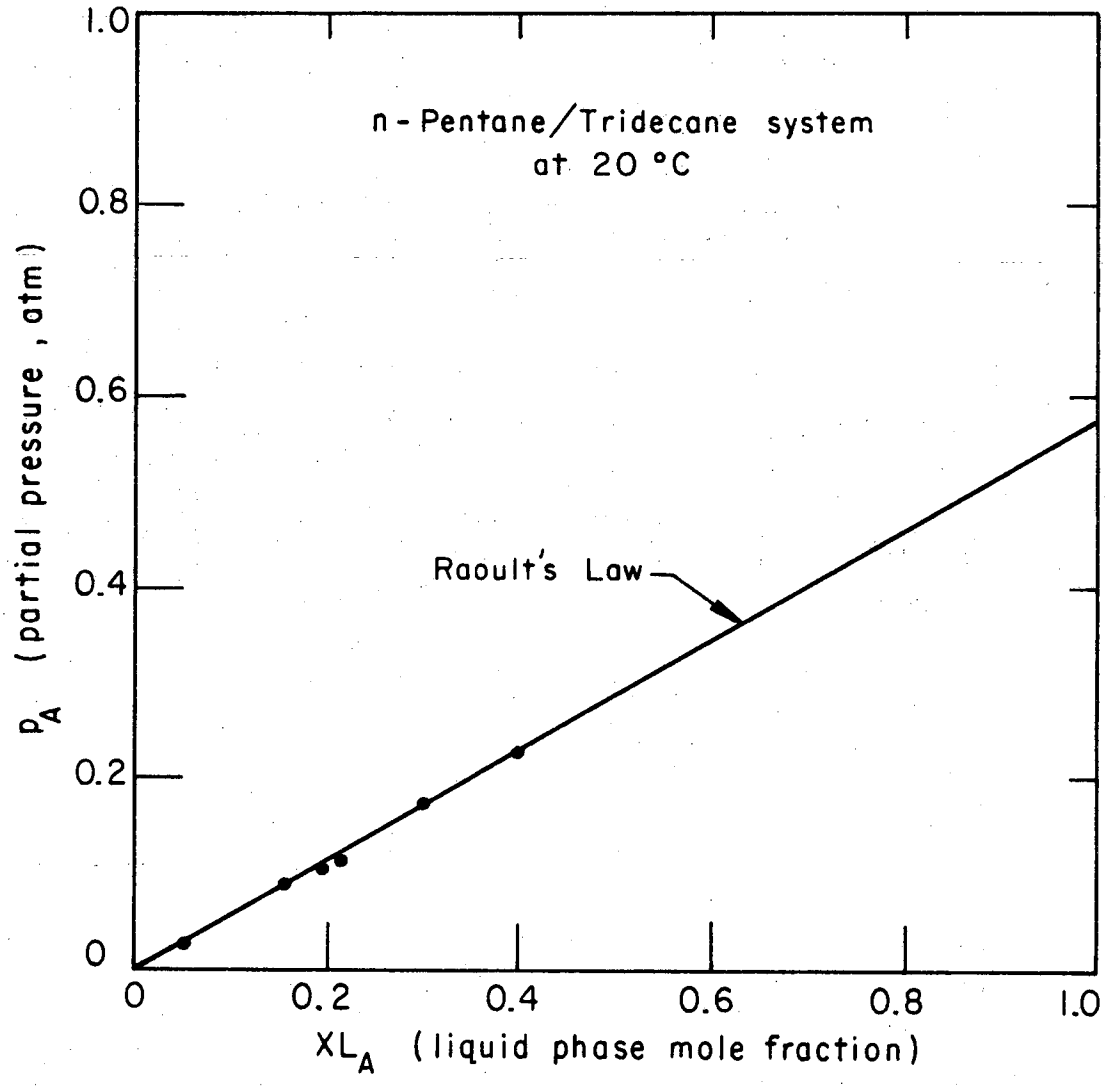

Fig. 34. Vapor pressure of n-pentane versus liquid phase mole fraction for the system n-pentane/tridecane.

● = experimental data points

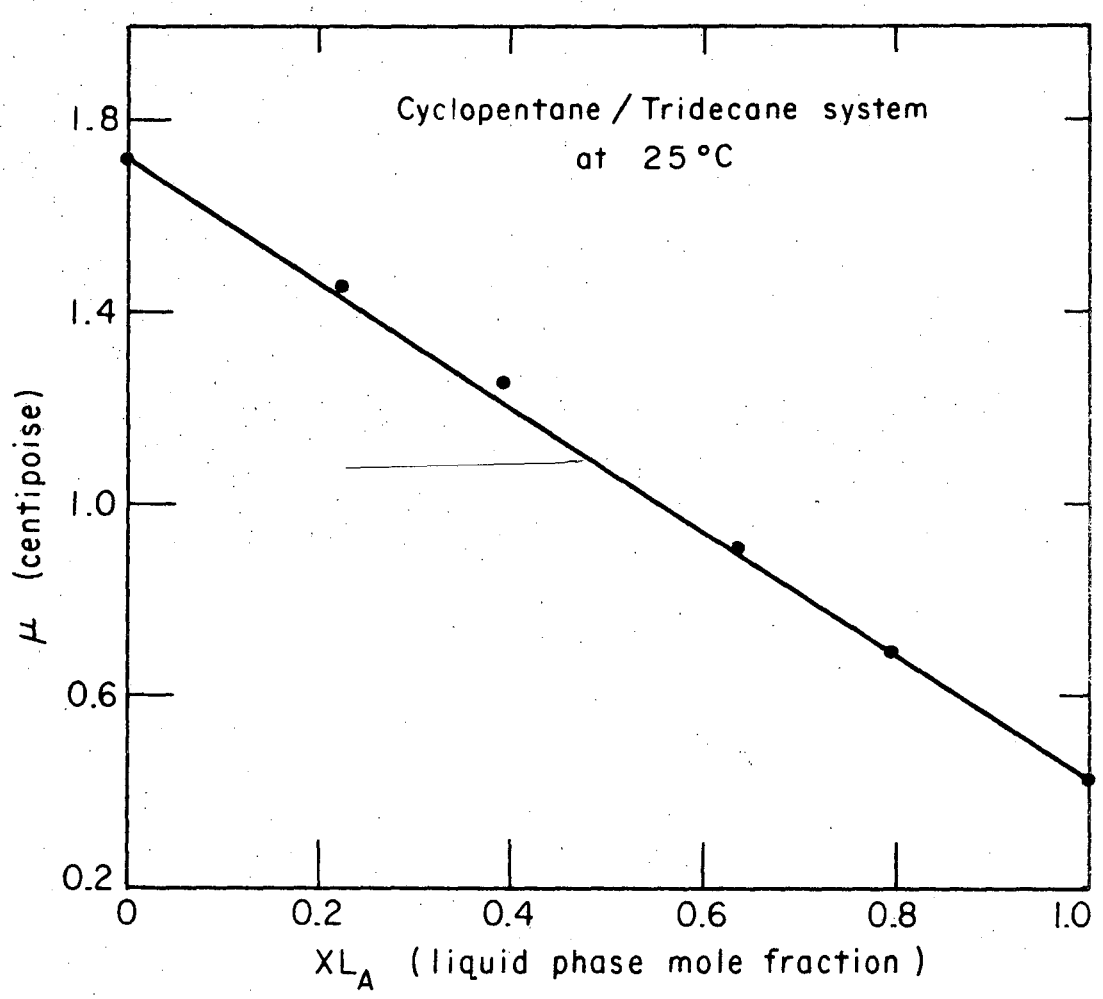

Fig. 35. Vapor pressure of cyclopentane versus liquid phase mole fraction for the system cyclopentane/tridecane.

● = experimental data points

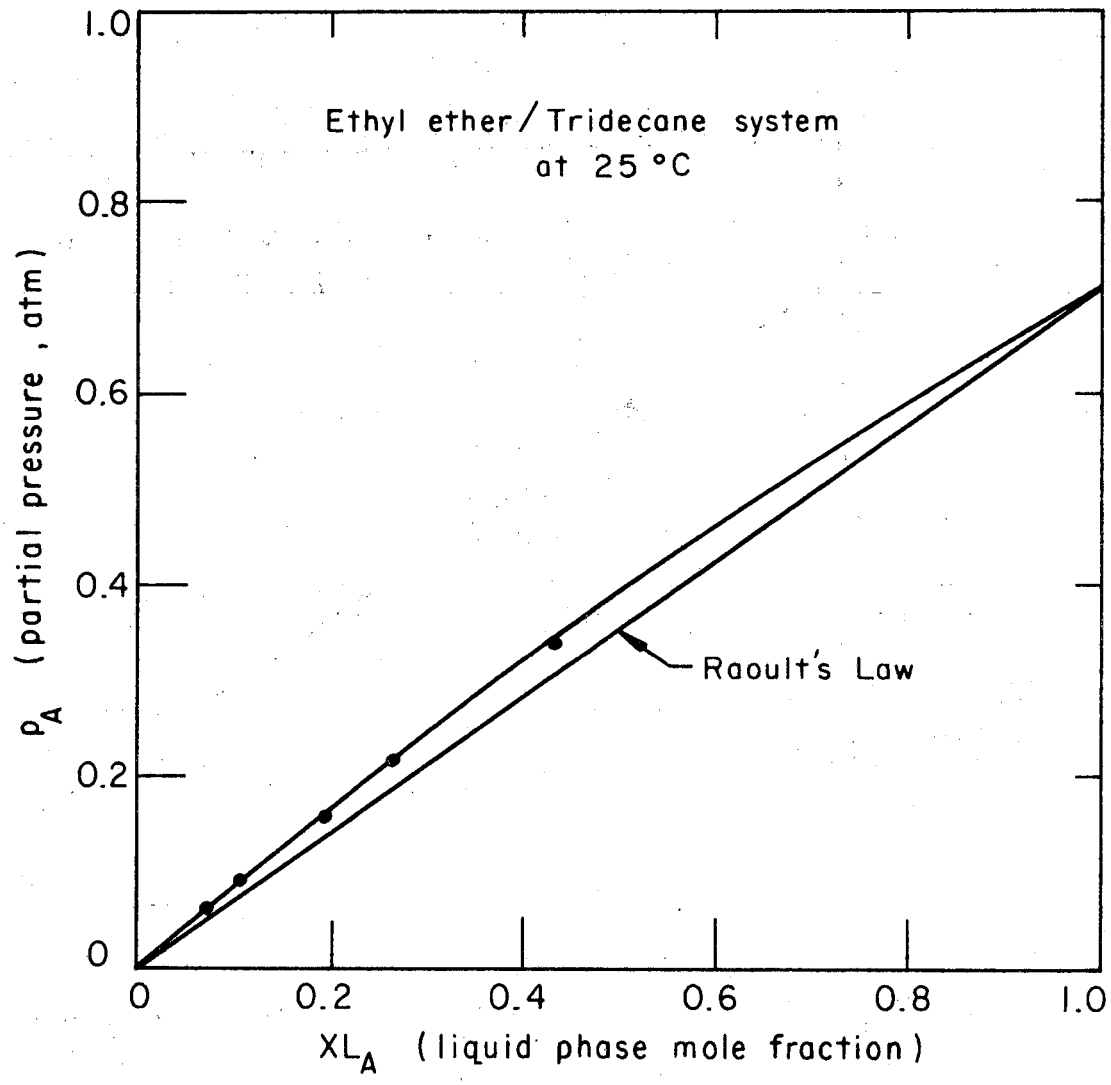

Fig. 36. Vapor pressure of ethyl ether versus liquid phase mole fraction for the system ethyl ether/tridecane.

● = experimental data points

A more recent work by Sprow and Prausnitz[72] promises somewhat better results for non-aqueous organic mixtures; however, it is also based on Regular Solution Theory and would thus tend to break down for the case of widely differing molecular size. The method also has the disadvantage of being quite difficult to apply, as it requires a trial and error computer solution to yield the final values of mixture surface tension versus composition.

Figure 37 represents surface tension data published by Koefoed and Villadsen[38] for the system heptane-hexadecane. For this system the linear approximation recommended by Reid and Sherwood[66] appears to be fairly good, yielding only 2.4% error in the absolute value of mixture surface tension at the worst point. Since the primary use in this work of the variation of surface tension with concentration was for calculation of the Thompson number, it is also desirable to estimate the accuracy of the derivative, $\partial\gamma/\partial x_A$, calculated using the linear approximation. A maximum error of 30% occurs for $X_{C_7} = 0.00$; however the most important concentration region for the study was between solute mole fractions of 0.20 and 0.50. Since only a portion of the mass transfer resistance was within the liquid phase, the values of x_{bulk} and $x_{interface}$ shown on Fig. 37 represent a typical run situation. A value of $\partial\gamma/\partial x_A$ calculated by connecting these points with a straight line differs by only 6% from the linear assumption. If we construct a tangent to the curve at $x_{interface}$, the error in $\partial\gamma/\partial x_A$ is found to be less than 12%. Thus for the most important region of interest, the values of $\partial\gamma/\partial x_A$ calculated by using the linear approach should be within 5 to 15% of the true value for the chemical systems utilized in this study.

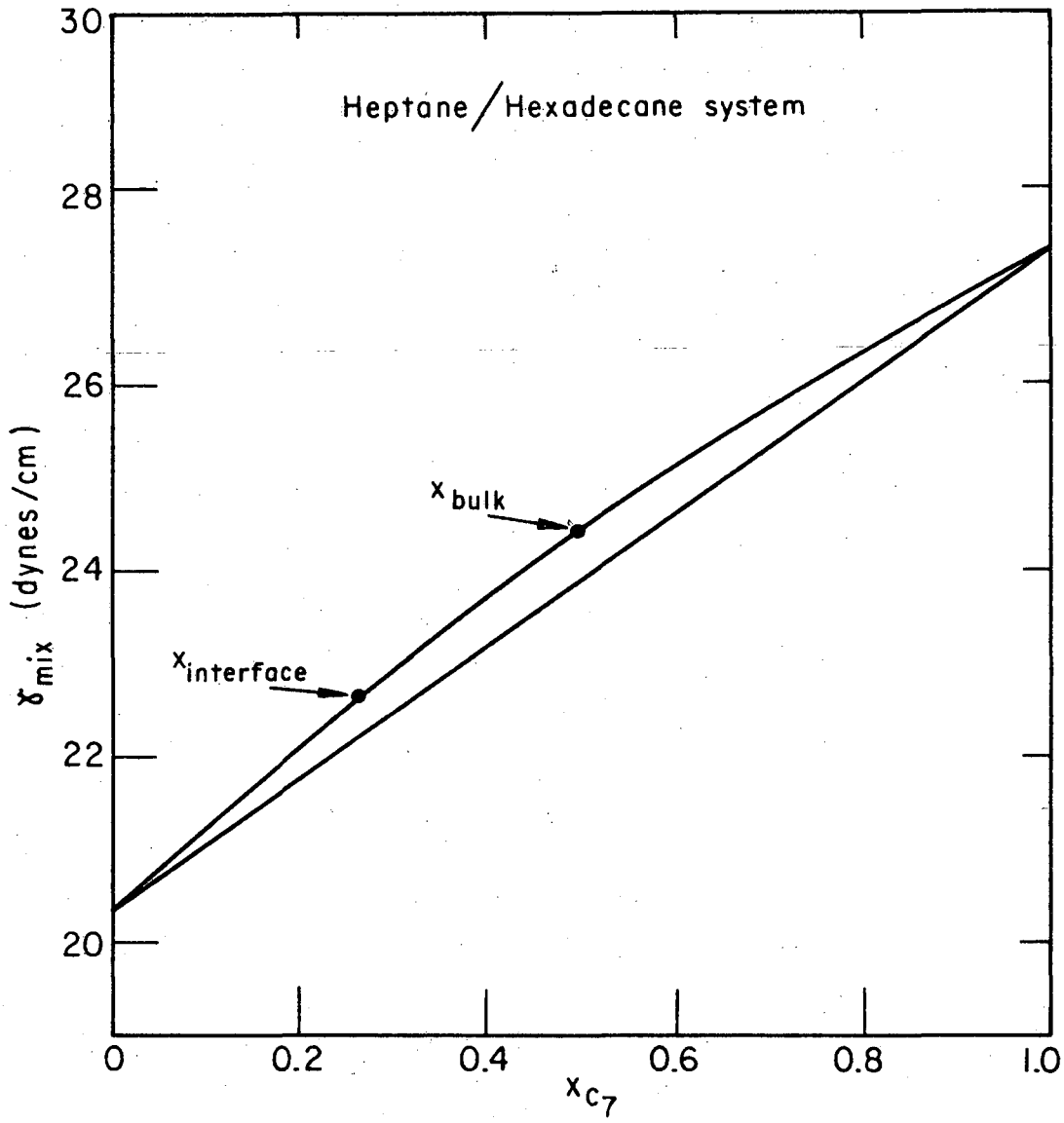

Fig. 37. Surface tension versus liquid phase mole fraction of n-heptane for the system n-heptane/n-hexadecane at 20°C, as obtained by Koefoed and Villadsen.[38]

upper solid line indicates experimentally observed behavior
lower solid line indicates ideal mixture behavior

3. Density and Viscosity

a. Pure substances. In addition to the two previously cited works on Organic chemicals,[3,79] the "Handbook of Physics and Chemistry"[31] was found to be helpful, particularly for the more common chemicals. As before, the practice of using the more recent of any conflicting data was followed. The following two tables give a listing of the density and viscosity used for each material. For interpolation between temperatures; density was assumed to vary linearly with inverse temperature (°K). Viscosity was assumed to vary with absolute temperature according to the equation[66]:

$$\mathrm{Log}_{10}(\mu) = A + B\ \mathrm{Log}_{10}(T) \quad ,$$

where A and B were constants determined from the existing data.

Substance	Viscosity in cp. (Temp. °C)	μ(°C)	μ(°C)
n-Pentane	0.239 (20°)	---	---
Cyclopentane	0.460 (15°)	---	0.388 (30°)
Isopentane	0.434 (0°)	0.396 (10°)	0.364 (20°)
Ethyl Ether	0.284 (0°)	0.233 (20°)	0.222 (25°)
Carbon disulfide	0.436 (0°)	0.363 (20°)	0.330 (40°)
Tridecane	1.920 (20°)**	1.731 (25°)**	---

** Indicates values obtained experimentally by the author, utilizing a capillary tube viscometer.

Substance	Density (gm/ml) at 20°C	25°C	30°C
n-Pentane	0.626	0.621	0.616
Cyclopentane	0.745	0.740	0.735
Isopentane	0.620	0.615	0.610
Ethyl Ether	0.714	0.708	0.702
Carbon disulfide	1.263	1.256	1.250
Tridecane	0.756	0.753	0.749

b. Mixtures. The density and viscosity of all the mixtures utilized were measured experimentally as a function of concentration. In all cases the density was found to be a linear function of volume fraction (i.e., very little volume change upon mixing); however the relationships for viscosity were not so well behaved. Figures 38 thru 40 show plots of viscosity versus mole fraction for the various experimental systems of interest. In all cases the viscosity values were obtained using a capillary flow viscometer, which was kept isothermal in a constant temperature bath. Density was determined experimentally using a 10 ml pycnometer.

4. Gas Phase Diffusivities

A recent work on the prediction of gas phase diffusion coefficients is an article by Fuller, Schettler, and Giddings.[25] This summary indicates that the use of the Wilke-Lee modification of the Hirschfelder-Bird-Spotz method,[87] yields by far the more satisfactory results for systems of the type utilized in this study (for example, nitrogen with a hydrcarbon). This method was applied to all the systems for which the required molecular properties could be found. For some of the systems the Lennard-Jones parameters could not be found; in these cases the Bird-Slattery approach was utilized.[11] Judging from the tabulation given by Fuller et al., either of the above approaches should yield a value of diffusivity accurate to within 5% or better, with the Wilke-Lee approach generally being better than 2%. To illustrate the above outlined calculational procedures, an example calculation is carried out below for the Nitrogen, n-Pentane system.

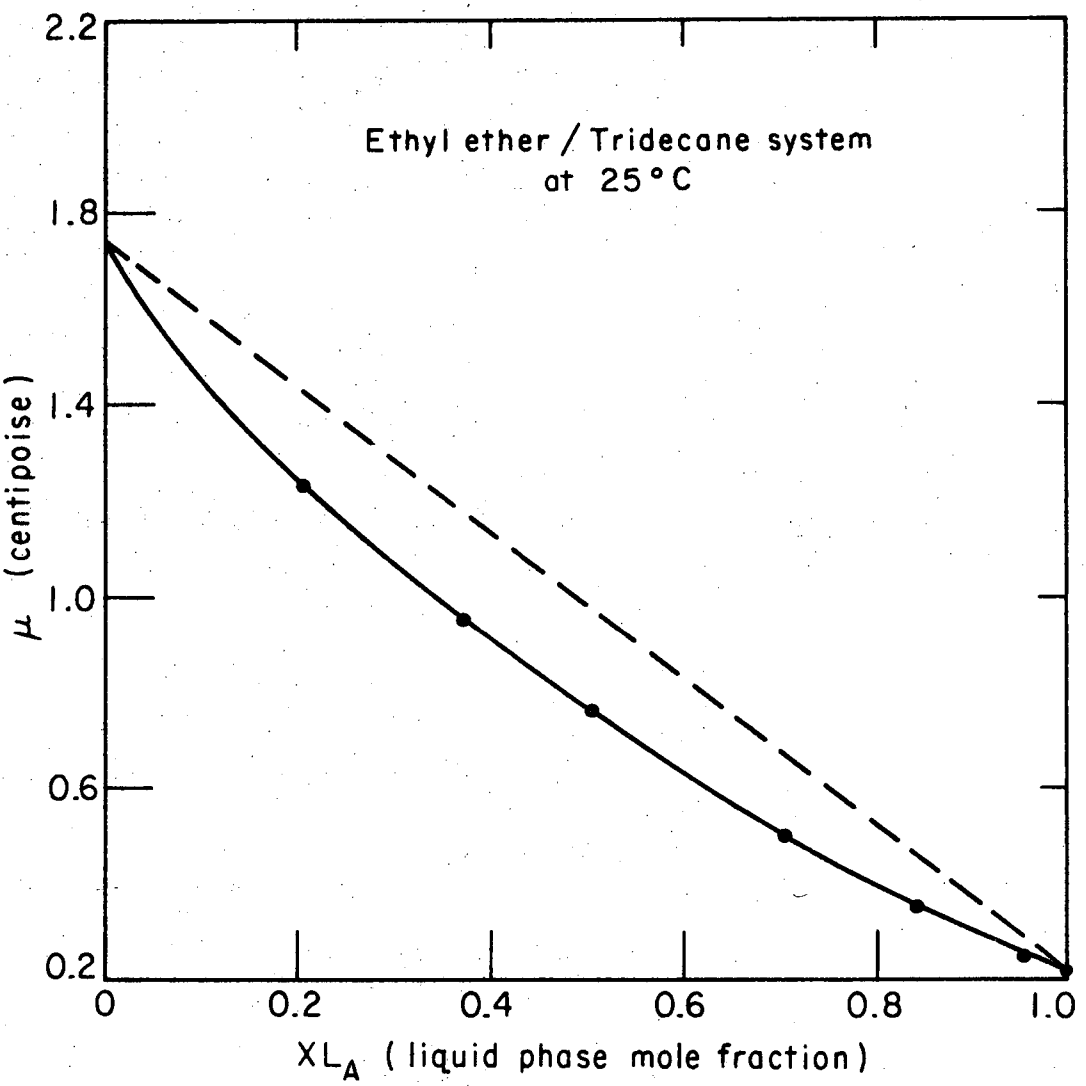

Fig. 38. Viscosity versus liquid phase mole fraction of ethyl ether for the system ethyl ether/tridecane at 25°C.

● = experimental data points, solid line is best fit to these data.

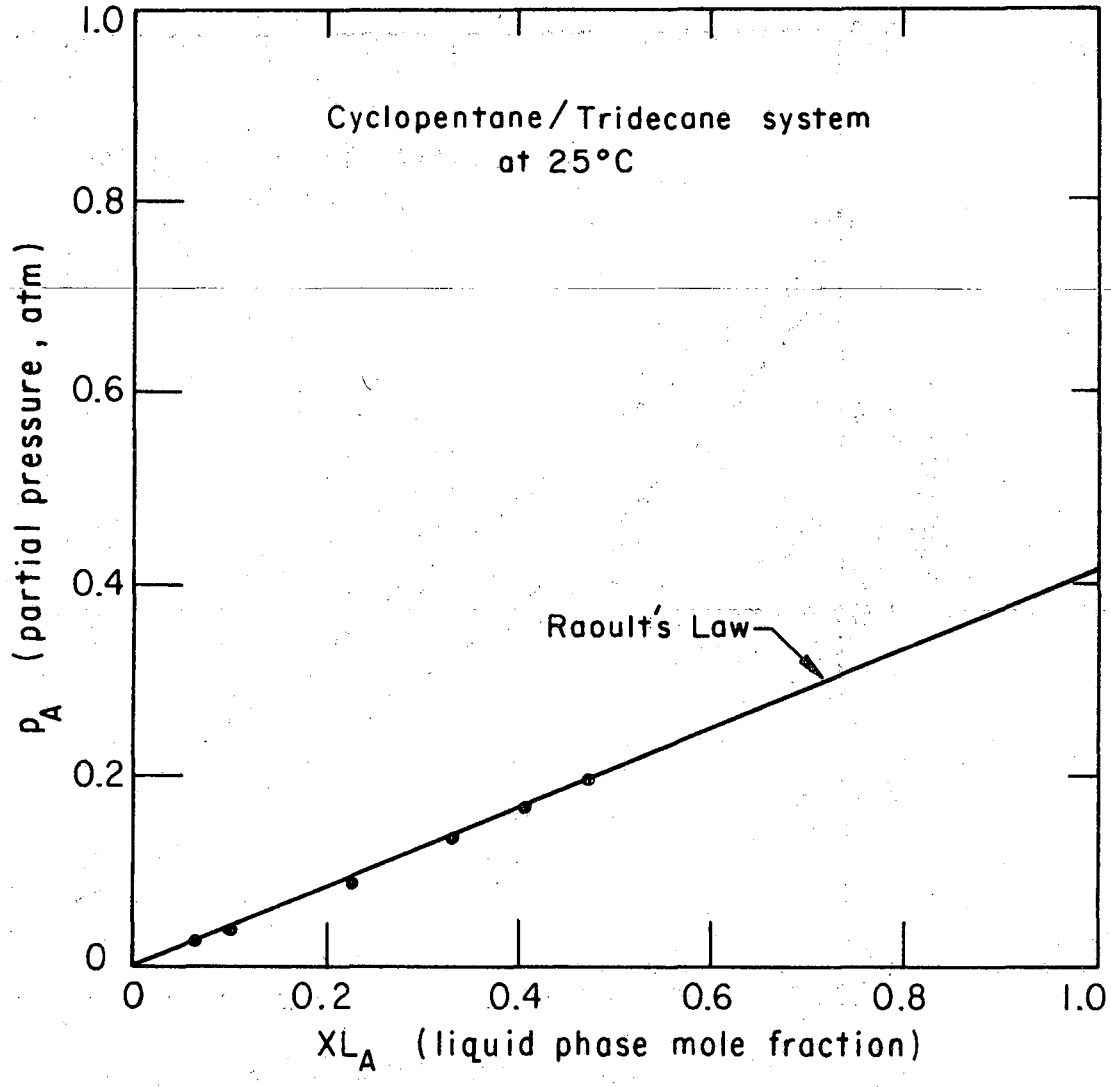

Fig. 39. Viscosity versus liquid phase mole fraction of cyclopentane for the system cyclopentane/tridecane at 25°C.

• = experimental data points, solid line is the best fit to these data.

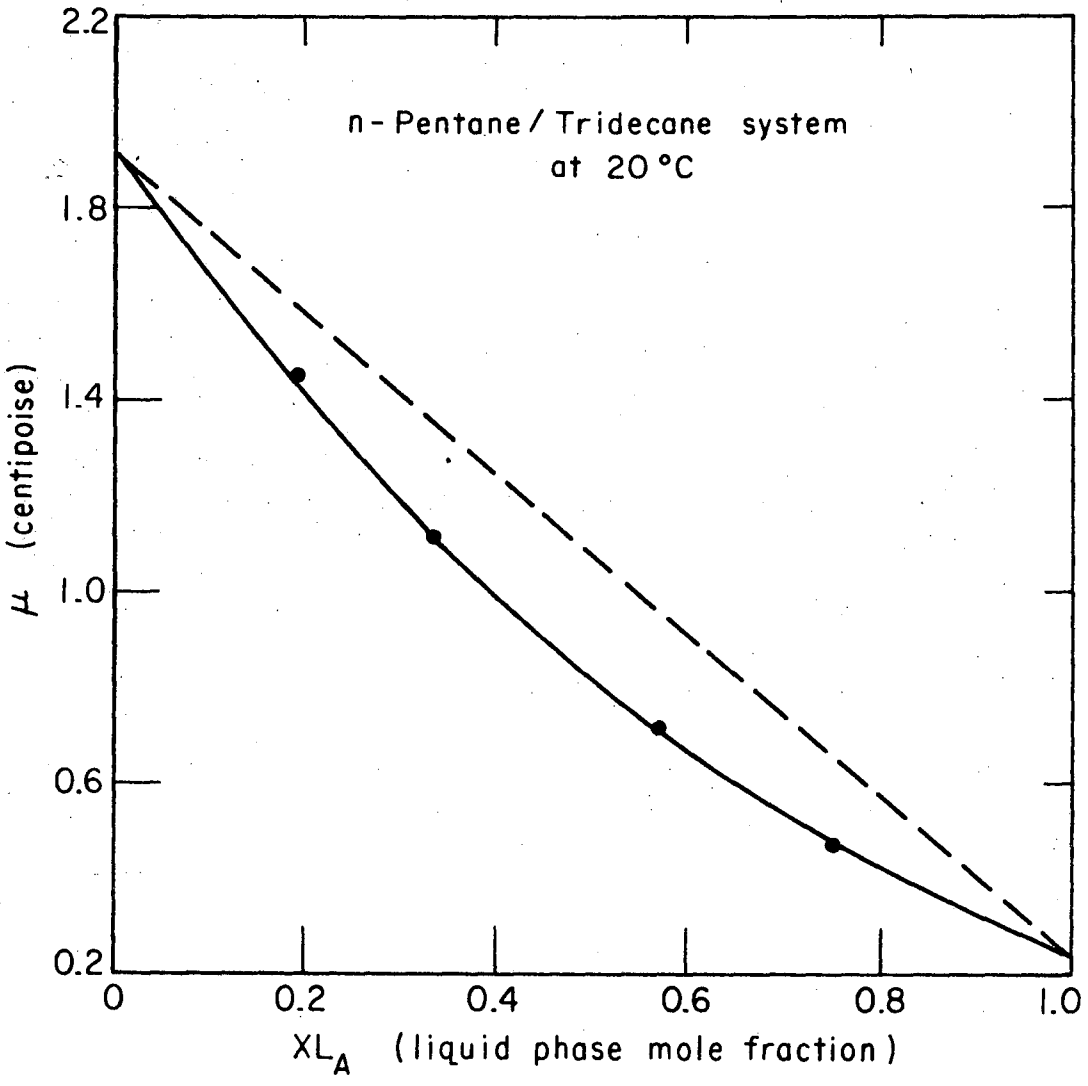

Fig. 40. Viscosity versus liquid phase mole fraction of n-pentane for the system n-pentane/tridecane at 20°C.

● = experimental data points, solid line is the best fit to these data.

1) Wilke-Lee Approach:

$$D_{12} = B\,T^{3/2}\left[(M_1 + M_2)/M_1M_2\right]^{1/2}/P(r_{12})^2\,W_{(1)}^{(1)}(1 - \Delta)$$

$$B = \left[10.7 - 2.46((M_1 + M_2)/M_1M_2)^{1/2}\right] \times 10^{-4}$$

Letting 1 = pentane, 2 = nitrogen; we can calculate the above parameters: Since $M_1 = 72.15$ and $M_2 = 28.0$, we find that,

$$B = 10.1 \times 10^{-4} \quad .$$

The temperature of interest is 20°C; T = 293.16; and P = 1.0 atm. From the Wilke-Lee paper[87] we find that for this system, $\Delta \tilde{=} 0.0$, and we need only to obtain the values of our Lennard-Jones parameters, r_{12} and ϵ/k in order to finish the above calculation. As the next steps,

$$r_{12} = (r_1 + r_2)/2$$

and the values for W, the collision integral, are tabulated versus kT/ϵ_{12}, where $\epsilon_{12} = (\epsilon_1\epsilon_2)^{1/2}$. From Table B-1, Bird, Stewart, and Lightfoot:[11]

$$r_1 = 5.769\ , \quad r_2 = 3.681\ ; \quad \epsilon_{1/k} = 345\ , \quad \epsilon_{2/k} = 91.5$$

Utilizing these values we see that,

$$r_{12} = 4.725$$

$$\epsilon_{12/k} = 177.7 \quad \text{or} \quad kT/\epsilon_{12} = 1.65$$

From page 746, Bird et al.,[11] we see that:

$$W = 1.153/2 = 0.5765$$

Accumulating all of these values into the expression for D_{12}, we find,

$$D_{12} = \frac{10.1 \times 10^{-4}(293.16)^{1.5}(0.0496)^{1/2}}{1.0(4.725)^{2}(0.5765)\ 1.0}$$

$D_{12} = 0.0882$ using Wilke-Lee Method.

A similar calculation was also made using the Bird-Slattery method,[11] wherein:

$$P\ D_{12}/(P_{c1}P_{c2})^{1/3}\ (T_{c1}T_{c2})^{5/12}\ (1/m_1 + 1/M_2) =$$

$$2.745 \times 10^{-4}(T/(T_{c1}T_{c2})^{1/2})$$

Substitution of the appropriate values into the above equation and solving for the value of diffusivity; we obtain:

$D_{12} = 0.0814$

The tabulated values below are those which were used in the calculations for the systems indicated.

System	Diffusivity (cm^2/sec)	Temp.
N_2 - n-Pentane	0.0882	20°
N_2 - Cyclopentane	0.0943*	25°
N_2 - Isopentane	0.0894*	20°
N_2 - Ethyl Ether	0.0975	25°
N_2 - Carbon disulfide	0.1112	30°

*Indicates use of the Bird-Slattery method due to inability to obtain the necessary molecular parameters for use in the Wilke-Lee approach.

5. Liquid Phase Diffusivities

The estimation of liquid-phase diffusion coefficients is the most uncertain of all the physical property calculations that were necessary in this study. This difficulty was anticipated, and in fact was one of the primary reasons for the choice of the liquids that were used in this investigation. Since the liquid phase concentrations were varied over an extremely wide range and in view of the strong dependence of the diffusivity on species concentration, a reliable method of predicting this behavior as a function of concentration was a necessity. Fortunately, such a method exists, and has been confirmed quite well experimentally in a work by Bidlack and Anderson.[10] The basic results of the Bidlack and Anderson study are that the group $(D_L\mu)$ varies linearly with mole fraction over the entire concentration region. This was experimentally confirmed for the systems hexane-dodecane and heptane-hexadecane, and to a lesser extent (5% error at the worst point) for the system hexane-carbon tetrachloride. The similarity of the first of the above systems to all of the systems used in this study (with the possible exceptions of Ether and CS_2) is obvious. It is then encouraging to note that the above method of prediction was good to better than 1.0% for hexane-dodecane over the entire concentration range. Thus, we need only the two limiting values of the diffusivity, and the functionality of viscosity against mole fraction to yield an expression for D_L vs XL_A.

Experimental data for viscosity versus mole fraction have already been presented in Figs. 38 thru 40. As can be seen, the experimental data are all quite well-behaved, and could be fitted to 0.5% accuracy with an expression of the form:

$$\mu = A + B(XL_A) + C(XL_A)^2 \quad ,$$

here the constants A, B, and C are determined from the best curve through the experimental data. The solid lines in Figs. 38, 39, and 40, were obtained from the above polynomial expression.

Two methods were employed to calculate the values of diffusivity at infinite dilution. The first was the familiar Wilke-Chang[86] equation:

$$D_{12} = 7.4 \times 10^{-8}(M_2)^{1/2}\, T/\mu_2 V_1^{0.6}$$

The second approach, which was found to yield values which agreed somewhat better with the experimental data published by Bidlack and Anderson,[10] was that of King, Hsueh, and Mao[37]:

$$\frac{D_{12}\mu}{T} = 4.4 \times 10^{-8}\left(\frac{V_2}{V_1}\right)^{1/6}\left(\frac{H_2}{H_1}\right)^{1/2}$$

Values determined from the two methods usually agreed to within a few per cent; and since the Wilke-Chang equation is less accurate when the difference in molecular size is large, the King et al., method was relied upon when a discrepancy existed between the two methods. With the two values of diffusivity at infinite dilution, D_{12} and D_{21}, we could then write a final equation for our diffusion coefficient:

$$D_L = \frac{D_{12}\mu_2 + (D_{21}\mu_1 - D_{12}\mu_2)XL_A}{A + B(XL_A) + C(XL_A)^2}$$

This procedure was carried out for each system, with the resulting equations tabulated below.

Pentane - Tridecane

$$D_L = 10^{-5}[(2.11 - 1.22\ XL_A)/(1.92 - 2.74\ XL_A + 1.06\ XL_A^2)]$$

Ethyl Ether - Tridecane

$$D_L = 10^{-5}[(2.024 - 1.176\ XL_A)/(1.730 - 2.332\ XL_A + .824\ XL_A^2)]$$

Cyclopentane - Tridecane

$$D_L = 10^{-5}[(2.00 - 1.20\ XL_A)/(1.730 - 1.323\ XL_A)]$$

(note that a linear viscosity-concentration curve was sufficient in this case).

APPENDIX E

Calculational Details

The major purpose of this section is to illustrate several of the more involved calculational procedures outlined in the main body of this work. Also, a small number of relatively simple, but important calculations which were not discussed elsewhere will be given in this section.

Gas Phase Reynolds Numbers

The motion of the liquid interface was ignored in calculating all the reported gas phase Reynolds numbers in this study, i.e., the calculations were carried out as though the gas were flowing through a rectangular channel with the dimensions 1/2 in. by 3 in. The appropriate formula for this situation is then given by,

$$N_{Re} = \frac{4 R_h G}{\mu} \qquad \text{(E-1)}$$

where R_h, the hydraulic radius is given by:

$$R_h = \frac{H \times W}{2H + 2W} \qquad \text{(E-2)}$$

and for the experimental channel, $R_h = 0.214$ in.

Liquid Phase Reynolds Numbers

The liquid phase Reynolds numbers were calculated with the drag on the upper surface ignored, i.e., using Eq. (E-1) but with R_h being given by,

$$R_h = \frac{H \times W}{2H + W} \qquad \text{(E-3)}$$

or for the experimental channel, $R_h = 0.375$ in.

The Calculation of Interfacial Temperature Differences Caused by an Evaporative Heat Flux

As was stated in Chapter 5, for the experimental system utilized in this study the solution to the heat transfer problem can be carried out quite accurately by ignoring the gas phase contribution. Thus the mathematical problem to be treated is that of a moving liquid which is subjected to an interfacial heat flux of the form:

$$Q_{int} = \Delta H_{vap}(N_{Ao}) \quad . \tag{E-4}$$

If we assume that the liquid motion can be represented by a constant velocity equal to the interfacial velocity, then the concept of penetration theory can again be used. The x-direction can be converted to t, the exposure time;

$$x = U_{int}(t) \quad . \tag{E-5}$$

We can now use, as a first approximation, the penetration approach for the calculation of the gas phase mass transfer coefficient, this somewhat underestimates the heat flux. Then for the case of $N_{Bo} = 0$, $\Delta H_{vap} =$ constant;

$$Q_{int} = \frac{k'_{x,loc}(x_{A\infty} - x_{Ao})}{1 - x_{Ao}} \Delta H_{vap} \tag{E-6}$$

where

$$k'_{x,loc} = c\sqrt{\frac{D_{AB}}{\pi t}}\ \theta_{AB} \tag{E-7}$$

The application of Fourier's law to the liquid interface gives

$$Q_{int} = - k_t \left.\frac{\partial T}{\partial y}\right|_{y=o} \tag{E-8}$$

In Eq. (E-8), k_t represents the thermal conductivity of the liquid in question, and T the liquid temperature. The preceeding set of assumptions defines the problem of a transient temperature penetration into a semi-infinite body, whose surface temperature gradient is given as a function of $t^{-1/2}$, i.e., $k_t \partial T/\partial y = \beta_1 t^{-1/2}$. The solution to such a problem has been carried out by Carslaw and Jaeger[17] with the assumption of a constant initial fluid temperature, T_∞. Their solution can be manipulated to yield an expression for the interfacial temperature of the form:

$$(T_{int} - T_\infty) = \frac{\beta_1 \alpha^{1/2} \Gamma(1/2)}{k_t} \qquad \text{(E-9)}$$

where α is the liquid phase thermal diffusivity. The value of β_1 can be determined from the combination of Eqs. (E-6), (E-7), and (E-8).

To demonstrate the order of magnitude of the interfacial to bulk temperature difference, let us now carry out several sample calculations for some representative run conditions.

1) Evaporation of pure n-pentane into nitrogen under the following flow conditions:

gas flow	$QG = 200\ cm^3/sec$
liquid flow	$QL = 0.40$ gpm
liquid bulk temperature	$T_\infty = 20°C$

The above given flow conditions correspond to an interfacial velocity of 5.3 cm/sec, or if we consider an exposure length of 45.7 cm the exposure time is 8.6 sec. Making use of Eq. (E-7) and the physical properties given in Appendix D, the value of $k_{x,loc}$ can be found to be:

$$k'_{x,loc} = 4.46 \times 10^{-5}(0.0882/3.14)^{1/2}\ t^{-1/2}\ \theta_{AB}$$

$$k'_{x,loc} = 7.45 \times 10^{-6}(t^{-1/2})\ \theta_{AB}\ \text{gm-moles/cm}^2\ \text{sec}$$

As a first approximation, let us use the bulk liquid temperature to establish the equilibrium value of $x_{Ao} = 0.572$ (from data given in Appendix D.) Substitution into Eq. (E-6) now yields;

$$Q_{int} = 3.26 \times 10^{-2}(t^{-1/2}) \text{ cal/cm}^2\text{sec}$$

Thus we can now solve for the parameter, β_1, by making use of its definition and Eq. (E-8);

$$\beta_1 = - 3.26 \times 10^{-2}$$

Substitution into Eq. (E-9) will now yield the final value of interfacial temperature to be,

$$T_{int} = 14.7°C \quad ,$$

or the bulk to interfacial temperature drop is predicted to be on the order of 5.3°C. If we carry out a second calculation using $14.7° = T_{int}$, a ΔT of 4.0°C is obtained. As was discussed in Chapter 5, this is somewhat larger than the observed temperature difference; however, cellular convection due to density effects could be observed in most of the pure component evaporation runs. Benard cells were more important than in interphase experiments primarily due to the much lower viscosity of the n-pentane and iso-pentane as compared with that of tridecane. Thus, an excellent test of the accuracy of the above calculational method is to apply it to the CS_2/tridecane runs at $XL_A = 0.200$, since there was no observable cellular convection of any kind under these run conditions for this system.

2) Evaporation of carbon disulfide from tridecane into nitrogen under the following flow conditions:

gas flow	= 166 cm^3/sec
liquid flow	= 0.400 gpm
liquid interface temperature	= 30°C
liquid bulk concentration (XL_A)	= 0.400

The above flow conditions correspond to an interfacial velocity of 5.2 cm/sec, or if we consider an exposure length of 45.7 cm, the exposure time is 8.8 sec. Since the interfacial temperature is given, the calculation is no longer trial and error, as the value of β_1 can be determined uniquely from the given conditions and a knowledge of the interfacial equilibrium constants.

From Eq. (E-7) and the physical properties found in Appendix D, the value of $k'_{x,loc}$ can be found,

$$k'_{x,loc} = 4.46 \times 10^{-5}(0.1112/3.14)^{1/2}\ t^{-1/2}\ \theta_{AB}$$

$$= 8.35 \times 10^{-6}\ t^{-1/2}\ \theta_{AB}$$

As a reasonable first approximation let us use the interfacial concentration predicted by the low flux solution and an approximate high flux correction factor to obtain a value of the interfacial mass flux,

$$x_{Ao} = 0.560(0.514) = 0.288$$

$$Q_{int} = 1.60 \times 10^{-2}\ t^{-1/2}$$

Again solving for for β_1 we obtain the value,

$$\beta_1 = -\ 1.6 \times 10^{-2}$$

and the predicted ΔT is 2.6°C, which compares very well with the experimental values of 2.4 to 2.7°C which were obtained for these conditions.

Calculation of High Flux Interphase Transfer Coefficients

Sample Calculation for the System n-pentane/tridecane

1) Conditions:

	nitrogen flow	= 166 cm^3/sec
	liquid flow	= 0.40 gpm
	temperature	= 20.0°C
	inlet liquid conc. $XL_{A\infty}$	= 0.500

2) Assumptions will be those indicated in Sec. 6(A)-1 for the high flux and high concentration level addition of resistances.

3) Using the assumption of no volume change upon mixing in the liquid phase, and letting n-pentane be component A, tridecane be component B, then the liquid phase mole fraction and volume fraction of A may be related by the equation;

$$XL_A = \frac{\phi_A}{\phi_A + (1-\phi_A)\frac{\rho_B M_A}{M_B \rho_A}} \qquad \text{(E-10)}$$

From the above equation we find that $\phi_{A\infty} = 0.330$. The low flux interphase numerical solution yields the result that

$$\phi_{Ao} = 0.524(\phi_{A\infty}) = 0.173$$

Using the equilibrium data for n-pentane we find that the interfacial equilibrium concentration in the gas phase is given by,

$$x_{Ao} = 0.172$$

Using the low flux prediction of the interfacial conditions we can now calculate the flux level correction factors:

$$R_{AB}(liq) = \frac{\phi_{Ao} - \phi_{A\infty}}{1 - \phi_{Ao}} = -0.190; \quad \text{or} \quad 1 + R_{AB}(liq) = 0.810$$

From Fig. 12, using the curve for penetration theory, we find that

$$\theta_{AB}(liq) = 1.16$$

A similar calculation for the gas phase yields:

$$R_{AB}(gas) = 0.209 \quad \text{or} \quad \theta_{AB}(gas) = 0.883$$

The low flux computer solution yields the fact that,

$$\frac{k_{x,avg}}{k_{\phi,avg}} = 0.908$$

If we now use, as a first guess, the low flux interfacial conditions then substitution into Eq. (6-10) gives,

$$\frac{k'_{x,avg}}{k'_{\phi,avg}} = 0.883(0.908)/1.16 = 0.691$$

If we now make use of this value to determine a new value of x_{Ao} from Eq. (6-10) (and hence ϕ_{Ao}) it is obvious that it will not agree with the low flux value; hence let us now try a new value (obtained by guessing) of $\phi_{Ao} = 0.600(\phi_{A\infty})$. Making use of this value, and the corresponding equilibrium value of $x_{Ao} = 0.192$, we can now calculate revised values for $\theta_{AB}(liq)$ and $\theta_{AB}(gas)$. The new values are:

$$\theta_{AB}(liq) = 1.140$$

$$\theta_{AB}(gas) = 0.860$$

Again, substituting into Eq. (6-10) we now obtain for the ratio of high flux coefficients a value of 0.685, which differs by only 1% from the initial value. Thus the calculations have converged to within about 1% after the second iteration, which is sufficiently close for our purposes. A comparison of the low flux and high flux results shows that the high flux value of ϕ_{Ao} is 0.198, as compared with a low flux value of 0.173. The value of x_{Ao} has also increased from 0.172 under the low flux conditions to a value of 0.192 at the high flux conditions.

The net effect therefore has been to decrease the liquid phase driving force and increase the gas phase driving force so that the two mass transfer rates remain equal. This occurred because the liquid phase mass transfer resistance had gone down more rapidly with the increase in flux and concentration than had the gas phase resistance. In order for the fluxes to remain equal, the driving forces had to change in the manner outlined above.

Thompson Number Calculations

A. Assumptions

1) All the important physical properties (D_{AB} and μ) will be assumed constant, at the values associated with the interfacial conditions.

2) For the sake of simplicity and to have a standard method of calculation, the concentration profile used to obtain $\partial C_A/\partial y$ will be calculated using the standard penetration theory approach.

3) The value of interfacial concentration will be assumed to be the same as that obtained using the interphase numerical Graetz solution carried out by Byers.

4) The value of h to be used in the Thompson number will be the "depth of penetration" of the concentration profile based upon a linearization of the interfacial value of $\partial C_A/\partial y$ to the bulk condition (see Eq. (E-12)).

B. Penetration Theory

The derivation of the penetration theory solution can be found on page 539 in Bird, Stewart, and Lightfoot.[11] The final expression for the concentration profile is given on a dimensionless basis as:

$$C_A/C_{Ao} = \text{erfc}\left[\frac{y}{\sqrt{4\ D_{AB}x/U_{int}}}\right] \qquad \text{(E-11)}$$

This equation gives the concentration as a function of both distance downstream and vertical distance. With a little further manipulation, Bird et al. obtain the expression for the distance to which the concentration profile has penetrated, based upon the interfacial slope being linearized to the bulk conditions;

$$h = \sqrt{D_{AB}x/U_{int}} \qquad \text{(E-12)}$$

The expression for the Thompson number, based upon a concentration dependent variation of surface tension is given by,

$$\text{Th \#} = \frac{\left(\frac{\partial \gamma}{\partial C_A}\right)\left(\frac{\partial C_A}{\partial y}\right) h^2}{\mu\, D_{AB}} = \frac{\left(\frac{\partial \gamma}{\partial x_A}\right)\left(\frac{\partial x_A}{\partial y}\right) h^2}{\mu\, D_{AB}} \qquad \text{(E-13)}$$

As a sample calculation, the n-pentane/tridecane system will now be considered under the following conditions:

$QG = 166\ cm^3/sec$ $\quad QL = 29.3\ cm^3/sec$ $\quad x_{A,bulk} = 0.05$

$x = 45.72\ cm$

From the interphase computer solution we find that,

$$x_{Ao} \cong 0.025 \quad \text{and} \quad U_{int} = 5.19\ cm/sec$$

For the n-pentane/tridecane system, $\partial\gamma/\partial x_A = 10.1$ dynes/cm. From the penetration solution we find that

$$h = 1.8 \times 10^{-2}\ cm, \text{ and } \partial x_A/\partial y = 1.33\ cm^{-1} \text{ at the channel exit.}$$

By placing each of these quantities into the appropriate position in the Thompson number expression and carrying out the indicated operations we find that,

$$\text{Th \#} = 20{,}900 \text{ at channel exit.}$$

These calculations can be carried one step farther to determine an average value of the Thompson number for the exposure, since each of the terms entering into the expression for the local Thompson number have a specified x-direction dependence. Putting this dependence into the expression for the local Thompson # we find that,

$$\text{Th \#} \sim x^{1/2} \quad ;$$

and by a simple integration we find that, averaging over the exposure length

$$\text{Th \#})_{avg} = 2/3\ \text{Th \#})_{local}$$

Thus for the sample exposure we can calculate an average value of the Thompson number for the total exposure as:

$$Th\ \#_{avg} = (2/3)\ 20,900 = 13,900$$

It should be noted at this point that all the mass transfer correlation calculations were based upon a critical value of the average Thompson number of 8000. This seemed to represent all of the systems studied fairly well, and has the added advantage of eliminating the measurement of the value of Th_{cr} for each of the systems.

APPENDIX F

Nomenclature

a	slope of the velocity profile at the interface (sec^{-1})
A	an arbitrary numerical constant
b	channel half width (cm)
B	an arbitrary numerical constant
c	total concentration ($gm\text{-}moles/cm^3$)
C_A, C_B	species concentration ($gm\text{-}moles/cm^3$)
C_1	constant defined by Eq.(5-22)
C_2	constant defined by Eq.(5-21)
C_p	heat capacity at constant pressure (cal/gm °C)
C_v	heat capacity at constant volume (cal/gm °C)
D_{AB}	diffusion coefficient in the binary system A-B (cm^2/sec)
D_{12}	diffusion coefficient of component 1 at infinite dilution in component 2
d_a	diameter of cylinder (cm)
F_s	fraction saturation of the gas phase (either temperature or concentration)
G	mass flow rate (gms/cm^2 sec)
G_r	Grashof number (dimensionless)
g	acceleration due to gravity (cm/sec^2)
H	Henry's law constant ($atm.\ cm^3/gm\text{-}moles$)
H	height of a fluid phase (cm)
ΔH_{vapn}	heat of vaporization (cal/gm-mole)
h	depth of a liquid layer (cm); also used in this study as the penetration depth of a concentration profile in the liquid phase
h_G	gas phase heat transfer coefficient ($cal/cm^2 sec$ °C)
J_A^o	molar flux of species A relative to the volume average velocity
J_A^*	molar flux of species A relative to the molar average velocity
k	mass transfer coefficient at low flux conditions ($moles/cm^2 sec$)
k'	mass transfer coefficient (applicable at high flux conditions) ($moles/cm^2 sec$)
k_G	gas phase mass transfer coefficient based on partial pressure driving force ($moles/cm^2 sec\ atm$)

k_t	thermal conductivity (cal/cm sec °C)
K_1	constant used in computer solution (see Eq.(5-24))
K_2	constant used in computer solution (see Eq.(5-24))
L	exposure length (cm)
L	length of cylinder (see Eq. (3-4)) (cm)
M_A	molecular weight of species A (gms/gm-mole)
N	dimensionless group used in solution to cylindrical heat transfer problem in Chapter 1 (see Eq. (3-4))
N_A	molar flux of component A relative to stationary coordinates (moles/cm^2 sec)
N_{Re}	Reynolds number (dimensionless)
P	total pressure (atm)
p_A	partial pressure of component A (atm)
P_c	critical pressure (atm)
P_{BM}	log mean pressure of component B
QG	gas flow rate (cm^3/sec)
QL	liquid flow rate (cm^3/sec)
Q_{int}	interfacial heat flux (cal/cm^2sec)
R	Rayleigh number (dimensionless)
R_h	hydraulic radius (cm)
R_{AB}	dimensionless flux ratio
r	molecular collision diameter (Å)
S	ratio of fluxes across interface (mass, molar, or volume)
S_c	Schmidt number (dimensionless)
Sh	Sherwood number (dimensionless)
T	temperature (°C)
T_c	critical temperature (°C)
Th	Thompson number (dimensionless)
t	time (sec)
U_m	mean gas phase velocity in the x-direction (cm/sec)
U_i	interfacial velocity in the x-direction (cm/sec)
u_x	velocity in the x-direction (cm/sec)
v	velocity vector (cm/sec)

v_y	velocity in the y-direction (cm/sec)
V_l	molar volume of component 1 at its boiling point (cm^3/gm-mole)
$\tilde{V}$	partial molal volume
W	channel width (cm)
$W_{(l)}$	collision integral
x	horizontal distance variable (cm)
X	dimensionless horizontal distance variable = x/L
x_A	mole fraction of component A
XL_A	liquid phase mole fraction of component A
y	vertical distance variable (cm)
Y	dimensionless vertical distance variable = y/b
z	length variable used in solution of cylindrical heat transfer problem (cm)
z_{Ao}	arbitrary interfacial concentration (dimensionless)

Greek Letters

α	thermal diffusivity (cm^2/sec)
α_1, α_2	arbitrary constants defined by Eq. (6-16, 6-17)
β_1	variable used in heat flux solution (see Eq. (E-9))
β_T	coefficient of volumetric thermal expansion ($cm^3/°C$)
γ	surface tension (dynes/cm)
Γ	gamma function
Δ	indicates the difference between two quantities
δ	film thickness (cm)
ϵ	maximum attractive energy between two molecules (ergs/molecule)
ζ	dimensionless variable defined by Eq. (3-4)
η	dimensionless distance defined by Eq. (4-3)
θ_A	dimensionless concentration of component A
θ_{AB}	dimensionless flux correction factor
λ	dimensionless variable defined by Eq. (4-3)
μ	viscosity (centipoise)
ν	kinematic viscosity (centistokes)
ξ	dimensionless variable defined by Eq. (4-4)
π	constant = 3.1416
ρ	density (gms/cm^3)
Φ	dimensionless temperature variable
ϕ_A	volume fraction of component A
Φ_{AB}	dimensionless flux ratio
ψ	dimensionless mass transfer rate defined by Eq. (5-15)
∇	vector differential operator

Variable Subscripts

1,2	refers to component 1, 2, etc.
A,B	refers to component A, B, etc.
AB	refers to the binary system composed of components A and B
avg	average of a quantity
cr	at or near the critical point for cellular flow instability
G	in the gas phase, or based upon the gas phase
i,int	quantity evaluated at the interfacial position
in,inlet	quantity evaluated at the inlet, or start of the exposure section
L	in the liquid phase, or based upon the liquid phase
loc	a local or point value
o	quantity evaluated at the interfacial position
mix	refers to a liquid mixture
x	based upon mole fractions
ϕ	based upon volume fractions
∞	quantity evaluated in the bulk, or at a large distance from the gas-liquid interface

Mathematical Operators

D/Dt	substantial derivative = $\frac{\partial}{\partial t} \quad (v \cdot \Delta)$
def	deformation operator = $\left(\frac{\partial u_i}{\partial x_j} + \frac{\partial u_j}{\partial x_i} \right)$
div	divergence of a vector = $(\Delta \cdot v)$
grad	operation of Δ on a scalar function
Δ	vector differential operator = $\sum_i \delta_i \frac{\partial}{\partial x_i}$, where δ_i are the unit directional vectors

REFERENCES

1. G. Ackermann, Forschungsheft 382, 1 (1937).
2. A. Acrivos, A.I.Ch.E.J. 6, 410 (1960).
3. American Chemical Society, "Physical properties of Chemical Compounds," Vol. 2, No. 22, Advances in Chemistry Series, New York (1959).
4. J. H. Arnold, Trans. A.I.Ch.E. 40, 361 (1944).
5. C. A. P. Bakker, P. M. Buytenen, and W. J. Beek, Chem. Eng. Sci. 21, 1039 (1966).
6. W. J. Beek and C. A. P. Bakker, Appl. Sci. Res. 10, 241 (1961).
7. H. Bénard, Ann. Chim. Phys. 23, 62 (1901).
8. J.C. Berg, A. Acrivos, and M. Boudart, "Advances in Chemical Engineering" Vol. 6, Academic Press, New York (1966).
9. J. C. Berg, Ph.D. Dissertation, University of California, Berkeley, California, 1964.
10. D. L. Bidlack and D. K. Anderson, J. Phys. Chem. 68, 3790 (1964).
11. R. B. Bird, W. E. Stewart, and E. N. Lightfoot, "Transport Phenomena," John Wiley and Sons, New York, (1960).
12. R. M. Butler and A. C. Plewes, Chem. Eng. Prog. Symp. Ser., No. 10, 121 (1955).
13. C. H. Byers, Ph.D. Dissertation, University of California Lawrence Radiation Report UCRL-16565, 1966.
14. C. H. Byers and C. J. King, Part I, A.I.Ch.E.J. (July 1967).
15. C. H. Byers and C. J. King, Part II, A.I.Eh.E.J. (July 1967).
16. R. C. Cairns and G. H. Roper, Chem. Eng. Sci. 3, 97 (1954).
17. H. S. Carslaw and J. C. Jaeger, "Conduction of Heat in Solids", Oxford University Press, 2nd ed., New York, (1959).
18. S. Chandrasekhar, "Hydrodynamics and Hydromagnetic Stability", Oxford University Press, London, (1962).
19. K. C. Chao and J. D. Seader, A.I.Ch.E.J. 7, 598 (1961).
20. A. P. Colburn and T. B. Drew, Trans. A.I.Ch.E. 33, 197 (1937).
21. S. R. M. Ellis and M. Biddulph, Chem. Eng. Sci. 21, 1107 (1966).
22. A. S. Emanuel and D. R. Olander, Int. J. Heat and Mass Trans. 7, 539 (1964).
23. Adolf Fick, Pogg. Ann. 94, 59 (1855).

24. J. B. J. Fourier, "Theorie Analytique de la Chaleur", Gauthier-Villars, Paris, (1822), English Trans. by Freeman (1878).
25. E. N. Fuller, P. D. Schettler, and J. C. Giddings, Ind. and Eng. Chem., 58, No. 5, 19 (1966).
26. F. Goodridge and G. Gartside, Trans. Inst. Chem. Engrs. 43, 74 (1965).
27. L. Graetz, Ann. Phys. Chim. 25, 338 (1885).
28. J. P. Hartnett and E. R. G. Eckert, "Recent Advances in Heat and Mass Transfer", McGraw-Hill Book Co., Inc., New York (1961).
29. R. Higbie, Trans. A.I.Ch.E. 31, 365 (1935).
30. J. O. Hirschfelder, C. F. Curtis and R. B. Bird, "The Molecular Theory of Gases and Liquids", John Wiley and Sons, New York (1956).
31. C. D. Hodgeman, "Handbook of Physics and Chemistry", 40th ed., Chemical Rubber Pub. Co., Cleveland (1959).
32. M. Jakob, "Heat Transfer", Vol. 1, John Wiley, New York (1949).
33. C. J. King, A.I.Ch.E.J. 10, 671 (1964).
34. C. J. King, Ind. Eng. Chem. Fund. 5, 146 (1966).
35. C. J. King, ScD Thesis in Chemical Engineering, Massachusetts Institute of Technology (1960).
36. C. J. King, Lawrence Radiation Laboratory Report 11196, "Mass Transfer During Short Surface Exposures in Countercurrent Flow", (1964).
37. C. J. King, L. Hsueh, and K. Mao, J. Chem. Eng. Data 10, 348 (1965).
38. J. Koefoed and J. V. Villadsen, Acta. Chem. Scand. 12, 1124 (1958).
39. J. G. Knudsen and D. L. Katz, "Fluid Dynamics and Heat Transfer", McGraw-Hill, New York (1958).
40. H. L. Kuo, J. Fluid Mech. 10, 611 (1961).
41. N. A. Lange, "Handbook of Chemistry", 6th ed., Handbook Publishers Inc., Sandusky, Ohio (1946).
42. L. Lapidus, "Digital Computation for Chemical Engineers", McGraw-Hill Book Co., Inc., New York (1962).
43. J. Leveque, J. Ann. Mines 12, 201, 305, and 381 (1928).
44. W. K. Lewis and C. K. Change, Trans. A.I.Ch.E. 21, 127 (1928).
45. W. K. Lewis, Mech. Eng. 44, 445 (1922).
46. E. N. Lightfoot, J. Electrochem. Soc. 113, 614 (1966).
47. E. N. Lightfoot and V. Ludviksson, J. Electrochem. Soc. 113, 1325 (1966).

48. A. R. Low, Proc. Roy. Soc. (London) A125, 180 (1929).
49. W. V. R. Malkus and G. Veronis, J. Fluid Mech. 4, 225 (1958).
50. N. G. Maroudas and H. Sawistowski, Chem. Eng. Sci. 19, 919 (1964).
51. J. B. Maxwell, "Data Book on Hydrocarbons", Van Nostrand, New York (1950).
52. H. Mendelson and S. Yerazunis, A.I.Ch.E. J. 11, 834 (1965).
53. R. L. Merson and J. A. Quinn, A.I.Ch.E. J. 11, 391 (1965).
54. R. L. Merson and J. A. Quinn, A.I.Ch.E. J. 10, 804 (1964).
55. A. D. Modine, E. B. Parrish, and H. L. Toor, A.I.Ch.E. J. 9, 348 (1963).
56. K. Muenz and J. M. Marchello, A.I.Ch.E. J. 12, 249 (1966).
57. R. J. Nunge and W. N. Gill, Int. J. Heat Mass Trans. 8, 873 (1965).
58. D. R. Olander, Int. J. Heat Mass Trans. 5, 765 (1962).
59. A. Orell and J. W. Westwater, A.I.Ch.E. J. 8, 350 (1962).
60. J. R. A. Pearson, J. Fluid Mech. 4, 225 (1958).
61. A. Pellew and R. V. Southwell, Proc. Roy. Soc (London) A176, 312 (1940).
62. R. H. Perry, "Chemical Engineers' Handbook", 4th ed., McGraw-Hill Book Co., Inc., New York (1963).
63. A. F. Pillow, Aeron. Res. Rept. Australia A79, 1 (1952).
64. W. E. Ranz and P. F. Dickson, Ind. Eng. Chem. Fund. 4, 345 (1965).
65. Lord Rayleigh, Phil. Mag. (6) 32, 529 (1916).
66. R. C. Reid and T. K. Sherwood, "The Properties of Gases and Liquids", 2nd ed., McGraw-Hill Book Co., In., New York (1966).
67. H. Schlichting, "Boundary Layer Theory", McGraw-Hill Book Co., Inc., New York (1960).
68. T. K. Sherwood and R. L. Pigford, "Absorption and Extraction", 2nd ed., McGraw-Hill Book Co., Inc., New York (1952).
69. H. L. Shulman and L. J. Delaney, A.I.Ch.E. J. 5, 290 (1959).
70. A. Seidell, "Solubilities of Organic Compounds", 3rd ed., Van Nostrand, New York (1940).
71. E. M. Sparrow, R. J. Goldstein, and V. K. Jonsson, J. Fluid Mech. 18, 513 (1964).
72. F. B. Sprow and J. M. Prausnitz, Can. J. Eng. 45, 25 (1967).
73. C. V. Sternling and L. E. Scriven, A.I.Ch.E. J. 5, 514 (1959).

74. J. Szekely, Chem. Eng. Sci. 20, 1063 (1965).
75. Y. P. Tang and D. M. Himmelblau, Chem. Eng. Sci. 18, 143 (1963).
76. Y. P. Tang and D. M. Himmelblau, A.I.Ch.E. J. 9, 630 (1963).
77. J. J. Thompson, Phil. Mag. (4) 10, 330 (1855).
78. J. J. Thompson, Proc. Roy. Phil. Soc. Glasgow 13, 464 (1882).
79 J. Timmermans, "Physico-chemical Constants of Pure Organic Compounds", Elsevier Pub. Co., New York (1950).
80. R. E. Treybal, "Mass-Transfer Operations", McGraw-Hill Book Co., Inc., New York (1955).
81. C. Varley, Trans. Roy. Soc. Arts Sci. Mauritius 50, 190 (1836).
82. J. E. Vivian and W. C. Behrmann, A.I.Ch.E.J. 11, 656 (1965).
83. W. J. Ward and J. A. Quinn, A.I.Ch.E.J. 11, 1005 (1965).
84. L. E. Westkaemper and R. R. White, A.I.Ch.E.J. 3, 69 (1957).
85. W. G. Whitman, Chem. Met. Eng. 29, 146 (1923).
86. C. R. Wilke and Pin Chang, A.I.Ch.E.J. 1, 264 (1955).
87. C. R. Wilke and C. Y. Lee, Ind. and Eng. Chem. 47, 1253 (1955).

This report was prepared as an account of Government sponsored work. Neither the United States, nor the Commission, nor any person acting on behalf of the Commission:

A. Makes any warranty or representation, expressed or implied, with respect to the accuracy, completeness, or usefulness of the information contained in this report, or that the use of any information, apparatus, method, or process disclosed in this report may not infringe privately owned rights; or

B. Assumes any liabilities with respect to the use of, or for damages resulting from the use of any information, apparatus, method, or process disclosed in this report.

As used in the above, "person acting on behalf of the Commission" includes any employee or contractor of the Commission, or employee of such contractor, to the extent that such employee or contractor of the Commission, or employee of such contractor prepares, disseminates, or provides access to, any information pursuant to his employment or contract with the Commission, or his employment with such contractor.